Fluorescence correlation spectroscopy (FCS) analysis of probe transport in cells from measurements to models

D I S S E R T A T I O N

zur Erlangung des akademischen Grades

doctor rerum naturalium
(Dr. rer. nat.)
im Fach Physik

eingereicht an der
Mathematisch-Naturwissenschaftlichen Fakultät
Humboldt-Universität zu Berlin

von
Msc.-Phys. Seyed Mohsen Jebreiil Khadem

Präsidentin der Humboldt-Universität zu Berlin:
Frau Prof. Dr. Sabine Kunst

Dekan der Mathematisch-Naturwissenschaftlichen Fakultät:
Herr Prof. Dr. Elmar Kulke

Gutachter:
1. Prof. Dr. I. M. Sokolov, Humboldt-Universität zu Berlin
2. Prof. Dr. Hans-Gerd Löhmannsröben, Potsdam University

3. Prof. Dr. Diego Krapf, Colorado State University

Tag der mündlichen Prüfung: 28.02.2018

Ich widme diese Arbeit
meinen Eltern.

Abstract

The objective of this thesis is to provide a toolbox for characterization of anomalous diffusion of tracer particle in crowded systems using fluorescence correlation spectroscopy (FCS). We discuss that the robust information about the probability density function (PDF) of the particle's displacement is contained in the asymptotic behaviour of the FCS curves at long and short times. Thus, analysis of the short-time behaviour provides reliable values of exponent of anomalous, diffusion coefficient and lower moments of the PDF. This allows one to to confirm or reject its Gaussian nature. The Gaussianity test could be then used to guess the correct form of the PDF from a set of competing models. We show the applicability of the proposed analysis protocol in artificially crowded systems and in living cell experiments.

Furthermore, we investigate the consequence of non-scaling PDF on the possible results of the FCS data. As an example of such processes, we calculate the FCS curve for a continues time random walk model with waiting times delivered from Lévy-stable distribution with an exponential cut-off in equilibrium. The results indicate that, although the deviations from Gaussian behaviour may be detected when analyzing the short- and long-time asymptotic of the corresponding curves, their bodies are still perfectly fitted by the fit form used for normal diffusion.

Finally, we propose an alternative approach for performing spot variation FCS using an ordinary FCS set-up. We introduce a non-linear transformation which applies on the smoothed intensity profile of the detected fluorescence photons with binning or smoothing kernel method. Autocorrelation of the generated intensity profiles mimic the FCS curves for the sizes of laser spots which are effectively smaller than the initial one in the experiment. The obtained FCS curves are used to investigate the presence of nano-domains or barriers in artificially crowded systems and in living cells.

Keywords: Fluorescence correlation spectroscopy, Spot variation fluorescence correlation spectroscopy, Anomalous diffusion, Living cell

Zusammenfassung

Ziel dieser Arbeit ist es eine Toolbox zur Charakterisierung der anomalen Diffusion von Tracerpartikeln in dicht gepackten Systemen mit

Ziel dieser Arbeit ist es eine Toolbox zur Charakterisierung der anomalen Diffusion von Tracerpartikeln in dicht gepackten Systemen mit Fluoreszenz-Korrelationsspektroskopie (FCS) zur Verfügung zu stellen. Es wird gezeigt, dass die robusten Informationen über die Wahrscheinlichkeitsdichtefunktion (PDF) der Verschiebung des Tracers im asymptotischen Verhalten der FCS-Kurven auf langen, sowie auf kurzen Zeitskalen enthalten sind. So liefert die Analyse des Kurzzeitverhaltens zuverlässige Aussagen über die Werte des Exponenten der anomalen Diffusion, des Diffusionskoeffizienten und der niedrigeren Momente der PDF. Dies erlaubt es eine Gaußverteilung zu bestätigen oder zu widerlegen. Der Test auf Gaußverteilung könnte als Index verwendet werden, um die richtige Form der PDF aus einer Reihe von konkurrierenden Ergebnissen zu erraten.

Darüber hinaus untersuchen wir die Konsequenz der nicht-skalierenden PDF auf Ergebnis der FCS-Kurven. Wir berechnen die FCS für ein Continuous Time Random Walk Modell mit Wartezeiten gemäß einer Lévy-stabilen Verteilung mit exponentiellem cut-off . Die Ergebnisse zeigen, dass obwohl die Abweichungen vom Gauß'schen Verhalten bei der asymptotischen Analyse erkannt werden können, ihre Körper immer an Formen für die normale Diffusion perfekt angepasst werden können.

Schließlich schlagen wir einen alternativen Ansatz für die Durchführung von Spot Variation FCS mit dem gewöhnlichen FCS-Setup vor. Wir führen eine nicht-lineare Transformation ein, die auf das mit Binning oder Kernel smoothing method geglättete Intensitätsprofil der detektierten Fluoreszenzphotonen angewendet wird. Ihre Autokorrelation imitiert die FCS-Kurven für die Größen des Laserspots, die im Experiment effektiv kleiner als die anfängliche Größe sind. Die erhaltenen FCS-Kurven werden verwendet, um künstliche dicht gepackte Systeme sowie lebende Zellen auf Nano-Domänen oder Barrieren hin zu untersuchen.

Schlagwörter: Fluoreszenz-Korrelationsspektroskopie, Spot-Variation Fluoreszenz-Korrelationsspektroskopie, Anomale Diffusion, Lebende Zelle

Contents

List of abbreviations

FCS	Fluorescence correlation spectroscopy.
ACF	Autocorrelation function.
$SV-FCS$	Spot variation fluorescence correlation spectroscopy.
$FCCS$	Fluorescence cross correlation spectroscopy.
SPT	Single particle tracking.
PDF	Probability density function.
MSD	Mean squared displacement.
$CTRW$	Continuous time random walk.
GLE	Generalized Langevin equation.
fBm	Fractional Brownian motion.

1 Introduction

1.1 Motivation

Deep understanding of probe particle transport within cells and their interactions with cells is an essential step in investigating physics of life. This is also required for further developments in medicine and biology, especially for targeted drug delivery. In a living cell, efficient transport of the drugs and proteins to their specific destinations is of great importance to its basic biological functionality and development. Such transportation processes may be categorized in two classes: active transport and passive transport. In active transport, the substance moves against its concentration gradient and therefore, its movement consumes energy. Passive transport, however, refers to the processes in which movement of a substance does not require energy.

One of the main forms of the passive transport processes is (passive) diffusion which refers to the erratic motion of particles in a system. This thermally driven motion which consists of short-scale random displacements, generally ranging in the scale of nano- to millimetre, plays a crucial role in different systems observed in nature and in the laboratory. Transportation of gasses, hydrophobic molecules and small uncharged molecules from the surrounding environments into the cell through the membrane and vice versa are examples of diffusion processes. Therefore, investigation of diffusion in biological systems is important in many innovative strategies. In such systems, molecular crowding and complexity in and around living cells influence the diffusion process. To understand such complexities, one considers artificial crowded fluids as toy models for mimicking the situation at hand. Such artificially crowded system could be studied in details and results could be to some extent generalized to explain the observations in living cell experiments.

While diffusion of a passive particle in many environments is "normal" (see Sec.1.2), in crowded heterogeneous systems such as living cells, anomalous diffusion (see Sec.1.3) is frequently observed. This anomaly is reported as non-linear growth of mean squared displacement (MSD) of the tracer particle with time and/or the non-Gaussian probability density function (PDF) of particle's displacement in disagreement with prediction of Fick's theory of diffusion. Deep understanding of the nature of such an ubiquitous process is has brought theoretical and experimental scientists together from from biological, physical ,chemical and mathematical sciences. Experimentalists have provided detailed information regarding the single molecule

activities in different systems. In the theoretical part, different models based on different physical assumptions have been introduced to explain the experimental observations and also to predict other properties of the systems. Different statistical tools were also developed by mathematicians in order to distinguish between different competing models for explanation of the experimental observations.

The advent of single molecule techniques providing the information on single molecule activity, on the other hand, has led to a revolutionary improvement of our understanding of transport processes in biological context. During the last four decades, different methods have been developed to characterize diffusion processes and have been properly modified in order to be used in biological experiments. Fluorescence recovery after photo-bleaching (FRAP), single particle tracking (SPT) and fluorescence correlation spectroscopy(FCS) are the most conventional tools that are widely used by experimentalists in different fields of science. Although the theory behind these techniques are so far trivial for the case of normal diffusion, interpretation of results obtained using these techniques for the case of anomalous diffusion has so far remained elusive. Fulfilling such a gap requires not only the theoretical understanding but also an experimental background of these techniques which is necessary for further developments. The main focus of this work is, essentially, to provide a theoretical framework for the use of the FCS technique for observation of anomalous diffusion which is often the case in biological experiments.

In this thesis we aim at addressing the following questions: What information is essentially contained in the results obtained from the FCS measurement and where? and How can one extract this information? Most information regarding the diffusing process and the substrate is encoded in the PDF of particle's displacement which is a function of two variables, coordinate and time. However, FCS measurements provide us results which are function of only one variable, temporal intensity-intensity correlation function. Therefore, to win information one considers some assumptions about the diffusion process in analysis of FCS data which are not necessary correct in all systems. The standard approach to obtain information from the FCS technique is to fit the results to some simple functions which are derived assuming a Gaussian form of the PDF of particle's displacement. In case the fits are not optimum, one adds an additional parameter to the fit functions and describes the anomalous diffusion with this parameter.

As we proceed to show in this chapter, many models for describing the anomalous diffusion possess non-Gaussian form of the PDF. Thus, this fitting approach may lead to unreliable results. Therefore, we attempt at going beyond the simple fitting method. With some mathematical analysis of the theory of FCS results, we show that some information about lower moments of the PDF of particle's displacement and about the fractal dimension of the substrate can be reliably won from FCS data. The interesting result was that such information is contained not where people are normally looking for it, but in the short time asymptotic of the FCS curves. With

using this information about the lower moments, one can develop a Gaussianity test which can be used in guessing the correct form of the PDF from competing models. We also show that, in case of scaling form of the PDf of particle's displacement one can obtain robust values of diffusion coefficient and exponent of anomalous diffusion form the asymptotic of data. With these considerations, we can introduce a general toolbox for analysis of FCS data.

To generalize our proposed toolbox, we study the characterization of the non-scaling PDF of particle's displacement in the FCS data. This was motivated by some observations in our experimental works and other reported researches in literatures in which the PDF of particle's displacement has a considerable deviation from Gaussian form in short times which ceases to exit in log times. Such processes are termed as "anomalous yet Brownian". Our studies show that, characterization of such process with use of FCS technique is possible, only if one considers the short and long time asymptotic in the analysis of data.

To solve the fundamental problem of finding the PDF of particle's displacement from the FCS data, some spatial information has to be known. This can be delivered by a variation of ordinary FCS technique named as spot-variation FCS which is an experimentally demanding technique. We show that the whole information is essentially contained in the single photon count time series for any given spot radius. Thus, with an appropriate analysis of this time series from a single experiment, one can mimic the FCS data for the spot sizes which are effectively smaller than the initial one. Such an approach to perform the spot-variation FCS with the possibility of avoiding the experimental difficulties, could be used in different analysis to obtain valuable information from an ordinary FCS technique.

This thesis is structured as follows: in following sections we define normal and anomalous diffusion and provide a review of the models describing such scenarios. Then we introduce the FCS technique including the experimental set-up and some general applications.

In chapter **2**, we discuss what information is contained in the FCS data. We first re-derive the existing formula for the FCS data and provide formula for the three dimensional case. Then we introduce the apparatus function. We then show that the FCS curves is consist of the moments of the displacement's. From this fact we establish a protocol which enables one to distinguish different models of anomalous diffusion. The theoretical results are then examined and supported by the FCS experiments in in-vitro systems. Finally, we apply the proposed method to study diffusion in living cells.

Chapter **3** discusses the observation of the non scaling PDF of particle's displacement using the FCS technique. We first formulate a theory explaining the observations of anomalous yet Brownian diffusion. As a model for this, we use a continuous time random walk model with an exponentially cut-off Levy distribution waiting time distribution in equilibrium. This in principal takes into account the

time that systems ages before the start of the measurement. The analytic form of FCS curve in short and long time asymptotic are then derived and the full FCS curves are calculated numerically for different ageing times. We then discuss how to observe the existence of such processes using FCS technique.

In chapter **4**, we introduce a new method to improve the spatial resolution of ordinary FCS. By exploiting the Gaussian form of the laser spot in FCS set-up, we propose a method to obtain the FCS curves of different spot sizes by post-processing of the recorded data from the original spot during the measurement. This theoretical development provides valuable information about the sub-diffraction limit scale which is generally not available using an ordinary FCS technique. The proposed method is confirmed using some in-vitro experiments and then applied to the in-vivo measurements.

1.2 Normal Diffusion

It was 1828, when Scottish biologist Brown, reported the observation of intriguing random motion of certain pollen in water using a light microscope. This observation, which is now called Brownian motion, motivated plethora of systematic experimental and theoretical studies in the Nineteenth century. First microscopic approach explaining the nature of such observations was introduced by **?** and one year later by **?**, considering the diffusion as a random walk problem, giving a probabilistic picture of Brownian motion of the tracer particle. Some time later in 1908, **?**, proposed another theory to the problem, assuming that the diffusing particle in a fluid medium obeys Newtonian mechanics which experiences the external force and friction. This approach seems to be quite different from the former ones in mathematical sense but in principal, is closely related to the others in physical aspects. The experimental measurement of the trajectories of colloidal particles by J.Perrin and his students in 1908 (**?**), which gave a direct support to this probabilistic picture of Brownian motion, was awarded with the Nobel prize in 1926 for providing the direct proof for existence of molecules.

In what follows, we give a brief description of Einstein's approach and define the MSD and PDF of the random walker's displacement. Then we smoothly shift to the models for anomalous diffusion, discussing the violations of assumptions made by Einstein for explanation of normal one. In this section, we closely follow the review literature by (**?**), (**?**) and (**?**). Einstein gave the following picture of the Brownian motion of the tracer particle: He assumed that the displacement, s_i, of a tracer particle in the time intervals, τ_0, to be identically distributed independent random variables. The total displacement is then defined as $x(t) = \sum_{i=1}^{N} s_i$ with $N = t/\tau_0$ being the total number of steps during the time t and due to symmetry, the mean of displacement at any time is zero.

The most conventional parameter which is used to describe the diffusion process

is MSD of the random walker. Despite the mean displacement, MSD is non-zero quantity and is defined in the sense of statistical average as: $\langle x^2(t)\rangle = \langle(\sum_{i=1}^{N} s_i)^2\rangle$. Rewriting the sum one gets

$$\langle x^2(t)\rangle = \langle(\sum_{i=1}^{N} s_i)^2\rangle = \sum_{i=1}^{N}\langle s_i^2\rangle + \sum_{i\neq j}\langle s_i s_j\rangle.$$

The second sum term in the expression above is zero due to independence of the jumps, namely absence of any correlation. Calling the assumptions that the second moment of jumps is finite, and in average is $< {s_i}^2 >= a^2$, and the step time intervals are equal, he reached the MSD to be

$$< x^2(t) >= 2Dt \tag{1.1}$$

where D is the diffusion coefficient being $D = \frac{a^2}{2\tau_0}$. Based on these assumptions, Einstein could derive the differential equation for PDF of tracer's displacement

$$\frac{\partial}{\partial t}P(x,t) = D\frac{\partial^2}{\partial^2 x}P(x,t) \tag{1.2}$$

which its solutions is a Gaussian function, $P(x,t) = \frac{1}{\sqrt{4\pi Dt}}\exp(\frac{-x^2}{4Dt})$, satisfying the initial condition of $P(x,0) = \delta(x)$. The same diffusion equation was first introduced by Fick (**?**), in 1985 following a phenomenological approach. Combining the linear response theory for concentration of diffusing particles and conservation of number of particles, Fick derived the same formula as of Einstein with simple replacement of number of particles with PDF of tracer.

Therefore, normal diffusion is characterized with the linear growth of MSD with time lag and Gaussian form of the PDF ofthe particle's displacement. Additionally, the PDF has a scaling form such that, higher moments of displacement can be written as a function of second moment. Therefore, knowing the MSD for a normal diffusion is sufficient to calculate the PDF and higher moments of the particle's displacement. Any deviation from these properties in diffusion process belongs to another class of diffusion, termed anomalous diffusion, which we will discuss in the following section.

1.3 Anomalous Diffusion

In Einstein's approach to the problem of diffusion, he made assumptions which are necessary not the case for diffusion of the particle in complex and heterogeneous systems such as biological ones. Plethora of observations unveiled different behaviours of the MSD and PDF of the particle's displacement compared to the predictions of Einstein's theory. The MSD of the particle in such observations did not follow

the linear dependence on time and showed a rather complicated non-linear dependence as: $\langle x(t)^2 \rangle = 2Dt^\alpha$ with $\alpha \neq 1$ being exponent of anomalous diffusion. The PDF of the particle's displacement, however, happened to be Gaussian or deviate from Gaussian form for different observations with the non-linear time dependency of the MSD. These deviations persist for time scales much larger than characteristics diffusion time and cease to exist in times which could be longer than a specific measurement time.

Those processes with exponent of anomalous diffusion greater than unity, $\alpha > 1$, are assigned to the class of super-diffusion. Such situations occur when the second moment of step length PDF does not remain finite. The other corresponding situation is when the steps in random walk are positively correlated such that the walk is persistent. As examples to such situations, one could refer to the random walk on the chemical space of polymer chains and transport of particle (protein) made by molecular motors(**???**).

The other class of anomalous diffusion which is the main subject of this work, is called sub-diffusion. Sub-diffusion refers to the case that the exponent of anomalous diffusion is smaller than unity, $\alpha < 1$. Diffusion process in this situation is much slower than normal one.

First physical scenario leading to sub-diffusion is when the mean waiting time to perform a walk is much longer than the observation time and in this sense diverges. This situation was first assumed to describe the transport process of charge carriers in amorphous material(**?**). In biological sense, one can imagine a trapping-untrapping effect in binding sites, for example in living cell. The mathematical model for such physical assumption is called continuous time Random Walk model (CTRW). In CTRW model, not only the MSD may shows a non-linear dependency on time lag but also the PDF of the particle's displacement sharply deviates from Gaussian.

The other scenario for sub-diffusion is when the displacements are anti-correlated. This means in the sense that in jump action, there is higher probability that a particle moves in the direction opposite to the last one. This anti-correlation of displacement may be imposed by a structural disorder in the media in which diffusion takes place. The model for such a situation generally referred as random walk on fractal. The PDF in this model is also non-Gaussian, however, the non-Gaussianity is much smaller then what is observed in CTRW model.

Another possibility for the anti-correlation of steps is diffusion in visco-elastic environments. In such cases, different parts of the system create an interacting complex and the particle has to move through a concreted way. The corresponding theoretical model is generalized Langevin equation (GLE) and the fractional Brownian motion (fBm) which is closely related to (GLE). Contrary to the other models of sub-diffusion, these models show a Gaussian PDF of the particle's displacement.

In what follows, we shortly discuss the mentioned mathematical models for the

sub-diffusion. Understanding the fundamental properties and differences between such models will be utilized to recognize them using fluorescence spectroscopy technique.

1.3.1 Continuous Time Random Walk

Continuous time random walk (CTRW) is one of the most popular methods to describe the sub-diffusion and is widely discussed in the recent book (**?**). In CTRW, the medium in which diffusion takes place is considered as a homogeneous space containing randomly distributed traps. Despite to the Einstein's picture of normal diffusion, sojourn time of the particle in these traps is not identical and varies depending on the depth of energetic traps encoded in waiting time probability distribution function, $\psi(t)$, from which the waiting time for next jump is drawn. If this probability density functions have the first moment, the mean sojourn time is finite , $\tau_0 = \int_0^\infty t\psi(t)dt$. Then the average number of steps in time t is $\langle n(t)\rangle = \frac{t}{\tau_0}$ and this results in normal diffusion.

For those waiting time probability density functions that lack the first moment, for example heavy tailed power law distribution function $\psi(\tau) \propto \tau^{-1-\alpha}$ with $0 < \alpha < 1$, the number of steps goes as $\langle n(t)\rangle = (\frac{t}{t_c})^\alpha$ with t_c being some characteristic time. The jump length of the particle is, however, given from the PDF of the jump length, $p(x)$. Assuming that the PDF of the jump length has the second moment in accordance to Einstein's assumption, $a^2 = \int_{-\infty}^{+\infty} x^2 p(x)dx$, the MSD of walker for sub-diffusion is then given as

$$\langle x(t)^2\rangle \propto \frac{a^2}{t_c^\alpha} t^\alpha. \tag{1.3}$$

To obtain the average number of steps at time t, $\langle n(t)\rangle = \sum_0^\infty n\chi_n(t)$, one may note the , χ_n, being the probability of performing exactly n steps by the time t. Probability of making no step is given by, $\chi_0 = \int_0^\infty \psi(t')dt'$, and other χ_n are calculated iteratively as $\chi_n = \int_0^\infty \psi(t')\chi_{n-1}(t-t')dt'$. Passing to the Laplace domain, one can obtain the correspondence of the internal clock n of CTRW and the physical time t given by $\chi_n(t)$ in the Laplace domain as

$$\chi_n(s) = \psi^n(s)\frac{1-\psi(s)}{s}. \tag{1.4}$$

The general form of the PDF of displacement for CTRW model may be derived from subordination approach as

$$p(x,t) = \sum_0^\infty p_n(x)\chi_n(t).$$

Passing to the Laplace domain and Fourier space, we note that the Fourier trans-

form of $P_n(x)$ is n-th power of its characteristic function $\lambda^n(k)$, substituting Eq.1.4 and calculating the sum one gets in Laplace-Fourier

$$P(k,s) = \frac{1-\psi(s)}{s}\frac{1}{1-\psi(s)\lambda(k)}. \tag{1.5}$$

Substituting $\lambda(k)$ and $\psi(s)$ as given functions in equation above and performing inverse Fourier and Laplace, one could in principle obtain the corresponding PDF of displacement in CTRW model. It should also be mentioned that substituting $\lambda(k)$ and $\psi(s)$ possessing second and first moment, respectively, results in normal diffusion with Gaussian probability distribution function and substituting $\psi(s)$ lacking the first moment results in anomalous diffusion with the strong deviation from Gaussian.

One important feature of the CTRW model which makes it easy to distinguish from other models is *aging*. Aging in fact, means at dependency of system's evolution on the time when the observation starts. Suppose the observation starts at time t_a after the preparation of system. The MSD, for instance, is then given as

$$\langle x^2(t)\rangle = \langle l^2\rangle(\langle n(t_a+\Delta t)\rangle - \langle (t_a)\rangle).$$

For those waiting time PDFs which the mean waiting time exist, we have $n(t) = t/\tau$ and the MSD has no dependency on t_a, $\langle x^2(t)\rangle \propto \Delta t/\tau$. For heavy-tailed waiting time PDF, however, we have $n(t) \propto t^\alpha$ so that $\langle x^2(t)\rangle = \langle l^2\rangle((t_a+\Delta t)^\alpha - t_a^\alpha)$. It is now clear that the MDS in time Δt explicitly depends on the time t_a, in other words the systems ages. Other features of the system in the same way are dependent on the age of the process. In chapter 3, we will discuss the CTRW model in more details.

1.3.2 Random Walk in Disordered Systems

In the previous sections, it was assumed that diffusion takes place in homogeneous media. This means that whole space for the particle was allowed to be explored and from probabilistic point of view, particles have equal chances to move in all directions, namely, an isotropic situation. In heterogeneous system, this is not the case and presence of large obstacles, such as macromolecules in living cells, prevents the diffusing element to access whole space and this imposes an anti-correlation of steps. Studying such situation from mathematical point of view is not easy and in general, in these type of problems, proposing a closed formalism is not possible, except for some idealised situations. One approach for better understanding of diffusion in obstructed systems is to map the situation at hand to the problem of transport in a fractal systems. The self-similarity of the fractal systems allows mathematicians to use the re-normalization approach to obtain some analytical results for the transport process in the system. Note that this self-similarity in real cases is not perfect but still provides a good estimation of the situation.

Let us now define some features of the fractal systems which will be used in the next chapter for our analysis of FCS data. Analogous to the space dimension in Euclidean geometry, one defines the fractal dimension, d_f, for the fractal system which determines the growth of mass with size of structure, $M(x) \sim x^{d_f}$ (**?**). The trajectory of random walker in the fractal substrate results also in another self-similar structure which its dimension can be attributed to a fractal dimension called walk dimension, d_w. If the mass of newly created trajectory grow with the number steps, n, then one obtains the MSD of random walker to be (**?**)

$$\langle x^2(n) \rangle \sim n^{2/d_w} \tag{1.6}$$

Assigning each step of random walker to an instant of time, one can simply replace, n and t in Eq.1.6. Note that exponent of anomalous diffusion is now given as, $2/d_w$, with $d_w = 2$ leading to normal diffusion.

Derivation of PDF of particle's displacement in fractal system is rather complicated and a general form is not available for arbitrary fractal structure. In principal, a long time simulation is required in order to estimate the form of PDF, see (**?**). Nevertheless, the probability of finding a random walker at the initial position at time t_0, after time t is given as $P(0,t) \sim t^{-\frac{d_s}{2}}$, which d_s is the spectral dimension of fractal. Spectral dimension can be considered as parameter determining the available sites for a random worker and may be interpreted as density of states in a fractal space (**?**). The connection between d_f, d_w and d_s was proposed by Alexander-Orbach (**?**) as

$$\frac{d_s}{2} = \frac{d_f}{d_w} \tag{1.7}$$

meaning that finding the walk and spectral dimension from a specific measurement, would lead to an estimation of fractal dimension of the substrate.

Percolation cluster

Percolation model has been continuously used to characterize many disordered systems and extensively studied by mathematicians and physicists in simulation and theory (**????**). Often use of percolation cluster in order to mimic the situation of complex systems such as living cells does not mean that this is the only one but it is the well understood one which is often invoked for explanation of anomalous diffusion in crowded systems. Consider a cubic (square) lattice in three (two) dimension, consisting of sites which are connected to nearest neighbours with bonds. Assuming that the p fraction of these bonds are being removed, percolation cluster is thought as a limiting situation in which $p_c = 0.592(0.401)$ fraction of these bonds are removed, where the lattice belongs to an incipient infinite cluster. Below this critical concentration, the system consists of a large cluster and above which there exist many finite clusters which the random walker can not percolate through the

system (**?**).

Plethora of researches have shown that the percolation cluster is well described by a fractal (**??**). Thus diffusion on the percolation lattice may be described by the language of the fractals as follows: Above the critical point, p_c, where there exist large clusters, the mean squared displacement starts to be anomalous and after some time, normal diffusion emerges. This is explained by the correlation or self-similarity length, $\zeta(p)$. For smaller length of the network compared to $\zeta(p)$, the self-similarity leads to anomalous diffusion, however, for larger sizes, the cluster turned to be homogeneous and diffusion is regular with $d_w = 2$ in Eq.1.6. Therefore, one observes a crossover from anomalous to normal diffusion. Below p_c, small clusters are created. Therefor, random walker is trapped on one of these clusters and after experiencing anomalous diffusion in short times, MSD goes to a constant being square of correlation length at long times. Exactly at percolation threshold, the incipient infinite cluster is self-similar in all length scales and anomalous diffusion takes place with $d_w > 2$, with no crossover to normal diffusion.

This anti-correlation of displacement in percolation threshold is closely related to the anomalous diffusion modelled with GLE with coloured noise which will be the topic of following section.

1.3.3 Visco-elastic Systems

Diffusion of a particle in a visco-elastic system is another physical picture where the anomalous diffusion appears to be the case. In such picture, the diffusing particle is a part of complex system and its movement is a function of dynamic of the whole system. This in principal imposes a long term memory in the particle's displacement which determines a concreted way for its movement (**??**). To mathematically approach this interpretation of anomalous diffusion, first we shortly mention the Langevin equation for normal diffusion and pass to the anomalous one.

Celebrated Lengevin equation (**?**) describes the Brownian motion of a spherical particle immersed in a solution with use of Newton laws for forces. It is assumed that the particle with mass m, experiences a random force $f(t)$ (Gaussian white noise) and consequently the deterministic friction force $-\gamma\dot{x}(t)$. Thus the trajectory is given by the following stochastic differential equation

$$m\ddot{x}(t) = -\gamma\dot{x}(t) + f(t) \tag{1.8}$$

where γ denotes the friction constant, directly connected to the viscosity of solution η and radius of particle a as $\gamma = 6\pi\eta a$. If the the system does not show a visco-elastic behaviour, ensemble average of the randomly fluctuating force (noise) is zero, $\langle f(t)\rangle = 0$, and the noise is delta correlated, namely the random force is a white Gaussian noise.

From the fluctuation-dissipation theorem, one gets the noise correlation function as:

$$\langle f(t).f'(t')\rangle = 2\gamma K_\beta T\delta(t-t')$$

with K_β and T being the Boltzmann constant and the temperature of the medium. Calculating the velocity-velocity correlation function from the noise correlation function and then using Green-Kubo relation (**?**), one obtains the linear MSD as Eq.1.3 for Brownian particle with diffusion coefficient being $K_\beta T/\gamma$.

Genrealized Langevin equation is essentially the modification of Eq.1.8, for the situation where the friction term contains an intrinsic memory of the environment $\Gamma(t)$, say visco-elastic system, realized as an integral expression in Langevin equation as

$$m\ddot{x}(t) = -\gamma\int_0^t \Gamma(t-t')\dot{x}(t')dt' + f(t). \tag{1.9}$$

Depending on whether the system is in equilibrium or not, the fluctuation-dissipation theorem applies or violates. In case of equilibration, the memory kernel and noise correlation function are connected as $\langle f(t).f'(t')\rangle = K_\beta T\gamma\Gamma(t-t')$ but, in essence, the connection between the noise, the friction term and the exponent of anomalous diffusion is connected to the setting of the system. The PDF of particle's displacement remains Gaussian as long as the noise , say the fluctuation, is assumed to remain Gaussian and therefore the dynamic is totally defined by the MSD of particle. Note that, assuming the memory to be described by power-law kernel $\Gamma(t) \propto t^{-\beta}$, Eq.1.9 could be reformulated with the Caputo fractional derivative (**?**) and the equation is then referred as fractional Langevin equation (FLE). A good example of application of GLE for explanation of observed anomalous diffusion in single protein molecule may be the work by Kou, et al (**?**).

Fractional Brownian motion (fBm), rigorously introduced by Mandelbrot and Van Ness (**?**), is also a process that is closely related to the limiting case of GLE for long times. Rather than being a physical model, fBm is a mathematical model for conveniently describing the anomalous diffusion. Suppose that the position of particle obeys fBm, $x(t) = B^H(t)$ with $H \in (0,1)$ being the Hurst parameter, $B^H(t)$ is Gaussian distributed trajectory with zero mean and a persistent position-position correlation as

$$\langle B^H(t)B^H(t')\rangle = \left(|t|^{2H} + |t'|^{2H} - |t-t'|^{2H}\right)/2. \tag{1.10}$$

fBm, in another words, takes the Brownian motion and incorporates a persistent correlation, which results in MSD of particle to be $< x^2(t) > \propto t^{2H}$, which $H = 1/2, 1$ leads to normal and ballistic motion. In connection to the GLE in over-damped situation, fBm may be written as integration over Gaussian noise (FGN), $f(t)$ in Eq.1.9, $B^H(t) = \int_0^t f(t')dt'$. Again, the PDF of fBm process is Gaussian but in

contrast to the Brownian motion it is not a Markov process and the whole statistic of process is not fully driven from the propagator.

1.4 Fluorescence Correlation Spectroscopy

Fluorescent correlation spectroscopy (FCS) is one the most prominent single molecule techniques which has been widely used in many fields of studies. It was first introduced by **?** as a method to measure the thermodynamic fluctuations in a reacting system. They measured the chemical rate constant, diffusion coefficients and the coupling for the binding of ethidium bromide to DNA. Although determining these parameters is the main domain of application of this method, there is much more other information one can obtain from a FCS measurement. The number of articles reporting the results obtained from this techniques is more than ten thousands and the systems investigated range from cells and single biological molecules to artificial materials of technical use. This explicitly indicates its influence in the nowadays science.

FCS has experienced a long journey in order to become an ideal well-established analytical method and people from different fields of science have contributed to achieve this accomplishment. The main development of FCS was the advent of the ground breaking confocal microscopy (**?**). Coupling the confocal microscopy technique, which provides a tiny detection spot, to the ordinary FCS, allows one to observe the significant fluctuation of the concentration in the spot. This is due to the fact that, as much as the number of particles inside the detection volume decreases, the fluctuation of the number of particles with respect to average number of detected particles signifies. This consequently, results in data with high signal to noise ratio. Using the low concentration of tracer particles together with the tiny confocal volume, essentially makes the FCS a single particle technique. The laser spot created with the confocal microscopy is still limited to the diffraction limit but can reach to the order of hundreds of nanometers ($\sim$ 200 nm), depending on the numerical aperture, NA, and the laser light wavelength, λ, as: $d = \frac{\lambda}{2NA}$ (**?**).

The other crucial progress in the FCS technique which has led to the higher time resolution of data obtained, is the improvement of detecting systems. The conventional detectors such as photomultipliers used in FCS measurement to deal with a bunch of photons emitted form the fluorescent particles. Therefore, the resolution of the detection was determined by the time width which the detectors could recover from the previous detection to bin the photons. The same situation, namely the dead time of the detector, is naturally still remained in the developed detectors such as single-photon avalanche diode. However, this time width has decreased considerably thanks to the technical improvements. Decreasing the dead time of the detectors, then, led to the arrival of generation of detectors which are able to detect the single photons. The single photon counting provided the tendency of

observation and separation of the successive coming fluorescence photons with the time lag of nano-seconds (**?**). Practically, the time resolution of nowadays FCS measurements are in the order of micro- seconds, noting that below $10 - 100\ \mu s$, usually, one observes the photo-physical properties of the fluorescent particle rather than the motion properties.

In the software level as well, the advancement of empowered computational methods for the fast calculation of the autocorrelation curves for large number of lag times together with the large data management methods have made the use of FCS very convenient(**?**). The possibility of pre-processing the data in software level, for instance the filtering the unwanted background photon counts using time gating has led to obtain more reliable results from a FCS measurements. Beside these technical progresses, sophisticated methods for data analysis, such as many components fit functions (**?**) and asymptotic analysis (**?**) resulted in deeper understanding of diffusion process in complex systems using the FCS method.

Furthermore, limited tracer particles only to those having fluorescent properties, fluorophores, was indeed a drawback for FCS technique in studying the chemical and transport processes of proteins and molecules under study which lack the fluorescence property. Novel methods for labeling the tracer particle with fluorescent molecules with a weak influence on their properties had then a great impact on promotion of FCS applicability, especially in biological systems (**?**). In addition to these progresses in advancement of different elements of FCS technique, different variations of FCS for specified purposes were also introduced. Fluorescence cross-correlation spectroscopy (FCCS) for studying the interactions by cross-correlating two or more fluorescent channels and Scanning FCS for obtaining the special information about the medium under study, are examples of these variations which were continuously made for different purposes broadening the application of this technique in different fields of researches (**??**). Nevertheless, what we mean by the term of FCS technique in this work is, essentially, a set-up which consists of all these basic developments. In this section, an introduction to the FCS set up with some general remarks on experimental details will be provided.

Fig.1.1 shows the essential components of a FCS set-up. The first element is the laser source which is typically a pulsed laser. The laser light can be automatically controlled with a shutter placed in front of the laser source for preventing the additional illumination right after the measurements. The wavelength is chosen based on having the most overlap with the excitation wavelength of the fluorescent tracer. Then, the laser light is guided with the mirrors into a microscope objective passing through the dichroic mirror. The objective with high numerical aperture (to reduce aberration and decrease the spot size) creates a confocal volume in the sample. The excited fluorescent particles inside the the confocal volume re-emit the fluorescence photons. These photons are again collected by the same objective and reflected to the dichroic mirror. Since the fluorescent photon are red shifted with respect to the

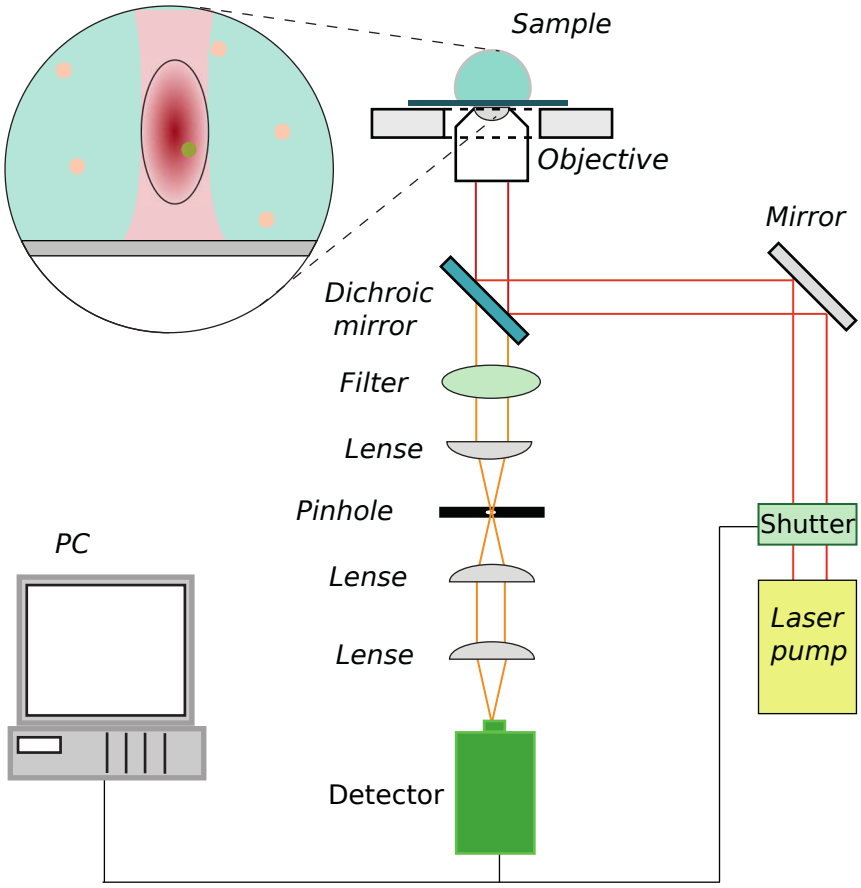

Figure 1.1. Schematic description of a ordinary FCS set-up. The pathway of incident laser light to the sample and that of re-emitted fluorescent photons by the tracer particles are shown. The red shifted fluorescence photons pass through the dichoric mirror and are collected by the detectors. The recorded intensity profile is the transformed to the PC for further analysis.

laser light, they can pass through the dichroic mirror. To eliminate the out of focus light in confocal microscopy, the photons pass from a pinhole and then are guided to the detector (s) which is (are) automatically controlled by PC to be open only during the measurement. The detected intensity is then recorded by the PC may be transformed for further analysis.

Fig.1.2 indicates a closer look at some details in the FCS measurement. The first remark is the form of the confocal volume which is created in the sample, shown in panel a. This intensity profile can be well approximated by an elongated Gaussian form. r_0 here is the lateral and sr_0 the axial $1/e^2$-radius of the confocal volume with s being the eccentricity of the confocal volume. s normally ranges from 4 to 6 in

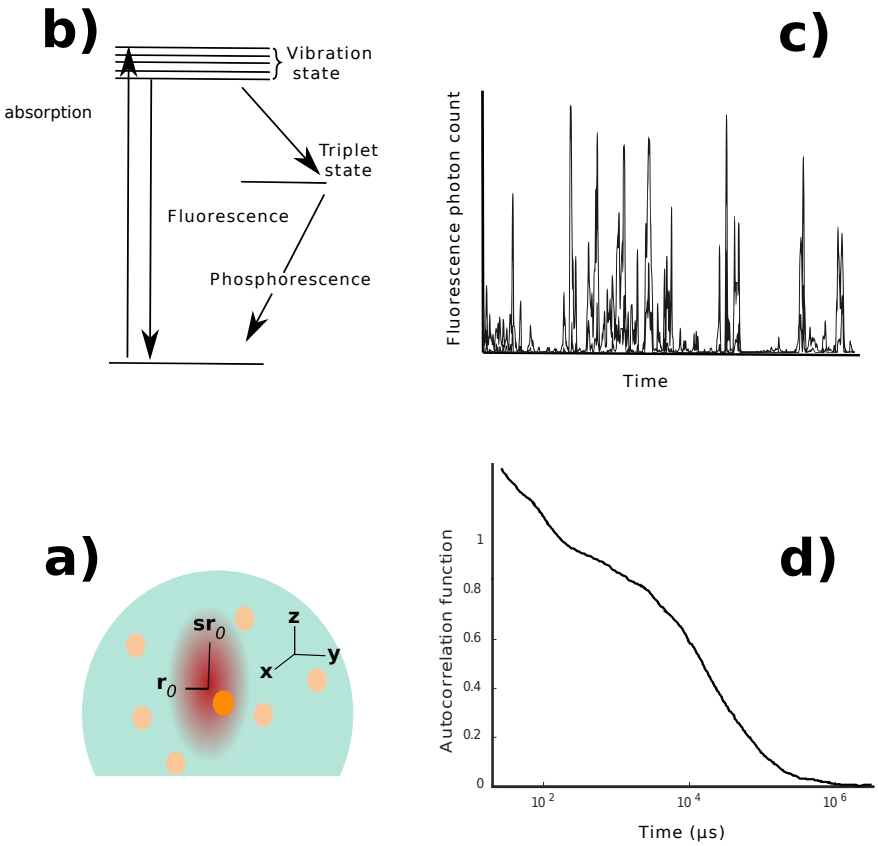

Figure 1.2. Schematic description of a) confocal volume created in the sample, containing tracer particles b) Jablonski energy diagram for explanation of emission fluorescence photos c) the recorded fluorescence intensity profile by detectors d) calculated autocorrelation function of the fluorescence intensity profile resulting in FCS curves.

typical FCS measurements. The average number of tracer particles in such confocal volume may be controlled by the concentration of particles in the sample. A trivial calculation indicates that, keeping the concentration of tracer particles in the sample below few nM, results in having less than one particle in average inside a confocal volume generated with confocal microscopy.

The panel b in Fig.1.2 shows the sketched Jablonski energy diagram for the fluorescent molecule (**?**). The first transition is the absorption of a photon with a particular energy by the fluorescent molecule. This is indicated by a straight arrow pointing up. In the absorption process, the energy of the incident photon excites one electron from the lower energy level to a higher one. This transition depends on

the energy of the photons which must correspond to the energy difference between two eigenstates of fluorescent molecule. This process is very fast and takes place in the time range of 10^{-15} s.

Upon the absorption of the energy by an electron, it attempts to dissipate the received energy. In fluorescent molecules, the most probable pathway to lose energy is to emit a photon. Since at higher energy levels there is higher probability that the energy is dissipated through the internal conversion and vibrational relaxation, the fluorescence occurs through relaxation of the electron from the first excited energy level. "In fact, at the first excited state, fluorescence can compete in regard to time-scales with other non-radiative processes which has lower energy compared to the incident photon". This is shown as a straight line going down. Therefore, the emitted fluorescent photon has lower energy compared to the incident one. The energy difference between the incident and emitted photona by the molecule is lost in the internal conversion and vibrational relaxation, where it is transferred away from the electron. This relaxation through vibration modes is, however, non-radiative and the electronic level of the electron does not change in this process. Compared to non-radiative processes which take place in the order of 10^{-14} s to 10^{-11} s, fluorescence is a slow process and takes place in the time range of 10^{-9} s to 10^{-7} s.

Another possibility for the energy dissipation by the excited electron is inter-system crossing. In this situation, electron changes the spin multiplicity from an excited singlet state to a triplet state. The spin-orbit coupling in molecules which show this behaviour is substantial. The probability that such a process occurrs is higher when the vibrational levels of the two excited states overlap. This process has a very low probability and is much slower than the fluorescence with many order of magnitude. Since in this process, no energy is gained or lost, the electron must undergo another transition to dissipate the energy. This can be done with a radiative decay from excited triplet state to the singlet ground state, which is called phosphorescence (**?**). There are other ways of non-radiative relaxations which are termed as dark-states. These types of transitions are essentially disturbing in a FCS measurement. In FCS curves, these photo-physical phenomena normally take place in time-scales less than 100 μs and may be excluded in the analysis by truncating the very short time autocorrelations. In slow process, specially, these problems are of minor importance since the dynamic of interest is much larger than these relaxation times.

Re-emitted photons from the excited fluorescent molecules which are red-shifted then are collected by the detectors. The schematic sketch of the fluorescence intensity is shown in panel c in Fig.1.2. The original intensity profile is, essentially, a trace of zero or one data (binary data) indicating the detection or lack of a fluorescence photon at a give time, t. The statistic of the detected photons may be recognized as a inhomogeneous Poisson distribution where the detection rate of the photons is locally dependent on the process by which the fluorescence particles pass

through the confocal volume. In principle, all the information about the diffusion process is contained in this intensity profile. Thus accuracy of collecting photons and excluding the unwanted backgrounds determines the quality of the final data in a FCS measurement.

The essence of the FCS technique is to take this intensity profile and calculate its autocorrelation function for different time lags. The schematic of calculated autocorrelation is depicted in panel *d*. All FCS curves are very similar to each other. Extraction of information from these curves is done with fitting procedure. For the case of normal diffusion, which is dominant form of diffusion in homogeneous systems, the hight of the non-normalized FCS curve determines the inverse number of the particles inside the confocal volume. Furthermore, the time corresponding to the autocorrelation function being at half of its maximum (autocorrelation at time zero) determines the average time which particles spend inside the confocal volume, termed as diffusion time τ_d. The diffusion coefficient of the particles can be, consequently, calculated as $D = \frac{{r_0}^2}{2\tau_D}$. Further information such as viscosity of the medium, η, and hydrodynamic radius of the diffusing particles, r may be obtained using Stokes Einstein-equation (**?**) as $D = \frac{k_B T}{6\pi\eta r}$ where K_B and T correspond to the Boltzmann constant and the absolute temperature of the medium, respectively.

Generally the extraction of information from the FCS measurements corresponds to fitting a function to the FCS curves. For normal diffusion, one uses the assumption of Gaussian form of the PDF and derives a closed form for the FCS curve, as we will discuss in next chapter. For the anomalous diffusion, however, no general closed formula exists and a general procedure to obtain reliable information is missing. The main aim of this work is , essentially, to provide such a toolbox which exploits the minimum assumptions on the motion of particles and simultaneously provides more information. This will be the main topic of next chapter and a comprehensive mathematical analysis of the FCS technique will be discussed.

2 What information is contained in Fluorecence correlation spectroscopy curve

In this chapter, we concentrate on the application of the standard FCS to processes which can be safely defined as normal or anomalous translational diffusion. While for the case of normal diffusion, the data processing in the FCS experiment corresponds to a fitting of the intensity autocorrelation curves to a relatively simple function with unknown parameters, the situations for anomalous diffusion are much more involved. In many cases one uses the same class of functions with the additional free parameter α defining the MSD, $R^2(t) = \langle r^2(t) \rangle$, of diffusing particles as a function of time, $R^2(t) = 6D_\alpha t^\alpha$, with D_α being the coefficient of the anomalous diffusion, (**???**). The fit assumes the Gaussian nature of the distribution of the particles' displacements, a fact which is discussed e.g. in (**??**), which in many cases (but not always) can be motivated by the physical (or biological) nature of the diffusion anomaly. The question arises, what kind of errors may one encounter using this procedure in the case of non-Gaussian displacement distributions, what is the reasonable way to proceed in such cases, and how to tell Gaussian and non-Gaussian cases appart having only the standard FSC autocorrelation functions (ACFs) as input.

To do answer these questions, one has to discuss in depth the mathematical theory behind the FCS formula, and to explicitly formulate the additional assumptions. After this, it will get clear what information can be extracted from the corresponding data and how this can be done. In what follows we only concentrate on the case of translational diffusion, and on the corresponding time range in the FCS autocorrelation functions. The results of this part of work are published in Physical Review E (**?**).

2.1 Preliminary Considerations

As we proceed to show, the intensity autocorrelation function $G(t)$, which we will call in what follows the "FCS curve" for the sake of brevity, can be mathematically seen as an integral transform of the diffusion's Green's function (particles' displacement distribution) $P(\mathbf{r}, t)$. We will assume that the transport process is homogeneous

in time (i.e. does not show aging effects), and that the diffusion takes place in a homogeneous and isotropic medium. In this case one can view the displacements' probability density $P(\mathbf{r},t) = P(r,t)$ as a function of two independent variables, the time lag t and the spacial distance r, and, as we discuss in Sec.2.2, the normalized FCS curve is given by the equation

$$G(t) = \int_0^\infty F(r)P(r,t)dr \tag{2.1}$$

where $F(r)$ will be called the apparatus function since it depends only on the properties of the setup characterizing the geometry of the light beam. This one typically has the Gaussian intensity profile

$$I(\mathbf{r}) = I_0 \exp\left(-\frac{2(x^2+y^2)}{r_0^2} - \frac{2z^2}{s^2 r_0^2}\right) \tag{2.2}$$

with r_0 being the diameter of the beam's waist in the direction perpendicular to the light propagation direction, and sr_0 being the corresponding axial dimension of the light propagation. In a typical FCS experiment the parameters of the beam are fixed and known in beforehand. The explicit form of $F(r)$ will be derived in Sec. 2.2 and is given by Eq. (2.11). Eq. (2.1) allows to explicitly calculate $G(t)$ provided $R(r,t)$ is known.

For normal diffusion the form of $P(r,t)$ is known

$$P(r,t) = \frac{1}{(4\pi Dt)^{3/2}} \exp\left(-\frac{r^2}{4Dt}\right), \tag{2.3}$$

and corresponds to a family of Gaussian functions parametrized by a single free parameter D, the diffusion coefficient. In this case the integral transform, Eq. (2.1), maps the family of $P(r,t)$ onto the family of FCS curves $G(t;D)$, again parametrized by D,

$$G(t;D) = \left(\frac{4D}{r_0^2}t + 1\right)^{-1} \left(\frac{4D}{s^2 r_0^2}t + 1\right)^{-\frac{1}{2}}, \tag{2.4}$$

and the parameter D can be found by fitting this expression to experimental data representing the ACF. If the corresponding fit is poor, there are reasons to assume the diffusion anomalies, which indeed are often observed in the crowded interiours of biological cells and in many artificial complex fluid systems (**???**).

In many cases, when the fit to the standard form, Eq. (2.4), is poor one considers a modified, two-parametric, family of fit functions

$$G(t;\alpha,D_\alpha) = \left(\frac{4D_\alpha}{r_0^2}t^\alpha + 1\right)^{-1} \left(\frac{4D_\alpha}{s^2 r_0^2}t^\alpha + 1\right)^{-\frac{1}{2}}, \tag{2.5}$$

which may give (and indeed gives) a reasonable fit. This form corresponds to assuming the Gaussian anomalous diffusion characterized by the displacements' PDF as

$$P(r,t) = \frac{1}{(4\pi D_\alpha t^\alpha)^{3/2}} \exp\left(-\frac{r^2}{4D_\alpha t^\alpha}\right). \tag{2.6}$$

As we proceed to show in Sec. 2.3 by considering simple numerical examples, even if such fit is reasonably or indeed very good, it does not guarantee that the value of the exponent α of anomalous diffusion is reproduced correctly since the true form of the FCS curve in its main part, close to the inflection point, mostly depends on the higher moments of $P(r,t)$ and not only on the MSD. This, however, does not mean that $G(t)$ contains no information on $P(r,t)$: on the contrary, the FCS curves contain a lot of important information, but simple parametric fitting is not the best way of extracting it.

The integral transformation Eq. (2.1) cannot be viewed as an integral equation of the Fredholm's type since the unknown function is the kernel of the transformation (i.e. the one with two variables, not with the single one). The corresponding mathematical problem is undetermined: it is impossible to uniquely restore a function of two variables $P(r,t)$ having only a function of a single variable t as an input. We note that using the spot variation FCS in which the parameters of the beam, say r_0, change during the experiment as we will discuss in chapter 4 (see also (**?**) for an example of such an experiment in a membrane) provides two-dimensional data $G(t,r_0)$ and may allow for full restoration of $P(r,t)$, although this is still quite a hard task. Moreover, such experiments are rare, and will not be considered in the present work devoted to the standard techniques.

As we proceed to show, all crucial information is contained in the short- and long-time asymptotic of the FCS curve. Thus, the initial (short time) part of the curve contains information about the particle's MSD (at short times), which can be obtained by asymptotic fitting, while the long time asymptotics contains information on return probabilities (at long times), the fact discussed in (**?**). As long as no additional assumptions are done, these two may provide valuable information but can hardly be connected with each other.

In many cases, however, it is reasonable to assume that the function $P(r,t)$ scales, i.e. retains its form in the course of the time. Physically, such an assumption means that one deals with the process which does not possess any internal time or length scale (like the typical size of the trapping domain or a typical trapping time), i.e. the self-similarity of the medium in which the diffusion takes place. This is the case for all Gaussian models like fractional Brownian motion (fBm), adequate for description of diffusion in viscoelastic media, for percolation models and other fractal geometries, and in many other cases. In this case, only the width of $P(r,t)$ changes in course of the time, while the relation between its higher moments, defining the form, remains constant. The assumption of scaling immediately allows for making

far reaching conclusions. Since the relation between the lower moments does not depend on the time, the short time asymptotic fitting may allow to obtain several lower moments to safely define α and to check whether the diffusion process is at least approximately Gaussian or not. Comparing short- and long-time asymptotics allows for decision whether the particles' motion is bounded to the fractal substrate.

In what follows, we will first discuss the general theoretical approach, numerical examples, the peculiarities of short- and long-time asymptitic fitting, and then show how the methods discussed work in application to real experimental data.

2.2 The Apparatus Function

The theory underlying the FCS measurement is well-described e.g.(**?**). We consider here the simple, one-component situation, and look for the normalized autocorrelation function

$$G(t) \propto \int\int d\mathbf{r}d\mathbf{r}' I(\mathbf{r})I(\mathbf{r}')C(\mathbf{r},\mathbf{r},t), \tag{2.7}$$

with $I(\mathbf{r})$ being the beam intensity profile and $C(\mathbf{r},\mathbf{r}',t) = \langle \delta c(\mathbf{r},0)\delta c(\mathbf{r}',t)\rangle$ being the correlation function of the molecular density fluctuations which are described as a time-homogeneous random process. The result is normalized over the value of $G(t)$ at zero time lag t. In the specially homogeneous and isotropic system $C(\mathbf{r},\mathbf{r}',t)$ depends only on the distance between the corresponding points: $C(\mathbf{r},\mathbf{r}',t) = C(|\mathbf{r}-\mathbf{r}'|,t)$. Our further discussion follows Höfling and co-workers, however, in a more complex tree-dimensional setting. The integral for $G(t)$ has the form of the double convolution, and therefore simplifies in the Fourier-domain. The normalized intensity autocorrelation function reads

$$G(t) = \frac{\int d\mathbf{k}|I(\mathbf{k})|^2 S(\mathbf{k},t)}{\int d\mathbf{k}|I(\mathbf{k})|^2 S(\mathbf{k},0)} \tag{2.8}$$

with $S(\mathbf{k},t)$, the intermediate scattering function, being the Fourier transform of $C(\mathbf{r},t)$, and $I(\mathbf{k})$ being the Fourier transform of $I(\mathbf{r})$. In the simple case considered here, $C(\mathbf{r},t)$ is proportional to the Green's function (propagator) of the corresponding diffusion operator, $C(\mathbf{r},t) \propto P(\mathbf{r},t)$, which gives the possibility to probe the diffusion in the corresponding medium. Therefore one can substitute $S(\mathbf{k},0)$ in the previous expression by the characteristic function of the corresponding propagator. Changing from $S(\mathbf{k},t)$ to the propagator's characteristic function,

$$P(\mathbf{k},t) = \int d\mathbf{r}\exp(i\mathbf{k}\mathbf{r})P(\mathbf{r},t)$$

we obtain from Eq. (2.8)

$$G(t) = \frac{\int d\mathbf{k}|I(\mathbf{k})|^2 \int d\mathbf{r} \exp(i\mathbf{kr})P(\mathbf{r},t)}{\int d\mathbf{k}|I(\mathbf{k})|^2 \int d\mathbf{r} \exp(i\mathbf{kr})P(\mathbf{r},0)}.$$

Interchanging the sequence of integration in $\mathbf{k}$ and in $\mathbf{r}$ we obtain

$$G(t) = \frac{\int d\mathbf{r} W(\mathbf{r})P(\mathbf{r},t)}{\int d\mathbf{r} W(\mathbf{r})P(\mathbf{r},0)}.$$

with $W(\mathbf{r}) = \int \exp(i\mathbf{kr})|I(\mathbf{k})|^2 d\mathbf{r}$. Noting that $P(\mathbf{r},0) = \delta(\mathbf{r})$ we obtain

$$G(t) = \int \frac{W(\mathbf{r})}{W(0)} P(\mathbf{r},t) d\mathbf{r}. \tag{2.9}$$

For the Gaussian intensity profile, Eq. (2.2),

$$I(\mathbf{r}) = I_0 \exp\left(-\frac{2(x^2+y^2)}{r_0^2} - \frac{2z^2}{s^2 r_0^2}\right),$$

the ratio $W(\mathbf{r})/W(0)$ is readily calculated:

$$\frac{W(\mathbf{r})}{W(0)} = \exp\left(-\frac{x^2+y^2}{r_0^2} - \frac{z^2}{s^2 r_0^2}\right).$$

The level surfaces of the Gaussian intensity profile are the spheroids characterized by the parameter e with $e^2 = 1 - 1/s^2$. For prolate spheroids ($s > 1$) the parameter e is real and fulfills the relation $0 \leq e < 1$: it corresponds to the eccentricity of the spheroid. For the oblate spheroid ($s < 1$) the parameter e is imaginary. In any case, e^2 fulfills the inequality $-\infty < e^2 < 1$. For the sake of brevity we will refer to e as to eccentricity, although in the oblate case it is not exactly the one. We note that throughout the text the letter e is used only for the eccentricity, and does not denote the base of the natural logarithm.

Substituting this in Eq. (2.9) we get

$$G(t) = \int \exp\left(-\frac{x^2+y^2}{r_0^2} - \frac{z^2}{s^2 r_0^2}\right) P(\mathbf{r},t) d\mathbf{r}.$$

Assuming the diffusion to be isotropic $P(\mathbf{r},t) = P(r,t)$, we now pass to spherical

coordinates:

$$\begin{aligned} G(t) &= 2\pi \int\int \exp\left(-\frac{r^2\cos^2\theta}{r_0^2} - \frac{r^2\sin^2\theta}{s^2 r_0^2}\right) P(r,t) r^2 dr d\cos\theta \\ &= 2\pi \int \exp\left(-\frac{r^2}{r_0^2}\right) \left\{ \int_{-1}^{1} \exp\left[\frac{r^2}{r_0^2}\cos^2\theta\left(1-\frac{1}{s^2}\right)\right] d\cos\theta \right\} P(r,t) r^2 dr \end{aligned}$$

Thus $G(t)$ can be expressed via a single integral, as in Eq. (2.1)

$$G(t) = \int_0^\infty F(r) P(r,t) dr$$

containing $P(r,t)$ and the apparatus function $F(r)$ which depends only on the beam's properties r_0 and e. The function $F(r)$ has the following integral representation:

$$F(r) = 4\pi r^2 \int_0^1 \exp\left[-\frac{r^2(1-e^2x^2)}{r_0^2}\right] dx. \tag{2.10}$$

The integral can be easily expressed through the imaginary error function $\operatorname{erfi}(z) = \frac{2}{\sqrt{\pi}} \int_0^z \exp(x^2) dx$. The final result reads:

$$F(r) = \frac{2\pi^{3/2} r_0}{e} r \exp\left[-\left(\frac{r}{r_0}\right)^2\right] \operatorname{erfi}\left(\frac{er}{r_0}\right). \tag{2.11}$$

$F(r)$ decays at infinity as $\exp(-r^2/r_0^2)$ for $s > 1$ or as $\exp(-r^2/s^2r^2)$ for $s < 1$ in the leading order, and has the integral of

$$B = \int_0^\infty F(r) dr = \frac{(2\pi)^{3/2} r_0^3}{\sqrt{1-e^2}}, \tag{2.12}$$

as can be seen by substituting the integral representation, Eq. (2.10), into Eq. (2.12) and exchanging the sequence of integration in r and in x.

Thus, the full expression for $G(t)$ is

$$G(t) = \frac{2\pi^{3/2} r_0}{e} \int_0^\infty r \exp\left[-\left(\frac{r}{r_0}\right)^2\right] \operatorname{erfi}\left(\frac{r}{r_0} e\right) P(r,t) dr. \tag{2.13}$$

This equation is the main result of the present section and the starting point of our further considerations. It is the most convenient for the numerical calculations (as done in Sec. 2.3).

For the standard case of normal diffusion the FCS curve

$$G(t) = \frac{2\pi^{3/2} r_0}{e} \int_0^\infty r \exp\left[-\left(\frac{r}{r_0}\right)^2\right] \mathrm{erfi}\left(\frac{r}{r_0} e\right) \frac{1}{(4\pi D t)^{3/2}} \exp\left(-\frac{r^2}{4Dt}\right) dr \quad (2.14)$$

can be obtained in quadratures. The integral is of the form

$$I = \int_0^\infty x \exp(-p^2 x^2) \mathrm{erfi}(qx) dx$$

with $p = \left[r_0^{-2} + (4Dt)^{-1}\right]^{1/2}$ and $q = r_0^{-1} e = r_0^{-1}\sqrt{1 - s^{-2}}$, and

$$p^2 - q^2 = \frac{1}{s^2 r_0^2} + \frac{1}{4Dt} > 0.$$

The last inequality guarantees that the integrand vanishes at the upper limit of integration. Performing partial integration and noting that $\mathrm{erfi}(0) = 0$ and that $\frac{d}{dx}\mathrm{erfi}(x) = \frac{2}{\sqrt{\pi}} \exp(x^2)$ we get

$$I = \frac{1}{2p^2} \int_0^\infty \exp(-p^2 x^2) \frac{d}{dx} \mathrm{erfi}(qx) dx = \frac{1}{\sqrt{\pi}} \frac{q}{p^2} \int_0^\infty \exp[(q^2 - p^2) x^2] dx,$$

a Gaussian integral which is equal to

$$I = \frac{1}{2p^2} \frac{q}{\sqrt{p^2 - q^2}}.$$

Substituting the values of p and q and inserting the corresponding expression into Eq. (3.17) we get, after trivial transformations, the standard result, Eq. (2.4), for a single-species FCS under normal diffusion

$$G(t) = \left(\frac{4D}{r_0^2} t + 1\right)^{-1} \left(\frac{4D}{s^2 r_0^2} t + 1\right)^{-\frac{1}{2}}.$$

For anomalous Gaussian diffusions, like fractional Brownian motion (fBm), one only has to change Dt in this expression for $D_\alpha t^\alpha$ where, D_α is the appropriately defined coefficient of the anomalous diffusion, to get the corresponding equation for the Gaussian anomalous diffusion, Eq. (2.5).

2.3 Numerical Examples and First Caveats

Eq. (2.5) is often used for fitting the data for anomalous diffusion of unknown genesis. As we show in Sec. 2.4, the form of the intensity ACF is, however, sensitive

to the higher moments of the diffusion propagator, and therefore to the departures from Gaussianity. This question was partially addressed in Ref. (**?**). Before going into the deeper analysis, we discuss here numerical examples and express some caveats with respect to this procedure.

The Gaussian propagator, as pertinent to normal diffusion, Eq. (2.3) and the propagator for the Gaussian anomalous case Eq. (2.6) scale as a function of the arguments r^2/Dt and $r^2/D_\alpha t^\alpha$, respectively, so that their form remains constant in the course of the time evolution. It is better to represent the functions as a function of the MSD $R^2(t) = 6D_\alpha t^\alpha$, in which case their form is universal:

$$p(r, R(t)) = \frac{3^{3/2}}{(2\pi)^{3/2}} R^{-3}(t) \exp\left(-\frac{3}{2}\frac{r^2}{R^2(t)}\right).$$

Thus, $P(r,t)$ in the Gaussian case has the scaling form

$$P(r,t) = R^{-3}(t) f\left(\frac{r^2}{R^2(t)}\right)$$

with the scaling function $f(\xi)$ given by

$$f(\xi) = \left(\frac{3}{2\pi}\right)^{3/2} \exp\left(-\frac{3}{2}\xi^2\right). \tag{2.15}$$

This function is normalized in 3D and has the second moment of unity.

Let us now consider the family of related scaling functions, characterized by the stretched or squeezed Gaussian form,

$$f_\beta(\xi) = A \exp[-a(\xi^2)^\beta], \tag{2.16}$$

with the parameters A and a guaranteeing normalization in three dimensions

$$4\pi \int_0^\infty f_\beta(\xi)\xi^2 d\xi = 4\pi A a^{-\frac{3}{2\beta}} \Gamma\left(\frac{3}{2\beta}\right) = 1$$

and the unit second moment

$$4\pi \int_0^\infty f_\beta(\xi)\xi^4 d\xi = 4\pi A a^{-\frac{5}{2\beta}} \Gamma\left(\frac{5}{2\beta}\right) = 1.$$

Solving these equations we get

$$a = \Gamma^\beta\left(\frac{5}{2\beta}\right)\Gamma^{-\beta}\left(\frac{3}{2\beta}\right) \tag{2.17}$$

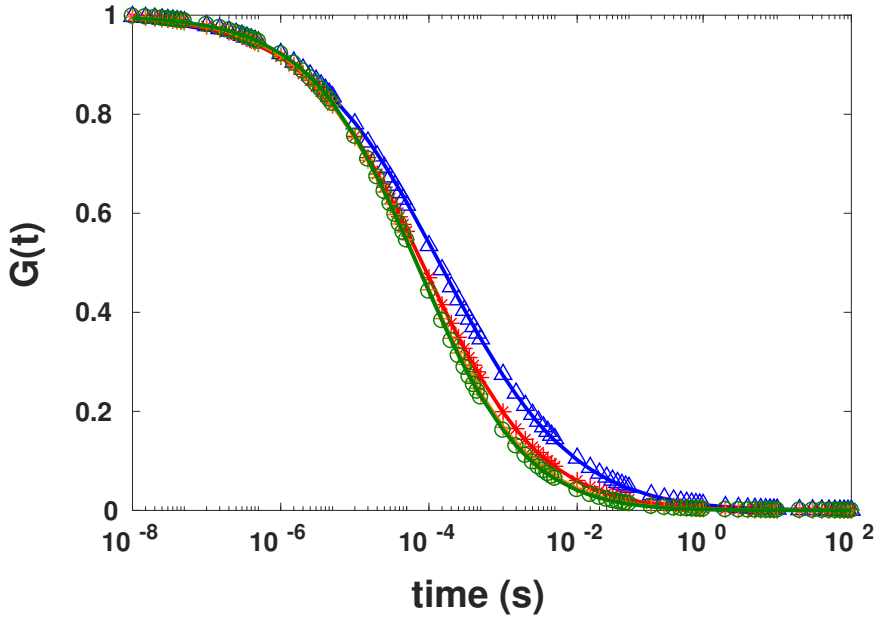

Figure 2.1. Numerically calculated FCS curves for $\beta = 0.5, 1, 1.875$ and 2.375 from right to left fitted to the standard formula for anomalous diffusion Eq.2.4.

and

$$A = \frac{1}{4\pi}\Gamma^{\frac{3}{2}}\left(\frac{5}{2\beta}\right)\Gamma^{-\frac{5}{2}}\left(\frac{3}{2\beta}\right). \tag{2.18}$$

For the Gaussian case ($\beta = 1$), we obtain exactly the coefficients in Eq. (2.15).

Let us now take the functions $f_\beta(\xi)$, Eq. (2.16), with the coefficients given by Eqs. (2.17) and (2.18), build the corresponding propagators

$$P_\beta(r,t) = R^{-3}(t) f_\beta\left(-\frac{r^2}{R^2(t)}\right),$$

all corresponding to the same MSD $R^2(t) = \langle \mathbf{r}^2(t)\rangle = 6D_\alpha t^\alpha$, insert them into the general equation Eq. (2.13), and obtain the hypothetical FCS curves $G_\beta(t)$ by the numerical integration. The curves for $\alpha = 0.53$ (mimicking the exponent of anomalous diffusion in percolation cluster), $D_\alpha = 1$, $e = 0.96$, $r_0 = 0.5\mu m$ and $\beta = 0.5, 1, 1.875, 2.375$ are shown in Fig 2.1.

All the curves look very much the same at short times, until the ACF falls approximately to $G(t) = 0.8$, and diverge afterwards. Since all these curves correspond to processes with exactly the same MSD and all other parameters except for β charac-

Table 2.1. Effective values of α for the examples in Fig.2.1

β	α_{eff}
0.5	0.4826 ± 0.0014
1	0.5308 ± 0.0002
1.875	0.5723 ± 0.0005
2.375	0.5845 ± 0.0005

terizing the form of the distribution, it is evident that the MSD cannot be estimated from the curve in a simple way. Now. we fit these curves by Eq. (2.5). The quality of fits is excellent, and the differences between the exact curves and the fits would be unobservable on the background of a whatever experimental noise. However, the values of the effective exponent α as given by the fit differ from the one used in the generation procedure (which is $\alpha = 0.53$) as can be seen from the 2.1.

This fact is evident when noting that if one plots $G(t)$, Eq. (2.5), on the logarithmic scale of Fig.2.1 the changes of D_α only shift the curve horizontally, while the changes in α alter the slopes. The slopes of the most prominent parts of the curves (the ones in vicinity of the inflection points) are evidently different, so indicating the extraction of only apparent values for α's.

Therefore we express the following caveat: *Although the fact of anomaly can be definitely detected by the standard fitting procedure, the value of the exponent of anomalous diffusion,α, given by the fit may differ considerably from the true one.* The value of α is underestimated for leptokurtic distributions (having sharper peak and heavier tails than the Gaussian one, $\beta < 1$) and overestimated for platykurtic ones (flatter peak and lighter tails, $\beta > 1$).

Further analysis will show that the part of the curve close to the inflection point is essentially a broad and non-universal crossover, hardly containing any information of immediate use. The short- and long-time asymptotic behaviours on the other hand may be analysed and lead to important conclusions about the form of the propagator. The discussion of the long-time asymptotics for the two-dimensional case is contained in (**?**) whereas, the discussion of the short-time behaviour is completely new to our best knowledge.

2.4 Short-time Asymptotics: Moments Expansion

Let us return to the integral representation Eq. (2.10), expand the exponential and perform the term-by-term integration. We get

$$F(r) = 4\pi r^2 \sum_{k=0}^{\infty} (-1)^k \frac{r^{2k}}{k! r_0^{2k}} \left[\int_0^1 (1 - e^2 x^2)^k dx \right], \tag{2.19}$$

i.e. a Taylor series which contains only contributions with even powers of r. We adopt here the following notation:

$$F(r) = 4\pi \left(a_0 r^2 + \frac{a_2}{r_0^2} r^4 + \frac{a_4}{r_0^4} r^6 + \frac{a_6}{r_0^6} r^8 + ... \right). \tag{2.20}$$

Since $-\infty < e^2 < 1$, the integrands of all integrals in Eq. (2.19) are positive, and the signs of the coefficients a_{2k} alternate. The integrals of the binomials can be easily computed:

$$\int_0^1 (1 - e^2 x^2)^k dx = \sum_{m=0}^{k} \binom{m}{k} (-1)^m e^{2m} \int_0^1 x^{2m} dx = \sum_{m=0}^{k} \binom{m}{k} (-1)^m \frac{e^{2m}}{2m+1}.$$

Therefore the expansion coefficients read:

$$a_{2k} = \sum_{m=0}^{k} \frac{(-1)^{k+m}}{m!(k-m)!(2m+1)} e^{2m},$$

and the first four coefficients are:

$$\begin{aligned} a_0 &= 1 \\ a_2 &= -1 + \frac{e^2}{3} \\ a_4 &= \frac{1}{2} - \frac{e^2}{3} + \frac{e^4}{10} \\ a_6 &= -\frac{1}{6} + \frac{e^2}{6} - \frac{e^4}{10} + \frac{e^6}{42}. \end{aligned}$$

Substituting the expression Eq. (2.20) into Eq. (2.1) and performing integration term by term we obtain

$$G(t) = 1 + a_2 r_0^{-2} M_2(t) + a_2 r_0^{-2} M_4(t) + a_6 r_0^{-6} M_6(t) + ... \tag{2.21}$$

with

$$M_{2n}(t) = 4\pi \int_0^{\infty} r^{2n} P(r,t) r^2 dr \equiv \langle \mathbf{r}^{2n}(t) \rangle$$

being even moments of the particles' displacements at time t. This is the main formula of this section which we will exploit continuously in what follows.

Eq. (2.21) shows that performing the asymptotic fitting of $1-G(t)$ at short times could provide the MSD $R^2(t) = M_2(t)$ (for these short times), but this knowledge is of limited value, if we do not assume that the form of $P(r,t)$ does not change with time. If, however, $P(r,t)$ scales (as it is the case for Gaussian processes, and in the case of percolation and other fractal models, as well as in random barrier setups) its higher even moments can be expressed through the MSD $R^2(t)$, and $M_{2n} = \kappa_{2n} R^{2n}(t)$ with coefficients κ_{2n} depending on the exact form of the distributions (with $\kappa_2 = 1$). In this case $G(t)$ as given by Eq. (2.21) can at short times be approximated by the polynomial in $R^2(t) = 6D_\alpha t^\alpha$:

$$G(t) = 1 + a_2 r_0^{-2} 6D_\alpha t^\alpha + a_4 r_0^{-4} \kappa_4 (6D_\alpha t^\alpha)^2 + a_6 r_0^{-6} \kappa_6 (6D_\alpha t^\alpha)^3 + \dots . \qquad (2.22)$$

Fitting this expression to experimental data one can (in principle) obtain α and several lower moments of particles' displacements, which can be used in subsequent analysis. Using them one can:

(i) Test whether the propagator is Gaussian or not,

(ii) try to guess the correct form of the propagator from a set of competing models,

(iii) Try to restore the function from the moments by solving the Stieltjes moment problem if large enough number of moments is available with a considerable accuracy.

We will show, however, that fulfilling these tasks is not trivial, and will not go beyond (i) in the present work (Sec.2.6).

2.5 Long-Time Asymptotic: Spectral Dimension and Beyond

Let us again assume that $P(r,t)$ scales:

$$P(r,t) = R^{-3}(t) f\left(-\frac{r^2}{R^2(t)}\right)$$

in full three-dimensional space, or

$$P(r,t) = R^{-d_f}(t) f\left(-\frac{r^2}{R^2(t)}\right)$$

in the case of the diffusion on a fractal substrate with fractal dimension d_f (in the three-dimensional Euclidean space $d_f = 3$). For long t , $R(t)$ gets very large, $R(t) \gg r_0$, and one can use the asymptotic expansion of Eq. (2.13). Let us assume that close to $\xi = 0$ one has $f(\xi) = C_1 - C_2 \xi^{2\beta} + \dots$ with $\beta > 0$ for any monomodal

distribution (e.g. as in our numerical examples). Inserting this form into Eq. (2.13) and noting that the value of $\int_0^\infty F(r)dr$ is given by Eq. (2.12) one gets:

$$G(t) = C_1 B R^{-d_f}(t) - C_2 R^{-d_f-2\beta}(t) \int_0^\infty F(r) r^{2\beta} dr + \dots .$$

The integral $\int_0^\infty F(r)r^{2\beta}dr$ converges under the restrictions assumed in the present work and has a representation via a hypergeometric function (following from Eq. (2.8.5.6) of (**?**)). The prefactors of the powers of R in this equation will be denoted by $\tilde{C}_1$ and $\tilde{C}_2$ in what follows.

Note that since $R(t) \propto t^{\alpha/2}$, the time-dependence of the first term (the slowest time dependence defining the asymptotic decay of the ACF) is $G(t) \propto t^{-\alpha d_f/2} = t^{-d_s/2}$ where d_s is the spectral dimension of the corresponding system. For normal diffusion this dimension is $d_s = 3$ as evident from the decay form of Eq.(2.4). Thus, the long-time behaviour is

$$G(t) = \tilde{C}_1 t^{-\frac{d_s}{2}} - \tilde{C}_2 t^{-\frac{d_s}{2}-2\beta}, \tag{2.23}$$

and the leading asymptotic in 3d is of the same type is in 2d case discussed by **?**.

Analysing the long time asymptotic of the FCS curve allows one to check whether the diffusion takes place on a fractal substrate or not. To do so, it is enough to fit the tail of the FCS curve by a power law and check whether the power is $-3\alpha/2$, as discussed in (**?**). In the case it is, the substrate is non-fractal, which excludes all kinds of percolation models. In the case it is not, one obtains d_f. Looking at the difference in the exponents of the main scaling term and of the correction to scaling (i.e. the sub-leading term) one obtains β, and has another test for Gaussianity, now in the vicinity of the peak of the distribution.

Note that the leading asymptotics of the short-time behaviour is

$$1 - G(t) \simeq t^\alpha$$

and the long time asymptotics in the non-fractal case is

$$G(t) \simeq t^{-3\alpha/2}.$$

As an exemplary study of Eq.2.23, we calculated the FCS curves for two different systems, one being a fractal system and the other being a diffusion in homogeneous system. For the non-fractal system, the example with $\beta = 1$ from Sec. 2.3 is used. For the fractal system, the propagator proposed by O'Shaughnessy and Procaccia (**?**),

$$P(r,t) = \frac{r^{d_f-d}}{t^{\frac{d_s}{2}}} \exp\left(-\frac{r^{d_w}}{t}\right) \tag{2.24}$$

mimicking the behaviour of diffusion on percolation clusters, is used.

Fig. 2.2 shows the calculated FCS curves for the fBm together with the percolation model. Both models were adjusted to have the same MSD and the exponent of anomalous diffusion being unity and 0.53, respectively. For adjusting the exponent of anomalous diffusion in percolation model, we used the discussion in sec.1.3.2 and set the walk dimension d_w, to be 3.77 and the spectral dimension d_s, to 1.33 and the fractal dimension is then calculated using Eq.1.7. As observed, the curves are very similar to each other and the standard fit hardly gives us information about the underlying processes. Note that the exponent of anomalous reproduced from the standard fit procedure is not the only parameter which may be incorrectly estimated. The diffusion coefficient also deviate strongly from the assumed one for the non-Gaussian PDF, however, we focus here only on the exponent of anomalous diffusion as the parameter of choice for our analysis.

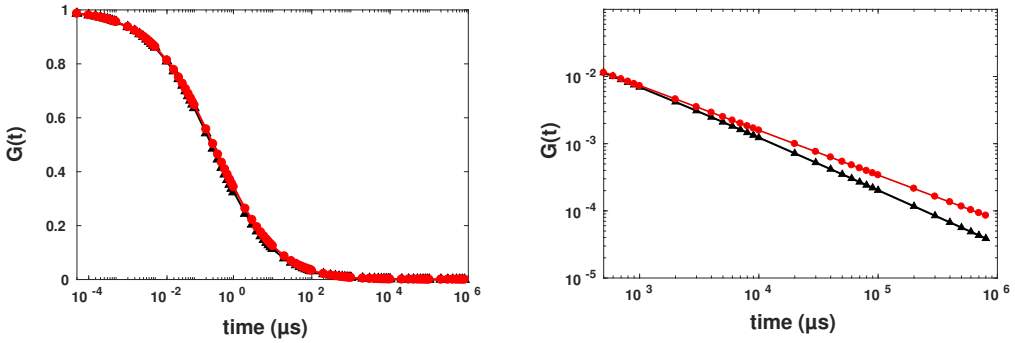

Figure 2.2. Numerically calculated FCS curves for fBm (black) and percolation (red) fitted to formula for anomalous diffusion (left). Linear fits to the end of curves for fBm and percolation in log-log scale (right).

Analysing the long time asymptotic of the same FCS curves, unravels the observable difference between two curves. Contrary to the FCS curve for the fBm model, the fitted curve to the data for the case of percolation model shows an extreme deviation in long asymptotic which in natural scale is not observed (not shown). Then long time asymptotic of the data (< 0.1) were fitted to a linear equation. The slope of long time asymptotic in FCS curves corresponds to $-3\alpha/2$ and $d_s/2$ for fBm and percolation models. This difference between slopes obtained from the fitting the body of the curve and from the long time asymptotic is a robust indication of non-Gaussianity of PDF. Results of the standard and long time asymptotic fits are given in Tab.2.2.

Another easy graphical way to grasp the fractality is to make a plot as shown in Fig.2.3. For this, one identifies the crossover time t_c from the FCS curves as the

Table 2.2. Results of fitting the FCS Curves shown in Fig.2.2 to anomalous diffusion formula leading to apparent α values and linear fits to the ends of FCS curves leading to different slopes. Data are shown as fit values and errors of fit)

PDF	*apparent* α_{eff}	*value of slope*
fBm	0.5334 ± 0.0001	-0.792 ± 0.001
percolation	0.5447 ± 0.0002	-0.665 ± 0.0002

time at which $G(t) = 1/2$ and plots $f_1(t) = \log[1 - G(t)]$ vs. $\log(t/t_c)$ for $t < t_c$ and $f_2(t) = (2/3)\log G(t)$ vs. $\log(t_c/t)$ for $t > t_c$ on the same plot. If the two curves get parallel at large negative values of abscissa, the substrate is non-fractal. If they are not parallel, one has to assume the fractality of the substrate. In real experimental data, however, this method is not perfectly applied due to the systematic errors in long time asymptotic.

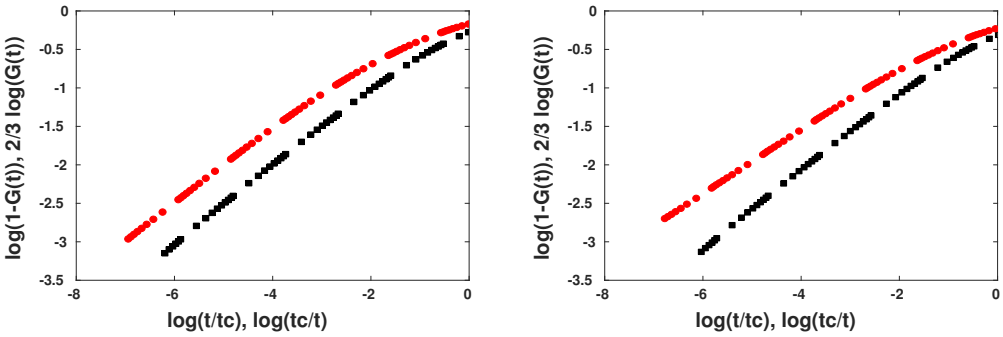

Figure 2.3. The comparison of the short-time asymptotic (red) and long time asymptotic (black) for the case of a non-fractal fBm model (left panel) and percolation model (right panel). In the non-fractal model the two curves run parallel in the asymptotic domain, while for the fractal one they show different slopes.

Generally, to obtain a robust data concerning the autocorrelation functions for long time lags, one needs to perform the measurement very long to obtain enough statistics. This is normally not the case in typical FCS measurements and especially in biological systems, the measurement is strictly limited due to destructive aspect of laser light on the sample. Beside this statistical error concerning the measurement time, there exists another type of noise which happens to appear in the long lag times, termed as "particle noise". The behaviour of this noise is dependent on the number of particles which cross through the confocal volume during large dwell

times. The advantage of the short time analysis to the long time is essentially arising from this point. Contrary to the long time noise, The noise at the beginning of the curves are simpler. Although the fact that shot noise in short times is disturbing and the noise is heteroscedastic, from time dependency view of the noise amplitude on the time, it is symmetric. Thus, such symmetric noise may influence the accuracy of fit and impose larger errors, but it does not change the nature of the results. Furthermore, for short lag times in typical FCS measurement time, there would be always enough statistic to obtain reliable results. Some comprehensive statistical analysis of the FCS technique may be found in literature by **??** and **?**.

2.6 Experimental Applications

Based on our theoretical findings in the previous sections, we proceed to develop a protocol for analysing the FCS curves in order to stablish a method for experimental applications. Before applying the method to experimental data, we introduce a simple form of equations and approaches for the short time and Gaussianity analysis. Starting from Eq.2.21, and assuming the scaling form of PDF, which has been discussed in sec.2.4, we suppose that $M_2(t) = b_2 t^\alpha$ and $M_4 = b_4 t^{2\alpha}$. In this case, the FCS curve, $G(t)$, at short times can be approximated by a polynomial in t^α, i.e

$$G(\tau) = 1 + c_2 t^\alpha + c_4 t^{2\alpha} + ... \tag{2.25}$$

where the prefactors read as $c_2 = a_2 {r_0}^{-2} b_2$ and $c_4 = a_4 {r_0}^{-4} b_4$. Fitting this expression to the experimental data at short times, one can essentially obtain the robust exponent and diffusion coefficient of anomalous diffusion. A simple estimation using numerical calculation of FCS curve and Eq.2.25 indicates that these three terms in the asymptotic form are enough to fit the FCS data to the point that it drops to 0.8 of its value in time zero(i.e. unity in n normalized form).

This allows to obtain the reduced kurtosis (non-Gaussianity parameter) of the displacement's PDF, i.e. the ratio of its fourth and its squared second moment:

$$\beta_2 = \frac{3M_4}{5M_2^2} - 1 = \frac{3b_4}{5b_2^2} - 1 = \frac{3c_4 a_2^2}{5c_2^2 a_4} - 1 \tag{2.26}$$

which for the three-dimensional Gaussian distribution has to be zero. The considerable deviation of K from this value (outside of the error bars) is a strong witness against the Gaussian diffusion model. If Gaussianity can not be rejected, there is a stronger reason to use the standard fit, Eq.(2.5), which may then refine the value of α. The coincidence of the two estimates, the asymptotic one and the one from the parametric fit, may indeed be considered as the proof of the Gaussian nature of the diffusion process.

Fitting the Eq.2.25 to the data may be done in two different ways which we tested

both methods on our own data described below and on the data courteously made available by Prof. Matthias Weiss at the University of Bayreuth (not shown).

The first approach to analyse the short time asymptotic, which is more convenient, is to cut the initial part of the curve $1 - G(t)$ down to 0.2 and fit it to the equation below at once

$$1 - G(t) = -c_2 t^{\alpha} - c_4 t^{2\alpha} \, . \tag{2.27}$$

This three parameter fit leads to the results with respectively large errors for the moments but the values for the exponent of anomalous diffusion and moments are equal to the one obtained from the first approach. In case that FCS curves are not smooth enough to get a reliable result for the anomalous exponent from the range of 0 to 0.1, one can perform the three parameter fit and then, by fixing it in the equation and perform a new two parameters fit for moments to get more accurate results.

The second approach which suits the data with high data to noise ration and provides robust results is as follows: one first performs the fit of $1 - G(t)$ vs. $-c_2 t^{\alpha}$ to obtain α from the asymptotic slope of the curve (0 to 0.1), then one substitutes $\tau = t^{\alpha}$ into Eq. (2.27), and performs statistically *linear* fit to a polynomial $G(\tau) = 1 + c_2\tau + c_4\tau^2$. Using this approach, one could also, in principle, investigate the scaling of the moments. In what follows, we show how does our proposed protocol perform for the analysis of real data. Then we compare the results from two different approaches and show that the difference only appears to be in the size of errors and not in the values themselves.

To obtain the experimental data, we performed a set of experiments on diffusion of the organic fluorescent dye, Atto655, in artificial crowded solutions and in living cells and estimated α and Gaussianity for these different systems, see the experimental details for the in Appendix A.1. The reason for using Atto655 in the experimental verification of our findings is that, this dye exhibits negligible isomerization or triplet kinetics at short time lags, see Fig.5 of (**?**), so that the photophysics of the tracer (not taken into account in our theoretical analysis) can be neglected.

For in-vitro systems, We performed six sets of experiments and obtained FCS curves of for Att0655 in water, water crowded by 44% and 66% Polyethylene glycol (PEG1500), in water with 30% dextran and in water with 75% sucrose. The experiment for PEG 66% repeated after 2 months and termed as 66%PEG-old. The acquisition time for each FCS curve was 10 minutes. In order to obtain parameters r_0 and s entering the apparatus function, we performed a calibration experiment with Atto655 diffusion in water at 293.15 K where the diffusion is normal and the diffusion coefficient is known: $D = 392\mu\text{m}^2/\text{s}$ (**?**). Calibration leads to the values of parameters $r_0 = (0.260 \pm 0.006)\mu m$ and $s = 6.3 \pm 0.1$, which corresponds to the values of $a_2 = 0.675$ and $a_4 = 0.271$.

Fig.2.4 shows the FCS results for the corresponding experiments. The curves were

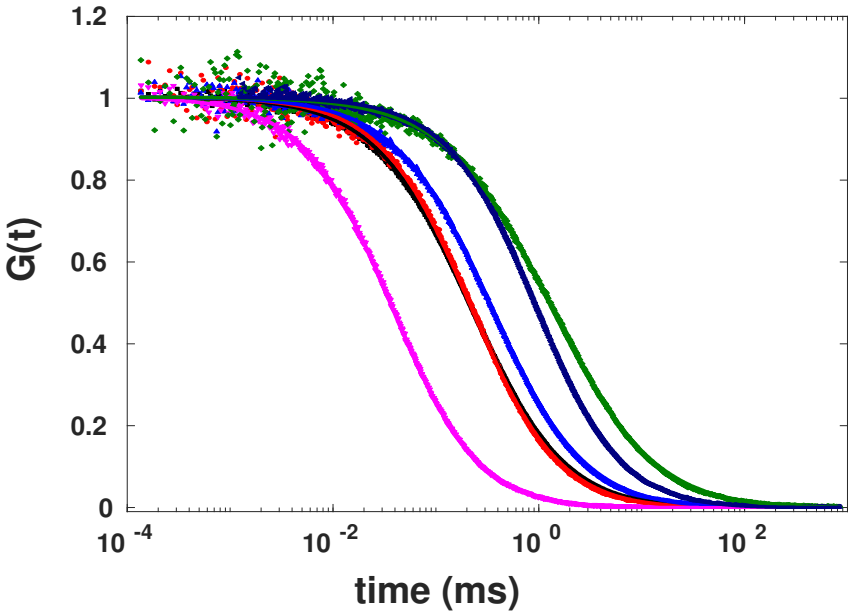

Figure 2.4. FCS curves for six in vitro systems: Atto655 in water(pink), 75% sucrose (black), 30% dextran (red), 44% PEG (dark blue), 66% PEG (dark blue) and 66% PEG-old (green) (from left to right) with data acquisition time of 10 min, fitted by Eq.(2.4).

first normalized and then transformed to the following analysis. The obtained FCS curves were fitted first to Eq.2.4. This led to the exponent of anomalous diffusion being $\alpha = 0.997 \pm 0.001$, $\alpha = 0.937 \pm 0.001$, $\alpha = 0.973 \pm 0.003$, $\alpha = 0.921 \pm 0.001$, $\alpha = 0.843 \pm 0.003$ and $\alpha = 1.000 \pm 0.001$ for water, 75% sucrose, 30% dextran, 44% PEG, 66% PEG and 66%PEG-old, respectively. These results indicate that all experiments except pure water and 66%PEG-old are slightly sub-diffusive. The fit was performed using the built-in Levenberg-Marquardt algorithm by the OriginPro 9.2 software. The errors reported for α above, as well as all the errors in this chapter are the uncertainties of the fit parameters returned by the algorithm and calculated using using standard error propagation method. these errors correspond to the data from a single experiments and do not represent the scattering of the values from different preparations.

Let us now return to the short time analysis. We initially use the first approach (three parameter fit) to investigate the exponent of anomalous diffusion. Table 2.3 represents the summary of the results for the short-time fits (denoted by α) for the data shown in Fig.2.5 together with the results of fitting the full FCS curves to

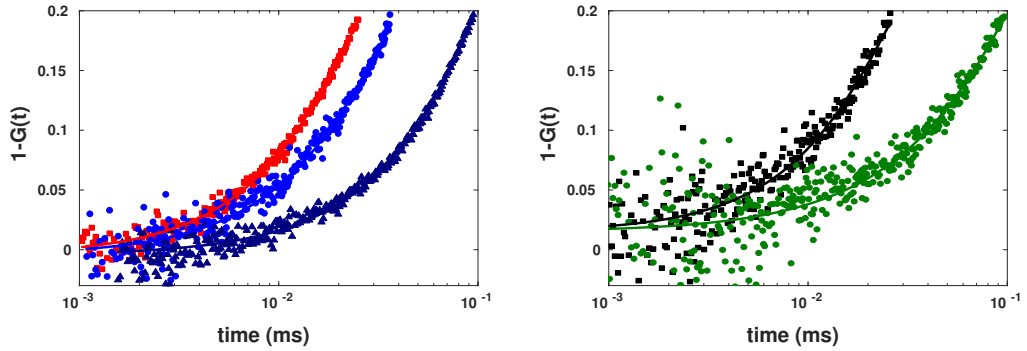

Figure 2.5. $1 - G(t)$ for Atto655 in water (right) crowded by 66% PEG-old , 44% PEG, and 75% sucrose from right to left and (left) for 66% PEG and 30% dextran, from right to left, fitted fitted to $1 - G(\tau) = -c_2 t^{\alpha} - c_4 t^{\alpha}$.

Eq.(2.4) (denoted by $\alpha_{\mathrm{Eq.(2)}}$).

Table 2.3. The results of fits for systems shown in Fig. 2.5

Medium	$\alpha_{\mathrm{Eq.(2)}}$	α	K
75% sucrose	0.937	0.94 ± 0.01	-0.011 ± 0.004
30% dextran	0.973	0.97 ± 0.06	-0.01 ± 0.02
44% PEG	0.921	0.92 ± 0.03	-0.03 ± 0.02
66% PEG	0.843	0.80 ± 0.07	-0.24 ± 0.36
66% PEG-old	1.000	0.89 ± 0.02	-0.33 ± 0.12

The uncertainties of the values of $\alpha_{\mathrm{Eq.(2)}}$ are smaller than the last reported digit. The results of standard fitting procedure and of the short-time fitting coincide within the error bars for 75% sucrose, 30% dextran, and 44% PEG and for 66% PEG. At the same time the deviations of the reduced kurtosis values from zero are either small or statistically insignificant. On the other hand, the results for 66% PEG-old differ considerably. The corresponding value of K indicates at the same time a strong deviation of the propagator's form from a Gaussian. The standard fit for this case has to be considered as unreliable. The analysis of the long-time of the curves for 66% PEG and 66% PEG-old, see Fig.2.6, indicates that none of the systems considered is fractal: all are fitted sufficiently well by a power-law $G(t) \propto t^{-3\alpha/2}$.

Cutting the beginning of the curves, Fig.2.7 shows that, we have two different qualities of data. These different qualities may arise from different count rate of

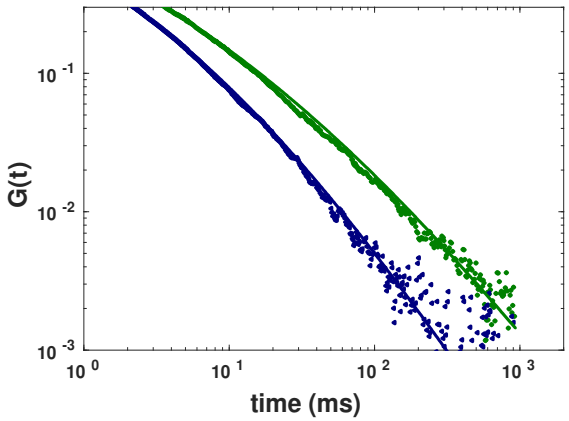

Figure 2.6. Long time asymptotic of FCS curves corresponding to 66% PEG (dark blue) and 66% PEG-old (green) together with their fit to Eq.2.4. Considerable deviations between fits and curves are not seen. This indicate no fractal property of the substrates.

photons recorded by detectors stemming from different transparency of media which leads to have less data in the measuring time. we note that measurement time can not be extended unlimited due to evaporation of solution for in-vitro solution samples which may cause the change of concentration of dye. However, the second strategy of the data fitting was applied to the short times of the FCS curves. Fitting the beginning of the curves gives us the characteristic values of α which differ only slightly from the ones obtained by fitting the full curve for the cases of 75% sucrose , 30% dextran and 44% PEG. This remarkably differs for the case of 66% PEG-old and 66% PEG. Comparing the results from both ways of fitting shown in table.2.4 is direct proof for effectiveness of the first method which is convenient to perform. This practically indicates the robustness of the estimation of α by a our proposed method in competition to the general fit model.

The observed relatively non-Gaussian PDF for diffusion in 66% PEG and 66% old PEG can be due to high concentration of PEG1500 crowding molecules which is close to it's solubility in water. Although the non-Gaussianity parameters observed in these systems are relatively small compared to what has been reported by **?** for simulation results of diffusion on percolating clusters, it is still interesting. Considering the fact that the long time fitting of these systems showed no fractality, percolation is no longer a proper model to explain this observed behaviour. this chapter was In next chapter, we will come back to this phenomenon and investigate the proper model that can potentially exhibit such behaviour.

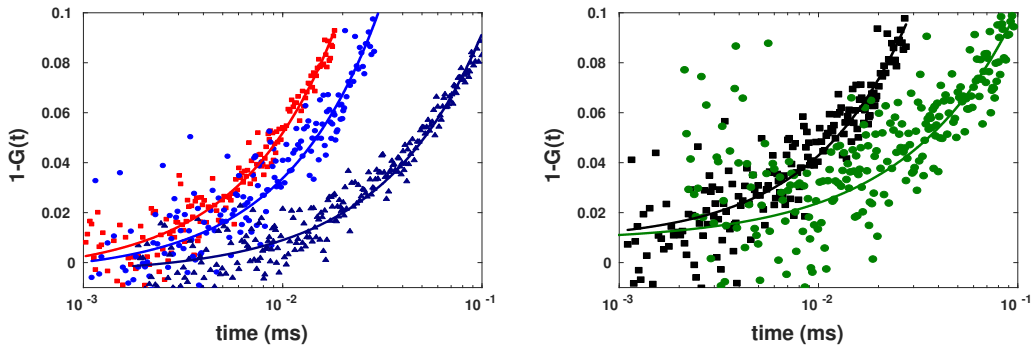

Figure 2.7. $1 - NG(t)$ for Att0655 in water (left) crowded by PEG 66% old, PEG 44% and sucrose 75% from right to left and (right)PEG 66% , dextran 30% from right to left both fitted to $c_2 t^{\alpha}$.

Table 2.4. Fit results for FCS curves obtained from Atto655 diffusion in artificial crowed systems with two different fitting approaches. For details see the text.

Medium	α	c_2	c_4	K
75% sucrose	0.94 ± 0.01	-4.62 ± 0.40	21.11 ± 5.2	-0.011 ± 0.004
	0.94 ± 0.02	-4.61 ± 0.04	21.01 ± 1.03	-0.011 ± 0.002
30% dextran	0.97 ± 0.06	-4.42 ± 1.30	19.32 ± 16.34	-0.012 ± 0.017
	0.97 ± 0.07	-4.41 ± 0.15	19.24 ± 3.71	-0.012 ± 0.005
44% PEG	0.92 ± 0.03	-2.72 ± 0.38	7.61 ± 3.03	-0.03 ± 0.02
	0.92 ± 0.04	-2.75 ± 0.05	7.8 ± 0.73	-0.03 ± 0.01
66% PEG	0.80 ± 0.07	-0.68 ± 0.17	0.36 ± 0.4	-0.24 ± 0.39
	0.80 ± 0.08	-0.68 ± 0.03	0.35 ± 0.1	-0.24 ± 0.13
66% PEG-old	0.89 ± 0.02	-0.79 ± 0.05	0.42 ± 0.1	-0.32 ± 0.12
	0.89 ± 0.02	-0.80 ± 0.01	0.43 ± 0.04	-0.33 ± 0.09

2.7 In Living Cell Experiment

After successful evaluation of our introduced method for FCS data analysis in artificial crowding materials, we attempted to apply this method to exemplary FCS data from living cells. The aim here was to investigate the Gaussianity of diffusing particle's PDF in such media. The experimental details concerning the preparation of cells and the injection process of dye is given in Appendix A.1. An exemplary bright-field image corresponding to this injection procedure is given in Fig.2.8.

Before injection, selected salivary gland ducts were excited at 635 nm and the fluorescence lifetime histogram as well as the overall fluorescence decay curve of the

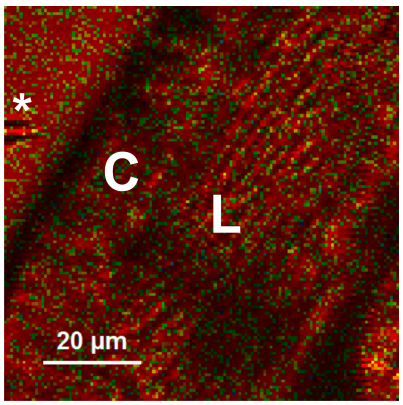

Figure 2.8. Bright field picture of salivary duct with duct cell. (C) and (L) indicate the duct cell and duct Lumen, respectively, as well as the microscopic tip (asterisk).

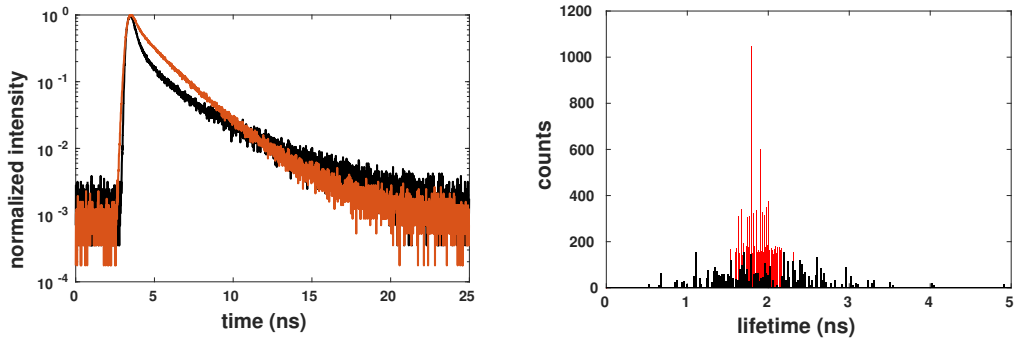

Figure 2.9. Normalized fluorescence decay curves (left) and fluorescence lifetime histograms (right) calculated from all pixels of an acquired time-resolved fluorescence images (80μm*80μm; 150 pixel*150 pixel; pixel dwell time 0.7 ms/pixel) of a selected salivary gland duct before (black) and after Atto655-injection (red).

cellular autofluorescence were recorded. To check the impact of autofluorescence in live cell FCS, FCS curves were measured for short (100 s) and long (800 s) recording times. After injection of Atto655 into one cell of the selected duct region, the measurements were repeated in order to compare it to the autofluorescence data Analysis of fluorescence lifetime histograms and fluorescence decay curves before and after injection confirmed the successful dye-injection. A retarded fluorescence decay behaviour and a shift in the fluorescence lifetime histogram could be observed after Atto655-injection. Fig.2.9 represent the data corresponding to these analysis.

Fig.2.10 shows the recorded FCS curves from the selected salivary gland duct cell

before and after dye-injection. FCS curves of cellular autofluorescence have been recorded for 100 s and 800 s (two lower red and blue data). At short recording time, autofluorescence could not be correlated and therefore FCS measurements after dye-injection was not significantly disturbed by the cellular background when applying 100 s recording time. An increased FCS data acquisition time of 800 s (in another similar cell) resulted in a slowly diffusing increment, which could be correlated and lead to autocorrelation. The amplitude of this autocorrelation, however, could be neglected in comparison to that obtained after dye-injection. When using only the beginning part of the autocorrelation curve for analysis, autofluorescence could be still neglected because of its low amplitude and large diffusion time. Therefore, in worst scenario, the autofluorescence contribution would only be a upper shift in the dye-related correlation curve. This essentially leads to an underestimated number of particles contributing to the correlation function but still does not disturb our analysis. In other words, since in our proposed model of FCS data analysis, we do not include the whole correlation curve, influences of any background and other errors can be further minimized.

To measure the intracellular diffusion behaviour after Atto655-injection, we kept the intensity of excitation laser low such that slight changes in the intensity of laser did not influence the behaviour of FCS curves due to photo-bleaching of Atto655. Fitting the whole FCS curve obtained after injection of dye to the standard formula for anomalous diffusion 2.4 , an anomalous diffusion exponent $\alpha = 0.58$ was determined. This extreme anomaly was also observed in other biological measurements with FCS and other single molecule techniques, (**???**) and (**??**). This slowness of diffusion in biological is essentially one of the secrets of the life. This not only leads to increasing the probability of eventually finding the target molecule by the diffusing element, but also provides a long search time (**?**).

To do answer the reliability of the α obtained from the standard fit method and concequently investigating the Gaussianiy of the PDF , we performed again the short time analysis. Analysis of the beginning part of the FCS curve by applying our proposed model resulted in the same anomalous diffusion exponent value, 0.58. In addition, two and three parameter fits resulted in $c_2 = 2.23 \pm 0.16$ and $c_4 = 4.81 \pm 1.6$. Using c_2 and c_4 the corresponding non-Gaussianity parameter could be calculated to -0.03 ± 0.01. This expresses that the behaviour of particle's displacement has a behaviour close to the Gaussian on. The reasoning behind this observation could be somewhat connected to the size of diffusing molecule. In fact, the small size of Atto655 in comparison to intracellular distances between sub-cellular structures may allows for performing diffusion in a visco-elastic like medium. Thus the extreme sub-diffusion behaviour, may appear without experiencing many hits from crowding increments inside cell during the data acquisition time. The results however, may differ from one to another cell type or when for instance a fluorescent marker of larger size is applied in the FCS measurements.

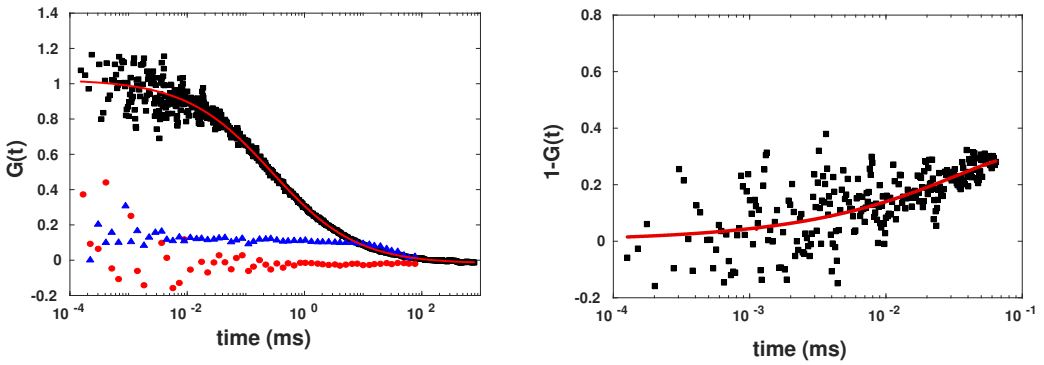

Figure 2.10. (left) Normalized FCS autocorrelation curves obtained from selected salivary gland duct cells before (red: $100\ s$ recording time; blue: $800\ s$ recording time) and after Atto655-injection (black: 100 s recording time). Black FCS curve was fitted to the equation of anomalous diffusion (Eq.2.5). (right) The beginning part of the FCS curve after Atto655-injection fitted to $1 - NG(\tau) = -c_2 t^{\alpha} - c_4 t^{\alpha}$.

2.8 Summary

We discussed the nature of data obtained in FCS in application to the situations showing anomalous translational diffusion. The FCS data are very similar to each other and extraction of data from these curves is a hard task. The standard approach assumes a Gaussian PDF of particle displacement and takes a closed formula to fit to the the FCS curves to obtain information such exponent and diffusion coefficient of anomalous diffusion. In our theoretical and numerical study of FCS technique, we showed that this simple fitting is not the best way to acquire information from FCS technique. We first demonstrated that the standard fitting procedure may lead to unreliable estimates for the exponent of the anomalous diffusion. This is because the precise form of the FCS curves strongly depends on the higher moments of the particle's displacement PDF. Therefore it is extremely sensitive to the departures from Gaussianity. Thus one had to develop a new strategy to obtain a better estimation of parameters from FCS data.

Then, we discussed that FCS curves contain a lot of valuable information about the diffusion process and its substrate. We showed that the exponent α of anomalous diffusion may be reliably estimated from the asymptotic fit at short times. The short time analysis also provides the possibility to obtain several lower moments. Using the second and fourth moment of the PDF at short times, one can develop a test for the Gaussian nature of the diffusive process. Another possibility to check the Gaussianity of the PDF is comparing the results for α obtained from short time and standard fit. If these two coincide one can assume the Gaussianity of

the PDF and also rely on the data from the standard method. Another piece of information concerning the fractality of the substrate is also hidden in the long time asymptotic of the data. Comparison of short- and long time behaviour allows for decision whether the diffusion takes place on a fractal substrate or not. All these developments in the theory of ordinary FCS technique was studied in the numerical level and furthermore, we showed how the methods discussed work in application to experimental data as well as living cells.

3 Fluorescence correlation spectroscopy in equilibrium

In the previous chapter, we introduced a general method to analysis the FCS curves using the short and long time asymptotics. Analysing the anomalous diffusion in in-vitro systems, we observed a very interesting phenomenon for the diffusion of Atto dyes in a fairly simple solution of water crowded by high concentration of crowding material, PEG1500 molecules. While the fit of the body and long time asymptotic of corresponding FCS curve showed a normal diffusion behaviour, a considerable sub-diffusion was observed in the short time asymptotic. With this we concluded that the form of the PDF in this experiment changes in course of time, it does not scale. This was in contrary to the expected normal diffusion where the PDF of particles displacement follows a Gaussian distribution which obeys the standard diffusion equation (second Fick's law). Such type of interesting phenomena which are termed as "anomalous yet Brownian" processes, have garbed our attention to investigate using the FCS technique.

Aside from our experimental observation of such phenomenon using novel analysis of FCS technique, recently, in some simulations and in experiments - using single particle tracking (SPT) (**?**), such a normal diffusion behaviour $\delta r^2 \propto t$ has also been observed together with non-Gaussian PDFs. Diffusion of colloidal beads along linear phospholipid bilayer tubes and in biofilament network (**?**), enhanced tracer diffusion in suspensions of micro-organisms (**?**), diffusion in lipid membranes (**?**), liposomes in nematic solutions of aligned F-actin filaments (**?**), nanoparticles in hard-sphere colloidal suspensions (**?**) and colloidal hard discs in solid and hexatic phases (**?**) are of examples showing such property. In some of these situations the deviation from Gaussian form is significant only at short times, while at longer times the PDF tends to the Gaussian form typical for the normal diffusion.

A theoretical model termed as "Diffusing Diffusivity" was introduced by **?**, can phenomenologically capture this observed behaviour. This model considers a "diffusivity memory" but no "directional memory " in the trajectory of the particles. By taking the distribution of diffusivities as an exponential form, they showed that PDF also decays as exponential with respect to the displacement in short times. Furthermore, they argued that other forms of the distribution of diffusivities may lead PDFS which are still well fitted to the exponential form. Another related model introduced by **?**, shows a very similar behaviour. This model exploits the diffusing

diffusivity idea of the previous one and considers a distribution of diffusivities which fluctuates in terms of time at times shorter than then diffusivity correlation time.

Demonstration of such phenomena in FCS technique is, essentially, the main task in this chapter. As we discussed in chapter 2, FCS is eligible to unravel the deviation of PDF from the Gaussian form (**?**). However, we discussed the analysis of FCS data assuming that PDF of displacement scales. This is the case in standard implementations of the methods as a whole, as it is for the normal diffusion, fBm model, and diffusion on percolation cluster. Therefore it is necessary to understand, what could be seen experimentally in the cases when the scaling is absent. The best way to proceed here is to consider, first, a simple model which to a large extent can be treated analytically. As such a model, we chose the CTRW scheme (**?**) with waiting time distribution given by a truncated power law.

Normally, in studying the CTRW the beginning of observation coincides with the first step of the walk process. However, in many experiments, especially in biological systems, the experiment is performed on a pre-existing system, or the techniques involve long data acquisition times. In this case the process at the beginning of observation is already strongly aged or even fully equilibrated. In this case the CTRW with a power-law waiting time distribution shows extremely slow diffusion, if any diffusion at all, while a CTRW with any waiting time PDF possessing the first moment (e.g. with a truncated power-law waiting time distribution) generically leads to normal diffusion in the entire time domain (**?**). However in this situation, the PDF of the particle's displacement may still be strongly non-Gaussian for time lags shorter than the truncation time, as is known for a long in mathematically similar econometric models (**?**). Such models can be proper candidates to explain the observed experimental results and may be useful to gain more information on systems showing such behaviour.

In what follows we discuss the corresponding model using an example of truncated one-sided Lévy stable PDF of waiting times, and concentrate mostly on the application of our results to fluorescence correlation spectroscopy. The FCS under ordinary CTRW process (as described by a fractional diffusion equation) was discussed in detail in Ref. (**?**). This process leads to anomalous diffusion in the whole time range and shows such exotic properties as aging and ergodicity breaking. In what follows, we discuss the same problem for a fully equilibrated CTRW model with a waiting time distribution following one-sided Lévy PDF with an exponential cut-off at long times. The model shows normal diffusion in the whole time domain, but the PDF of particles displacements shows a crossover from a non-Gaussian form at shorter times to a Gaussian asymptotic long-time behaviour, which is clearly seen in the behaviour of the fourth moment of the corresponding distribution. Then we calculate the FCS curves for such situation, and discuss how the information on this "anomalous yet Brownian" diffusion can be extracted from these curves, if at all.

In our examples we mostly consider the two-dimensional situation (diffusion in

a membrane), and use the dimensional units corresponding approximately to the parameter of the FCS apparatus used chapter 2. The results of this part of work are published in Physical Review E (**?**)

3.1 Equilibrated CTRW

The introduction to the CTRW model in the ordinary processes is given in the sec.1.3.1. Here we focus on the equilibrated CTRW where the starting point in not anymore the first step of the walker. We briefly review the ordinary CTRW method and pass to the equilibrated one which is a nice exactly solvable model of a stationary random process whose displacement's PDF is not scaling as a function of elapsed time. We first derive the lower moments of the model demonstrating the the normal diffusion in MSD and violation of scaling observed in fourth moment. We then define the reduced kurtosis using theses two moment. Next we obtain the PDF of displacement using subordination approach and exploit it to obtain the corresponding FCS curves. The analysis of the FCS curve are then done based on investigation of short and long time asymptotic compared to our results from chapter 2.

3.2 Moments of Displacements

In a CTRW a random walker performs instantaneous jumps choosing its displacement according to a probability density function $p(\mathbf{r})$ and waiting time between two jumps according to a PDF of waiting times $\psi(t)$. For the ordinary process, the PDF of particles displacement in Fourier-Laplace representation (i.e. the Laplace transform of the characteristic function of the displacements' distribution, $P(\mathbf{k},s) = \int_0^\infty \langle e^{-i\mathbf{kr}}\rangle e^{-st}dt$) obeys the Montroll-Weiss equation defined in Eq.1.5 as

$$P(\mathbf{k},s) = \frac{1-\psi(s)}{s}\frac{1}{1-\lambda(\mathbf{k})\psi(s)}. \tag{3.1}$$

Here $\lambda(\mathbf{k})$ is the characteristic function of displacements in a single step being the Fourier transform of $p(\mathbf{r})$, and $\psi(s)$ is the Laplace transform of waiting time PDF.

For the equilibrated CTRW, PDF has a slightly different form as:

$$P_1(\mathbf{k},s) = \frac{1-\psi_1(s)}{s} + \frac{1-\psi(s)}{s}\psi_1\frac{\lambda(\mathbf{k})}{1-\lambda(\mathbf{k})\psi(s)}, \tag{3.2}$$

where $\psi_1(s)$ is the Laplace transform of the forward waiting time for the first step after the beginning of the observation. The detailed derivation of the this formula is given in literature and in recently published book by (**?**). here we skipped the

derivation and only use the results for the further considerations. In our following discussions and simulations, we will concentrate on a two dimensional case and on the Gaussian distribution of step length, first, however, we will discuss the situation in some generality.

For the waiting time distribution, however, we will stick to a particular model waiting time PDF, namely to a one sided Lévy function with exponential cut off (tempered stable law (**?**))

$$\psi(t) = A \exp\left(-\frac{t}{t_c}\right) L_\alpha\left(\frac{t}{t_0}\right). \tag{3.3}$$

Here t_0 is a characteristic time scale of a jump, t_c is the cutoff time, and $A(t_0, t_c)$ is a normalization constant. In what follows we will put t_0 to unity (i.e. all times are now measured in units of t_0). In this case $A = \exp(t_c^{-\alpha})$. The Laplace transform of $\psi(t)$ then reads:

$$\psi(s) = \exp\left\{\left[-\left(s + \frac{1}{t_c}\right)^\alpha + \frac{1}{t_c^\alpha}\right]\right\}. \tag{3.4}$$

Exponential cut-off enforces the waiting time PDF to possess a mean which leads to establishing equilibrium at long times after process has started. In the case the waiting time PDF possesses a mean, the forward waiting time PDF in Laplace domain has a form (**?**)

$$\psi_1(s) = \frac{1 - \psi(s)}{s\tau}. \tag{3.5}$$

with τ being the mean waiting time and can be calculated from first derivative of waiting time PDF in Laplace domain

$$\tau = -\left.\frac{\partial \psi(s)}{\partial s}\right|_{s=0} = \alpha {t_c}^{\alpha-1} \tag{3.6}$$

Now Eq.(3.2) reads:

$$P_1(\mathbf{k}, s) = \frac{s\tau - 1 + \psi(s)}{s^2\tau} + \frac{[1 - \psi(s)]^2}{s^2\tau} \frac{\lambda(\mathbf{k})}{1 - \lambda(\mathbf{k})\psi(s)}. \tag{3.7}$$

Let us now return to the spatial part of the distribution. The characteristic function $p(\mathbf{k})$ of a probability distribution is the generating function of its moments. For an isotropic d-dimensional situation the Taylor expansion of $p(\mathbf{k})$ starts as (**?**):

$$p(\mathbf{k}) = 1 - \frac{k^2}{2d} m_2 + \frac{k^4}{8d(d+2)} m_4 + O(k^6) \tag{3.8}$$

where m_2 and m_4 are the second and the fourth moments of the distribution (the odd moments vanish due to symmetry). Applying this general expression to $\lambda(\mathbf{k})$

we get

$$\lambda(\mathbf{k}) = 1 - \frac{k^2}{2d}\langle l^2\rangle + \frac{k^4}{8d(d+2)}\langle l^4\rangle + O(k^6)$$

with $\langle l^2\rangle$ and $\langle l^4\rangle$ being the second and the fourth moment of the step length, respectively. Substituting this into Eq.(3.7) and expanding it in Taylor series in k we get:

$$P_1(\mathbf{k}, s) = \frac{1}{s} - \frac{k^2}{2d}\frac{\langle l^2\rangle}{s^2\tau} + \left[\frac{1}{4d^2}\frac{\psi(s)}{1-\psi(s)}\frac{1}{s^2\tau}\langle l^2\rangle^2 + \frac{1}{8d(d+2)}\frac{1}{s^2\tau}\langle l^4\rangle\right]k^4 + O(k^6).$$

Comparing this with the moment expansion, Eq.(3.8), which now reads

$$P_1(\mathbf{k}, s) = 1 - \frac{k^2}{2d}\delta r^2(s) + \frac{k^4}{8d(d+2)}\delta r^4(s) + O(k^6) \tag{3.9}$$

we get the expressions for the second and the fourth moments of the displacement in the Laplace domain, $\delta r^2(s)$ and $\delta r^4(s)$, which then can be transformed back to the time domain. In particular, we get that

$$\delta r^2(t) = \frac{\langle l^2\rangle}{s^2\tau}. \tag{3.10}$$

The second moment of PDF of distribution has a generic form and is independent of the particular form of the waiting time PDF (**?**). Its inverse Laplace transform grows linearly with time:

$$\delta r^2(t) = \frac{\langle l^2\rangle}{\tau}t. \tag{3.11}$$

The fourth moments is

$$\delta r^4(s) = \frac{\langle l^4\rangle}{s^2\tau} + \frac{2(d+2)}{d}\frac{1}{s^2\tau}\frac{\psi(s)}{1-\psi(s)}\langle l^2\rangle^2 \tag{3.12}$$

in the Laplace domain. Translating this back to the time domain gives different results for long times $t \gg t_c$ and for short times $1 \ll t \ll t_c$, corresponding to $s \ll 1/t_c$ and to $1/t_c \ll s \ll 1$ respectively (note that the non-universal domain $s \ll 1$ is of no interest here). In the long time domain $\psi \approx 1 - s\tau$ and therefore

$$\delta r^4(s) = \frac{\langle l^4\rangle}{s^2\tau} + \frac{2(d+2)}{d}\frac{1}{s^3\tau^2}\langle l^2\rangle^2$$

which translates into

$$\delta r^4(t) = \langle l^4 \rangle \frac{t}{\tau} + \frac{(d+2)}{d} \langle l^2 \rangle^2 \frac{t^2}{\tau^2} \tag{3.13}$$

and is dominated by the second term. For $1 \ll t \ll t_c$ we have $\psi(s) \approx 1 - s^\alpha$,

$$\delta r^4(s) = \frac{\langle l^4 \rangle}{s^2 \tau} + \frac{2(d+2)}{d} \frac{1}{s^{2+\alpha}\tau} \langle l^2 \rangle^2$$

which in the time domain translates into

$$\delta r^4(t) = \langle l^4 \rangle \frac{t}{\tau} + \frac{2(d+2)}{d\Gamma(2+\alpha)} \langle l^2 \rangle^2 \frac{t^{1+\alpha}}{\tau} \tag{3.14}$$

indicating strong non-Gaussianity of PFD of displacement in short times, and the absence of scaling of the distribution as a whole.

3.2.1 The Form of PDF

The Montroll-Weiss approach is a straightforward method to calculate the moments of the distribution, but is less convenient for obtaining the form of the PDF in the space-time domain, since it involves both the inverse Laplace and the inverse Fourier transforms which have to be performed numerically. One can exclude the Fourier transform when applying the subordination approach. The same approach will be used for direct calculation of the FCS autocorrelation curves, and therefore is discussed here in some detail. The PDF of displacement can be written as

$$P_1(\mathbf{r}, t) = \sum_{n=0}^{\infty} \chi_n(t) P(\mathbf{r}, n) \tag{3.15}$$

where $P(\mathbf{r}, n)$ is the PDF of particles displacements in a simple random walk after n steps, and $\chi_n(t)$ being the probability of taking exactly n steps up to the time t. The number of steps is the internal temporal variable of the subordination scheme (operational time).

For an aged or equilibrated CTRW the probability $\chi_0(t)$ of making no step from the starting point of measurement $t = 0$ till time t is given in the Laplace domain by

$$\chi_0(s) = \frac{1 - \psi_1(s)}{s},$$

and all other $\chi_n(s)$ are

$$\chi_n(s) = \psi_1(s)[\psi(s)]^{n-1} \frac{1 - \psi(s)}{s}.$$

In Laplace domain Eq.(3.15) transforms to

$$P_1(\mathbf{r},s) = \frac{1-\psi_1(s)}{s}\delta(r) + \psi_1(s)\frac{1-\psi(s)}{s}\sum_{n=1}^{\infty}[\psi(s)]^{n-1}P(\mathbf{r},n). \tag{3.16}$$

For n large the function $P(\mathbf{r},n)$ can be well approximated by a Gaussian

$$P(\mathbf{r},n) = \frac{1}{\pi\langle l^2\rangle n}\exp\left(-\frac{r^2}{\langle l^2\rangle n}\right). \tag{3.17}$$

Eq.(3.16) is then rewritten as follows: Each term in the sum is multiplied by $\psi(s)$, and the whole sum is then divided by the same function, and $\psi_1(s)$ is written in the explicit form given by Eq.(3.5). Now we obtain:

$$P_1(\mathbf{r},s) = \left[\frac{1}{s}-\frac{1-\psi(s)}{s^2\tau}\right]\delta(r) + \frac{[1-\psi(s)]^2}{s^2\tau\psi(s)}\sum_{n=1}^{\infty}[\psi(s)]^n P(\mathbf{r},n). \tag{3.18}$$

For $t \gg t_0$ the typical number of steps taken is large and n can be considered as a continuous variable, and the sum changed to the integral:

$$P_1(\mathbf{r},s) = \left[\frac{1}{s}-\frac{1-\psi(s)}{s^2\tau}\right]\delta(r) + \frac{[1-\psi(s)]^2}{s^2\tau\psi(s)}\int_0^{\infty}P(\mathbf{r},n)e^{n\ln\psi(s)}dn \tag{3.19}$$

The integration corresponds to the Laplace transform of $P(\mathbf{r},n)$ in its temporal variable n:

$$\int_0^{\infty}P(\mathbf{r},n)e^{n\ln\psi(s)}dn = \tilde{P}[\mathbf{r},-\ln\psi(s)].$$

Here and below the tilde denotes the Laplace transformed, when it is not evident from the variable used as the Laplace frequency, i.e. when it is not simply s. We note that typically one expands $-\ln\psi(s)$, but for the PDF given by Eq.(3.3) this logarithm is simpler than its expansion! Thus,

$$P_1(\mathbf{r},s) = \left[\frac{1}{s}-\frac{1-\psi(s)}{s^2\tau}\right]\delta(r) + \frac{[1-\psi(s)]^2}{s^2\tau\psi(s)}\tilde{P}[\mathbf{r},-\ln\psi(s)]. \tag{3.20}$$

Taking the Laplace transform of $P(\mathbf{r}, n)$, Eq.(3.17), explicitly, we get

$$P_1(\mathbf{r}, s) = \left[\frac{1}{s} - \frac{1-\psi(s)}{s^2\tau}\right]\delta(r) + \frac{[1-\psi(s)]^2}{s^2\psi(s)\tau}\frac{2}{\pi\langle l^2\rangle}K_0\left[2r\sqrt{\frac{-\ln\psi(s)}{\langle l^2\rangle}}\right] \tag{3.21}$$

with $K_0(z)$ being the modified Bessel function of the second kind. The numerical

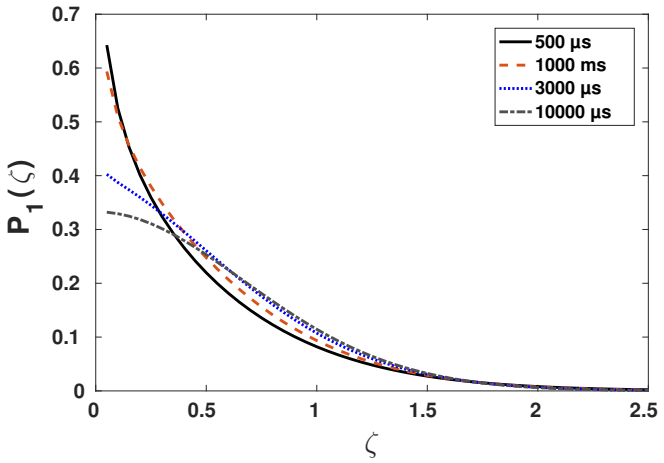

Figure 3.1. The probability density function of displacements as obtained by numerical inversion of Eq.3.22 for times t being 500, 1000, 3000 and 10000 μs with $t_c = 1000$ μs and $\alpha = 0.6$. See text for details.

inversion of this expression can be easily performed using the Gaver-Stehfest algorithm (**?**). The results for different times are shown in Fig.3.1. To compare the forms of the PDF for different times, we plot them as a function of a dimensionless variable $\zeta = \frac{r}{\sqrt{\delta r^2(t)}}$, which is the displacement normalized with respect to r.m.s. displacement. Fig. 3.1 shows the PDFs for times t being 500, 1000, 3000 and 10000 μs with $t_c = 1000$ μs and $\alpha = 0.6$ (the rapidly decaying δ-peak at zero is not shown).

The form of the distribution for $t < t_c$ (here $t = 500$ μs) is shown in Fig. 3.2. Analyzing the distribution at short times indicates that they possess an exponential tail (resembling the prediction of the diffusing diffusivity model) by higher peak. Similar behaviour has been found in many experimental works, mentioned in introduction, using sampling the PDF from SPT measurements.

As it could be concluded from Fig. 3.1, this distribution for short times is strongly

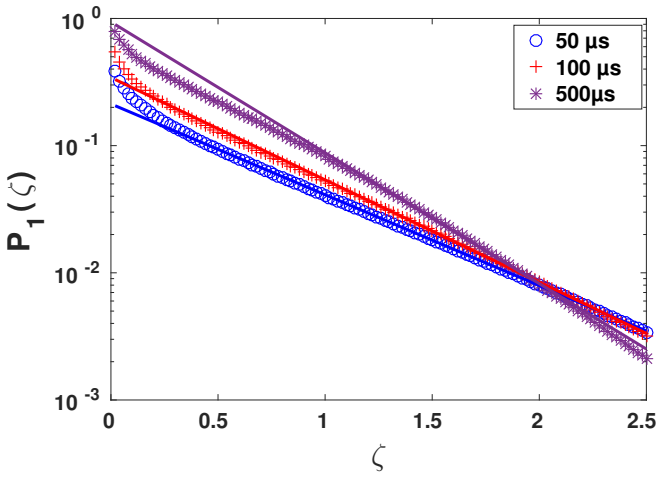

Figure 3.2. Probability density function of displacement for $t = 500\ \mu s$, $t = 100\ \mu s$ and $t = 50\ \mu s$ (symbols). Red lines show the exponential fit to the tail of the distributions ($\zeta > 0.5$) plotted in the whole ζ-domain.

peaked, and tends to a Gaussian at $t \gg t_c$.

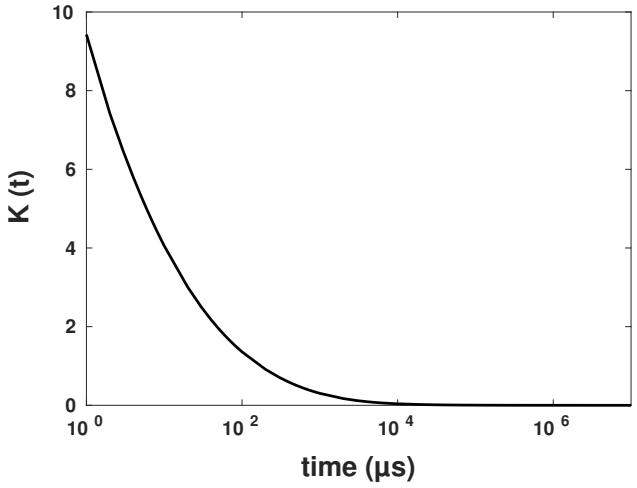

Figure 3.3. Non-Gaussianity parameter, Eq.3.22, as calculated using the previous result and Eq.3.11 for $t_c = 1000\ \mu s$ and $\alpha = 0.6$. Deviations from zero indicate strong non-Gaussianity; these vanish for vanishes for $t \gg t_c$.

The deviations from the Gaussian form of the distribution can be easily characterized when considering the reduced kurtosis (non-Gaussianity parameter)

$$K = \frac{d}{d+2}\frac{\delta r^4(t)}{\delta r^2(t)} - 1, \tag{3.22}$$

as following from Eqs. (3.10) and Eq.3.13 or Eq.3.14. At times $1 < t < t_c$ the second term in Eq.3.14 dominates unless the fourth moment in a single step displacement is exceedingly large. The distribution then is highly leptocurtic, and the non-Gaussianity decays essentially as $t^{\alpha-1}$. At long times, when Eq.3.13 is applicable and the result is dominated by its second term. The reduced kurtosis vanishes, indicating the transition to a Gaussian. This behaviour is clearly seen in Fig.3.3 which shows the non-Gaussianity parameter as a function of time as obtained by numerical Laplace inversion of Eq.3.12: Extreme strong deviations from Gaussianity at short times decay at times larger than the characteristic cut-off time t_c. Compare the value of the reduced kurtosis obtained in Fig.3.3 with the non-Gaussianity parameter, for example, for the 3-D Lorentz model reaching the maximum of $K = 3$ close to the percolation threshold (**?**).

We note that situations with slow convergence to Gaussian are known e.g. in truncated Lévy flight models (**??**) where the speed of convergence is governed by the Berry-Esseen theorem (**?**). In our case the situation is slightly different, since our process ist not the one with independent increments, but a more complicated subordinated construct. Eq.3.22 gives the possibility to assess numerically the speed of convergence.

3.3 Realization in Fluorescence Correlation Spectroscopy

Let us now discuss the consequences of the absence of scaling in PDF for the fluorescence correlation spectroscopy.

Generally FCS curve can be expressed via a single integral of the PDF of the absolute displacement, $P(r,t)$, and an apparatus function, $F(r)$, defining the laser intensity distribution in the detection volume, see sec.2.1:

$$G(t) = \int_0^\infty P(r,t)F(r)dr. \tag{3.23}$$

Assuming a Gaussian intensity distribution in the detection volume, the apparatus function in two dimensions reads

$$F(r) = 2\pi r \exp\left(-\frac{r^2}{r_0^2}\right). \tag{3.24}$$

with r_0 being the beam's waist. We note that $G(t)$, given by Eq.3.23, is a linear functional of $P(r,t)$ involving only the manipulation of spatial variables (weighted integration). Therefore, one can again use the subordination approach. Thus first pass to the Laplace domain, $G(s)$ via $P(r,s)$, and then perform the the numerical inversion to the time domain.

Let us calculate

$$G_1(s) = \int_0^\infty P_1(r,s)F(r)dr.$$

Substituting the series for $P_1(r,s)$ given by Eq.3.20 and performing term-by-term integration over spatial variables leads to the expression

$$\begin{aligned} G_1(s) = \quad & \frac{1}{s} - \frac{1-\psi(s)}{s^2\tau} \\ & + \frac{[1-\psi(s)]^2}{s^2\tau\psi(s)} \sum_{n=0}^{\infty} [\psi(s)]^n G(n) \end{aligned} \tag{3.25}$$

with $G(n)$ coinciding with the FCS curve for normal diffusion in the operational time:

$$G(n) = \left(\frac{\langle l^2 \rangle}{r_0^2} n + 1 \right)^{-1}.$$

Similar to the previous discussion, the summation corresponds to the Laplace transform of $G(n)$ in the changed Laplace variable:

$$\sum_{n=0}^{\infty} [\psi(s)]^n G(n) \approx \int_0^\infty G(n) e^{n \ln \psi(s)} dn = \tilde{G}[-\ln \psi(s)].$$

Replacing the explicit form of the Laplace transform of $G(n)$ we get

$$\begin{aligned} G_1(s) = \quad & \frac{1}{s} - \frac{1-\psi(s)}{s^2\tau} + \frac{[1-\psi(s)]^2}{s^2\psi(s)\tau} \frac{r_0^2}{\langle l^2 \rangle} \times \\ & \exp\left[-\frac{r_0^2 \ln \psi(s)}{\langle l^2 \rangle} \right] \Gamma\left[0, -\frac{r_0^2 \ln \psi(s)}{\langle l^2 \rangle} \right] \end{aligned} \tag{3.26}$$

with $\Gamma(a,z)$ being an incomplete Gamma function. The results of numerical inversion of this expression are shown in Fig. 3.4. Here we plot the results of numerical inversion of Eq.3.26 with the same Gaver-Stehfest algorithm (symbols) for t_c being 10, 100, 1000, 10000 and 100000 μs. The numerical FCS data points were fitted to a standard two-parametric expression

$$G(t) = \left(\frac{4D_\beta}{r_0^2} t^\beta + 1 \right)^{-1} \tag{3.27}$$

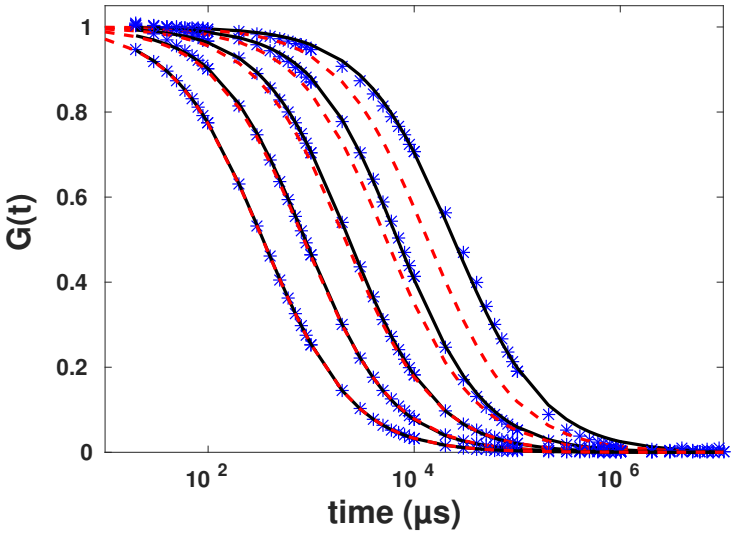

Figure 3.4. The FCS curves obtained by numerical Laplace inversion of Eq.3.26 (symbols) together with the FCS curves for normal diffusion with the corresponding diffusion coefficient (dashed lines) and their best fits to Eq.3.27 (full lines). The curves correspond to t_c being 10, 100, 1000,10000 and 100000 μs from left to right.

with free parameters β and D_β; the results of these fits are shown as full lines. In addition we plot the FCS curves which would be obtained for the case of normal diffusion

$$G(t) = \left(\frac{4D}{r_0^2}t + 1\right)^{-1} \tag{3.28}$$

with the terminal diffusion coefficient $D = \langle l^2 \rangle / 4\tau$. While for small t_c the differences between the inversion results and their fits from the normal diffusion curves is minor, they gets larger as t_c increases. At larger t_cs Fitting numerical FCS data to Eq.3.27 still indicates normal diffusion with $\beta = 1 \pm 0.03$, but with the diffusion coefficient D_1 which is considerably smaller than the terminal diffusion coefficient D. For example, for the largest $t_c = 10^5$ μs the terminal diffusion coefficient is $D = 0.0041$ while the one obtained by the fit is almost two times smaller: $D_{\text{fit}} = 0.0023$.

3.3.1 Exemplary Simulation

To check our theoretical predictions we also performed an exemplary lattice simulation of CTRW for the values of parameters used in our calculations. Simulations are done using the standard random walk on a square lattice with equal proba-

bility to jump to four nearest neighbours. Having arrived to a site particles were set to wait for a time chosen from waiting time according to Eq.3.3 with $t_0 = 1\mu s$ and $t_c = 1000\mu s$. The waiting times were generated using the acceptance-rejection method (**?**). The essence of this method is explained in Appendix A.5. First a random variable y distributed according to a Lévy law is generated. Then a random variable u uniformly distributed between 0 and 1 was generated. Waiting times meeting the condition, $\exp(-y/t_c) < u$, were accepted as actual waiting times, otherwise the trial was repeated. The size of the simulation box was taken to be $L = 300$ in each direction, with periodic boundary conditions. The lattice constant representing the step length was taken to be $1\mu m$. The confocal volume with $r_0 = 15\mu m$ was positioned in the center of box and intensities according to the distance of particles from the center of confocal volume were calculated at each step of simulation, $I_i = \exp(-r^2/r_0^2)$. The total number of particles was chosen such that their mean number within the confocal volume did not exceed unity. Simulation is run for 10^8 time steps. The results for these values of parameters are plotted in Fig. 3.5. This parameters chosen correspond to the middle curve (third from the left) from the previous Fig.3.4. This exemplary result shows the applicability of our semi-analytical

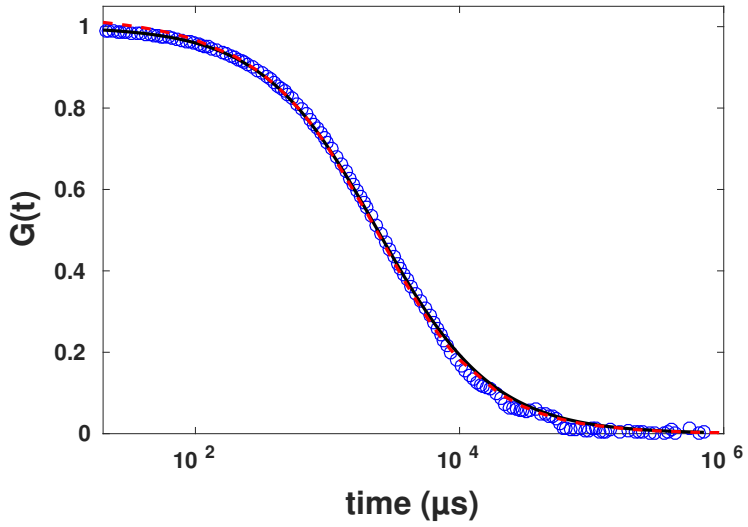

Figure 3.5. Simulated FCS curve (open circles) together with its fit to Eq.3.27 (full line, color online: black), and with the result of the numerical inversion of Eq.3.26 (dashed line, color online: red).

approach. The deviations at very short times are mainly caused by the lattice nature of the model used in simulations.

3.4 Asymptotic Behaviour

Let us now investigate the short and long time asymptotic of Eq.3.26 with respect to the characteristic time t_c. For $t \gg t_c$ ($s \ll 1/t_c$), $\psi(s)$ can be approximated by $\psi(s) \approx 1 - \tau s$ and $-\ln \psi(s) \approx \tau s$. Substituting this approximation into Eq.3.26 we see that the first two terms vanish, and the third term coincides with the Laplace transform of $G(n)$ with $n = t/\tau$. Therefore in this asymptotic domain

$$G_1(t) \sim \left(\frac{\langle l^2 \rangle}{\tau r_0^2} t + 1 \right)^{-1} \tag{3.29}$$

which is the normal diffusion with terminal diffusion coefficient $D = \langle l^2 \rangle / 4\tau$.

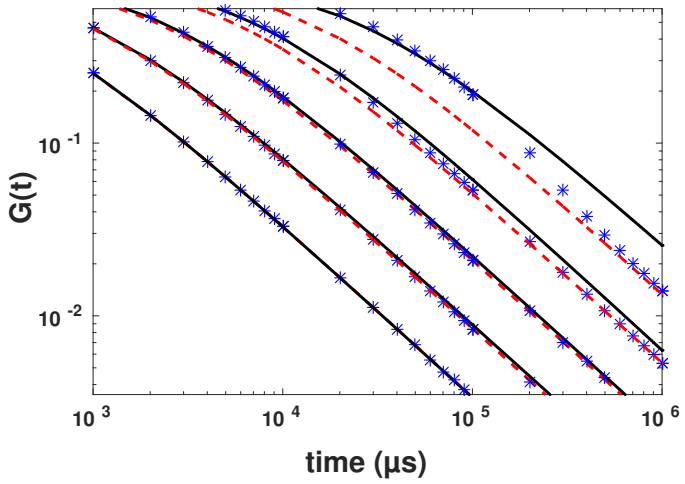

Figure 3.6. The FCS results from Eq.3.26 (stars) together with the FCS curves for normal diffusion with the terminal diffusion coefficient (dashed lines) and the fitted curves from Fig. 3.4 (full lines) at long times. The transition between the intermediate domain and the terminal asymptotic behavior is clearly see for larger t_c. The curves correspond to t_c being 10, 100, 1000,10000 and 100000 μs from left to right. Note the double logarithmic scales.

For short times, $t_0 \ll t \ll t_c$ ($1 \gg s \gg 1/t_c$), one has $\psi(s) \approx 1 - s^\alpha$ and $\ln \psi(s) \approx -s^\alpha$, and therefore Eq.3.26 reads as

$$G_1(s) \approx \frac{1}{s} - \frac{s^{\alpha-2}}{\tau} + \frac{s^{2\alpha-2}}{\tau} \int_0^\infty G(n) e^{-ns^\alpha} dn.$$

Expanding $G(n)$ as

$$G(n) \approx 1 + \frac{\langle l^2 \rangle}{{r_0}^2} n + \frac{\langle l^2 \rangle^2}{2{r_0}^4} n^2$$

and performing term-by-term integration one gets

$$G_1(s) \approx \frac{1}{s} - \frac{\langle l^2 \rangle}{\tau {r_0}^2} s^{-2} + \frac{\langle l^2 \rangle^2}{\tau {r_0}^4} s^{-\alpha-2}.$$

The inverse Laplace transform of the expression above reads:

$$G_1(t) \approx 1 - \frac{\langle l^2 \rangle}{\tau {r_0}^2} t + \frac{\langle l^2 \rangle^2}{\tau {r_0}^4} \frac{t^{1+\alpha}}{\Gamma(1+\alpha)}. \tag{3.30}$$

The same results for the short time asymptotic of FCS curve can be derived immediately from Eq.3.23 using the approach of (**?**). Expanding the apparatus function one gets

$$G(t) = 1 - \frac{\delta r^2(t)}{r_0^2} + \frac{\delta r^4(t)}{2 r_0^4} + \dots .$$

Using the explicit expressions for the moments and noting the the terms containing $\langle l^2 \rangle^2$ are negligible in the time window considered, namely for $t \gg t_0$, we again arrive at Eq.3.30. The corresponding behaviours are analyzed in Figs. 3.6 and 3.7.

Fig. 3.6 indicates the asymptotic transition of FCS data to Eq.3.29. This asymptotic behaviour is clearly seen in the last two set of data corresponding to $t_c = 10000\mu s$ and $100000\mu s$.

Expected behaviour for the short time asymptotic from Eq.3.30 is also observed in Fig. 3.7. The approximations we used to derive this equation are actually applicable for the large t_c in this figure, for the time window $t \ll t_c$ and $t \gg \tau$.

The conclusion is that the strongly non-Gaussian behaviour at short times, and the absence of scaling of the displacements' PDF as a whole may stay unnoticed in the FCS experiments, when these are analysed using the standard fit of the whole curve to the FCS data. Such a fit will hint onto normal diffusion, but deliver a wrong estimate for the diffusion coefficient. The deviation of data from the normal diffusion curves in the short and long time domain (i.e. asymptotic fitting) give us the way to spot normal, yet non-Gaussian behaviour and the lack of scaling. In experiment these deviations might be obscured by noise being strong exactly in these domains, and the short-time behaviour might be influenced by the photophysical properties of the dye. Therefore large statistics and careful data analysis are necessary for getting reliable conclusions.

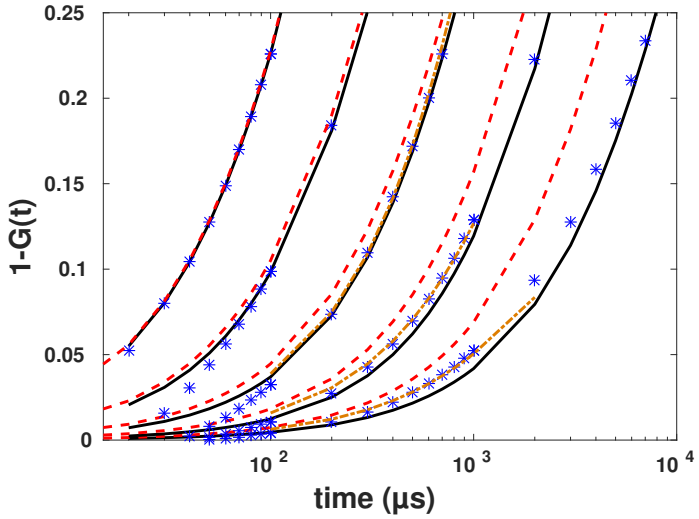

Figure 3.7. The FCS results from Eq.3.26 (stars) together with the FCS curves for normal diffusion with the terminal diffusion coefficient (dashed lines) and the fitted curves from Fig. 3.4 (full lines) at short times. The curves correspond to t_c being 10, 100, 1000, 10000 and 100000 μs from left to right. Curves corresponding to the theoretical approximation for the short times from Eq.3.30 are plotted as dotted lines for the time domain where the approximation is applicable.

3.5 Summary

In this chapter, we demonstrated the realization of "normal yet anomalous" processes in FCS technique, which normally was reported using SPT technique. This process is defined by its PDF which varies at time and therefore, does not scale. As an example of such non-scaling situation, we considered the CTRW of tracers with waiting time probability density function following a Lévy-stable law with exponential cut off (tempered stable law) in equilibrium in two dimensions. This is the case corresponding to the essentially normal diffusion, with the second moment of displacement growing linearly in time. The PDF of particles displacements is, however, strongly non-Gaussian at shorter times, and does not scale.

First, the first two even moments of the corresponding process were obtained analytically using the Montroll-Weiss equation. Then, using the sub-ordination approach, we obtained the exact form of PDF with such waiting time PDF. We derived the PDF of displacement in Laplace domain and used the numerical inversion to capture it in real time domain for different characteristic times. The characteristic time in waiting time PDF determines the time when the PDF tends to become Gaussian. Having the PDF at hand, we could proceed to obtain the corresponding FCS curves again for different characteristic times. An exemplary simulation of equilibrated

CRTW also corroborated the theoretical results. Then, to investigate the FCS curves, we studied their asymptotic behaviours as its importance was demonstrated in Chapter 2. The results showed that the deviations from Gaussian behaviour may be detected when analyzing the short- and long-time asymptotic behaviour of the corresponding curves. The bodies of the curves are still perfectly fitted by the fit forms obtained for normal diffusion. The diffusion coefficients obtained from these global fits may however differ considerably from the true tracer diffusion coefficient as describing the time-dependence of the mean squared displacement of the tracer.

4 Spot variation fluorescence correlation (SV-FCS) spectroscopy without spot variation

In this section, we focus on the spacial information which one can obtain about the diffusion propagator from an ordinary FCS measurement. As we have extensively discussed in chapter 2, one of the main difficulties of solving the inverse problem of finding the diffusion propagator is that, while the propagator is a function of two variables, coordinate and time, the measurement provides us a curve as a function of only one variable, time. The mathematical efforts of transferring the Eq.2.1 to a Laplace transform assuming a scaling form of the propagator, namely coupling between time and coordinate, also fail to work due to the ill-pose feature of the problem. This means that the presence of small noise in the data leads to extreme fluctuation in inverted form. Therefore, these considerations impose the necessity of inventing some tools to acquire some spacial information from FCS measurements not only to make a possibility to fully solve the inverse problem, but also to obtain indirect information about the structural organization of the medium in which diffusion takes place.

Different variations of the ordinary FCS method have been introduced to improve this deficiency of standard FCS method. Scanning FCS was developed to measure the point FCS in different points of the sample (**???**). In this method, the laser spot is driven along different lines or circles to calculate the autocorrelation functions, providing information on the concentration of tracers in the sample as well as their motion. This method is suitable for immobile (slowly diffusing) particles such that their lateral displacements may be ignored compared to the speed of laser spot. This method is easy to implement and the impact of moving laser spot may be included in the theoretical analysis. Multiple confocal spot is also another variation which simultaneously measures autocorrelation functions at different positions (**?**). This provides the possibility to investigate the mobility of different types of molecules with different colour labelling. A good description of these methods with their applicability in investigation of dynamics of the intracellular process may be found in literature (**?**)

Among many variations of the ordinary FCS technique, *Spot variation fluorescence correlation spectroscopy* (SV-FCS), is one the main variants which provides information about the local structure of the medium in the illumination spot. In

the SV-FCS, the size of confocal volume is tuned, and the autocorrelation functions for different sizes are then calculated. Although performing SV-FCS requires repetition of experiments for many times and is more involved, the set of obtained data from this technique includes spacial change as a parameter to the results of FCS measurements. This is, in theory, enough to obtain a complete information about the diffusion process in a medium and to fully obtain the full form of PDF in some situations. However, the noisy nature of the data is still disturbing and handling the special term as a well-controlled semi-continuous parameter is not realistically feasible. Therefore, the main idea behind SV-FCS is to use few changes in the size of the confocal volume in order to extrapolate the dependence of the particle's residence time on the illuminated spot size.

The framework of extracting information from SV-FCS was first introduced by Wawrezinieck (**?**), termed as diffusion law analysis. A schematic depiction of the diffusion law is given in Fig.4.1. Diffusion law in principle, exploits the relation between the residence time of the particle in the confocal volume and the spot size to predict the presence of nano-domains or nano-barriers in the medium in which diffusion takes place. Diffusion law studies a phenomenological relation as

$$\tau_d = t_0 + \frac{r_0^2}{4D_{eff}} \tag{4.1}$$

where τ_d and D_{eff} are diffusion time and effective diffusion coefficient. t_0 here is the off-set time which its sign determines the type of diffusion process as follows: The analysis of Wawrezinieck et al.(**?**) states that the existence of barriers in the confocal volume would lead to non-vanishing negative t_0, this is depicted in panel c in Fig.4.1. On the other hand, if there is a nano-domain in the confocal volume, in which the tracer molecule is trapped for longer times, one would expect positive t_0, panel b in Fig.4.1. Thus, the zero intercept, namely $t_0 = 0$, in this analysis is the proof for homogeneity of the system,panel a in Fig.4.1. Therefore, performing this analysis one could, in principle, obtain valuable information about the structural conformation of the system at the nano scale.

Experimentally, different methods were applied to continuously vary the size of confocal volume, each having specific advantages and disadvantages. In our novel proposed method for SV-FCS, we show that the same results can be obtained by post-processing the photon count data from ordinary FCS measurements. By using this method, one obtains the fluorescence autocorrelation functions for sizes of confocal volume, which are effectively smaller than that of the initial FCS measurement. The photon counts of the initial experiment are first transformed into a smooth intensity trace using kernel smoothing method or to a piecewise-continuous intensity trace using binning. Then a non-linear transformation is applied to this trace. The result of this transformation mimics the photon count rate in an experiment which

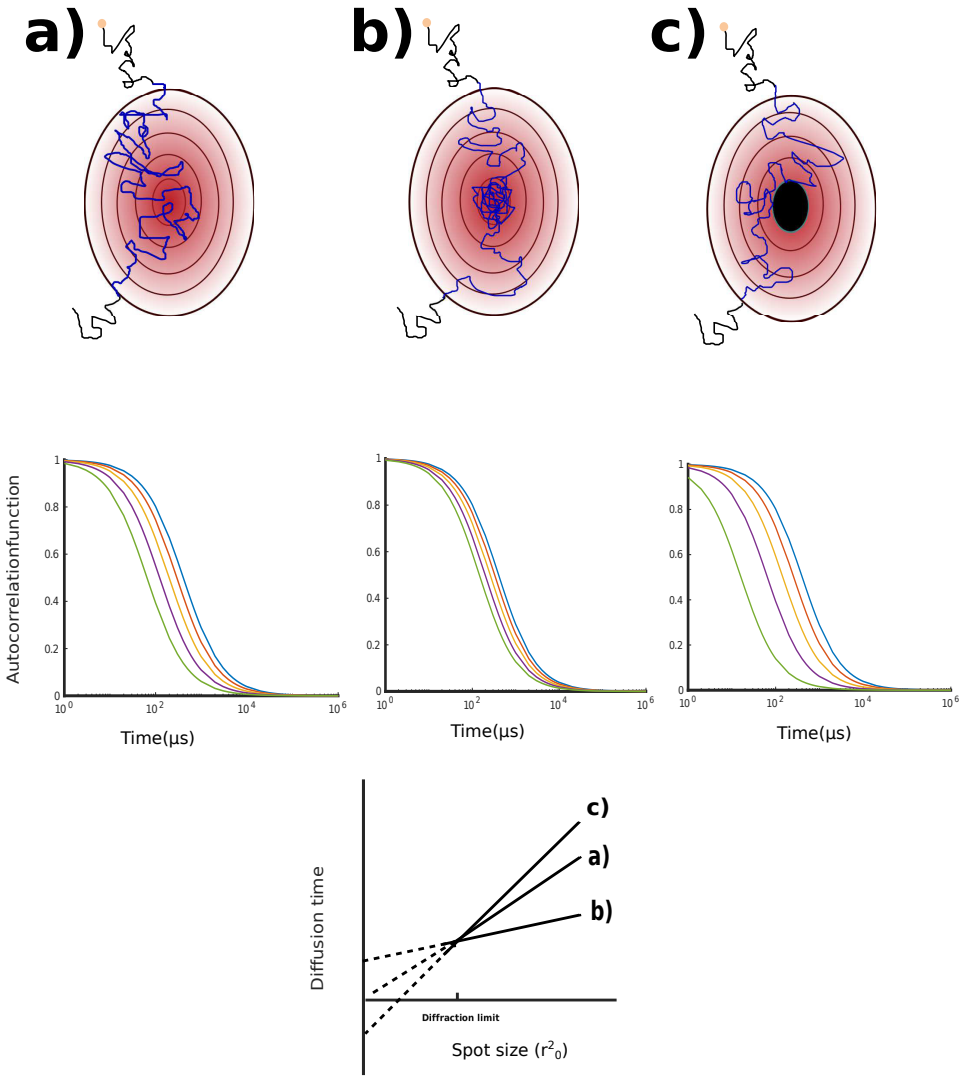

Figure 4.1. Schematic description of diffusion law analysis including different sizes of the confocal volume together with the calculated FCS curves for each spot size and the dependency of the diffusion time on the spot size for a created spot a) in a homogeneous medium b) in a medium containing traps for slowing down the diffusion c) in a medium containing barriers for hindering the diffusion.

is performed with a smaller confocal volume. The applicability of the method is established in extensive numerical simulations and directly supported in in-vitro experiments. The procedure is then applied to the diffusion of AlexaFluor647-labeled streptavidin in living cells. The results of this of work are published in Scientific

Reports (**?**).

4.0.1 Methods of Spot Variation

In general, there are three methods to vary the spot size. Here, we briefly explain these methods categorizing them in two classes. The first class corresponds to those methods which, essentially, start the FCS measurement with relatively large size of confocal volume and using some mechanical adjustment to decrease the size of the spot. These methods are limited to the diffraction limit size and measurements can not be performed beyond this size limit. The diffraction limit is defined with the minimum spot size, d, which is possible to create with a lens with numerical aperture, NA, and the laser light wavelength,λ as: $d = \frac{\lambda}{2NA}$ (**?**). Thus, they use the diffusion law to extrapolate the data from diffraction limited measurements in order to obtain the information about nano-scale infrastructures. The second class, however, is denoted to a method which physically goes beyond the diffraction limit and will be explained in the following section.

The first diffraction limited method is introduced by Steinberger et al. (**?**). They measured the fluorescence autocorrelation function of a planar system at different positions with respect to the confocal volume in z-direction with step size of typically 100-200 nm (z-scan). Changing the position of the planar system with respect to the beam's waist led to change in the illuminated spot size. Assuming the quadratic dependence of residence time and number of particles inside the confocal volume on the diameter of the spot, one could measure the diffusion coefficient, the beam's waist, and the particles' concentration. Although this method needs no additional calibration steps, it is limited to 2D-systems. The main error sources in this method are inaccurate positioning of the sample, thermal instability during subsequent measurements and deviation from the assumed Gaussian form of the spot (**?**).

Another method, spot-variation FCS (SV-FCS), was developed independently by Masuda et al. (**?**) and Wawrezinieck et al. (**?**). It is based on the under-filling of the back aperture of the objective by the laser beam. Wawrezinieck et al. introduced a diaphragm between laser beam expander and the dichroic mirror in order to select the extension of the beam on the back aperture of the microscope objective. Using the direct dependence of the point spread function on the diaphragm aperture, they could tune the size of the confocal volume. Masuda et al. also motorized the variable beam expander to adjust the size of incoming laser beam before objective. With these techniques one can continuously adjust the spot size in the range of 0.2 μm up to 0.5 μm.

Eggeling et al. (**?**) coupled FCS with stimulated emission depletion (STED) microscopy in order to lift diffraction limitations for confocal volumes (STED-FCS). An interesting feature of STED is its ability to tune the size of confocal volume by increasing the power of the depletion laser. Performing the calibration of the

laser intensity with respect to the resulting size of the confocal volume, one can in principle attain the desired size of confocal volume in three dimensions. Nevertheless, this calibration may not be accurate and therefore introduces errors in results of analysis. Moreover, higher intensities of the depletion laser for smaller spots may lead to deviations from the Gaussian intensity profile in the confocal volume which is assumed in further data processing procedures (**?**). This technique is in a wider use but demands for a sophisticated setup and high-power lasers, which could be considered as disadvantage.

In all methods mentioned above one has to perform many repetitions of the experiments. In each repetition the confocal volume has to be adjusted mechanically or electronically, which may lead to errors and artifacts in measured FCS curves. Thus, the size of the confocal volume is controlled only indirectly by considering its theoretically assumed dependence on the parameters changed, which can be altered due to minor deviations in the setup. Repeating the experiment many times can be a source of artifacts due to thermal instability of the system's environment or to unanticipated changes in the sample itself. This can be a crucial issue when considering experiments in living cells which have to be exposed to laser illumination for a long time.

In what follows we propose a new method providing the possibility of mimicking the spot sizes with any desired step size on the level of data post-processing. This is done by utilizing the data from a single run of the standard FCS measurement with diffraction-limited confocal volume. We apply a non-linear transformation to the smoothed fluorescence intensities, and with this, mimic the exclusion of intensities arising from the outer parts of confocal volume. Here we assume a linear relationship between the intensity of the excitation beam and the resulting florescence intensity, which is valid in standard FCS measurements with moderate intensities. Since only a single FCS measurement is required to perform our proposed method, all challenges arising from repeating the measurements are excluded. There is no need for extra calibration and no more assumptions than have been made for the FCS measurement. Since this method uses a common FCS setup, there is also no demand for extra equipments. We consider the method in a three-dimensional setup, although it can also be applied in planar, two-dimensional, systems.

4.1 Theory of Post-processing

In essence, the basic idea of spot variation without spot variation is to utilize the correspondence between the position of the tracer particle in the confocal volume and the intensity profile, measured by the detectors. As it is schematically illustrated in Fig.4.2, particles crossing the outer parts of confocal volume emit less fluorescence photons compared to those crossing the central part. This is direct consequence of the form of the confocal volume, intensity profile $W(\mathbf{r})$, which is commonly assumed

to be Gaussian, as discussed in chapter 2. Thus, if one excludes the lower intensities in the detected fluorescence intensity profile, it results in fact, in decreasing the size of the confocal volume. Although this linear filtering of the lower intensities, as depicted Fig.4.2, is convenient to perform, it includes a discontinuity in the FCS curve. Theoretically, the new intensity would have the form as $I'(t) = I(t)\theta(I(t)-I_c)$, where θ is the stpe function and I_c is the filtering threshold. Presence of this step function in the calculation of the autocorrelation, leads to non-analytic solution for the integration in Eq.2.7. Nevertheless, one could find some analytical form for the asymptotic limits of the FCS curves. Another difficulty with the linear filtration arises from attributing an arbitrary intensity threshold to a specific size of confocal volume. This, essentially, requires an extra calibration to find a correlation between the intensity and the position of the particle.

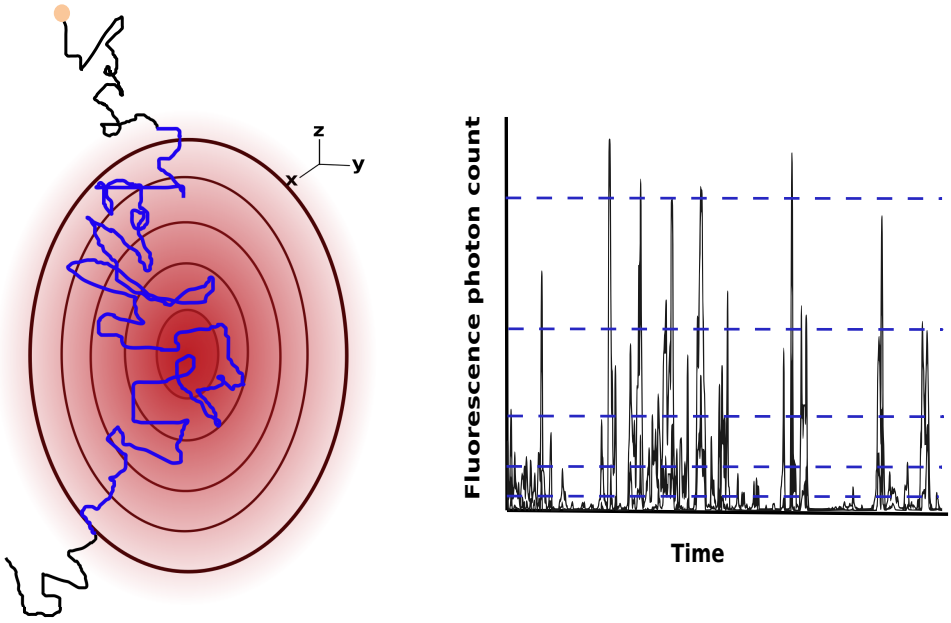

Figure 4.2. Schematic description of the idea of SV-FCS without spot variation. The outer parts of the confocal volume having lower laser intensities result in less fluorescence photons emitted by the tracer particle. Truncating the lower intensities in the intensity profile means at decreasing the size of the confocal volume.

Mentioning the problems with the linear filtration approach, we have attempted to invent a method which not only holds the continuity in the mathematical sense, but also provides a possibility of calibration free variation of the confocal volume.

Recalling the basic equation for the intensity of detected photons at time t, we have

$$I(t) = \epsilon \int d\mathbf{r} W(\mathbf{r}) c(\mathbf{r}, t) \tag{4.2}$$

where ϵ denotes the total quantum efficiency of fluorescence. This indicates that the intensity of emitted light depends on the laser intensity profile $W(\mathbf{r})$ and on the local fluorophore concentration $c(\mathbf{r}, t)$,

The standard FCS method can be considered as a single particle technique: the measurements are preformed at very low fluorophore concentrations so that one can safely assume, there is no more than one fluorophore particle in the confocal volume at each instant of time. Therefore the instantaneous concentration $c(\mathbf{r}, t)$ in Eq.4.2 is essentially $\delta(\mathbf{r} - \mathbf{r}(t))$ where $\mathbf{r}(t)$ is the instantaneous particle's position. The instantaneous fluorescence intensity at time t is thus

$$I(t) = \epsilon W(\mathbf{r}(t)). \tag{4.3}$$

The laser beam excitation profile $W(\mathbf{r})$ is commonly approximated by a Gaussian form

$$W(\mathbf{r}) = I_0 \exp\left[-2\frac{x^2 + y^2}{r_0^2} - 2\frac{z^2}{s^2 r_0^2}\right]$$

with I_0 being the characteristic intensity, r_0 being the diameter of the beam's waist in the direction perpendicular to the light propagation direction, and sr_0 being the corresponding dimension in the light propagation direction, so that

$$I(\mathbf{r}(t)) = \epsilon I_0 \exp\left[-2\frac{x^2(t) + y^2(t)}{r_0^2} - 2\frac{z^2(t)}{s^2 r_0^2}\right]. \tag{4.4}$$

Here the origin of coordinates is put to the center of the confocal volume. In a typical FCS experiment the parameters of the beam are fixed and known in beforehand from calibration.

Here we note that the logarithm of $I(r(t))$ as given by Eq.4.4 is immediately related to the particle's position . Therefore, we introduce a non-linear transformation which defines a modified intensity profile as

$$I'(t) = I(t) \exp\left(\frac{\ln I(t)}{r_c}\right), \tag{4.5}$$

with r_c being the free parameter of the transformation. substituting the Eq.4.5 in Eq.4.4, one gets

$$I'(t) = \epsilon I_0 \exp[\ln(\epsilon I_0)/r_c] \times \exp\left[-2\frac{x^2(t) + y^2(t)}{r_0^2}\left(\frac{r_c + 1}{r_c}\right) - 2\frac{z^2(t)}{s^2 r_0^2}\left(\frac{r_c + 1}{r_c}\right)\right] \tag{4.6}$$

Comparing Eq.4.4 with Eq.4.6, indicates that this non-linear transformation holds the form of the initial intensity profile, namely the Gaussian form, and simultaneously mimics a recorded intensity from a smaller confocal volume with the waist size

$$r_0' = \sqrt{\frac{r_c}{r_c + 1}} r_0 \tag{4.7}$$

and with the same elongation parameter s. In Eq.4.7, when r_c is taken to be large, r_0' tends to r_0 and when r_c is small, r_0' is reduced by the factor $\sqrt{r_c}$. The pre-factor in Eq.4.6 is not disturbing, since the autocorrelation of modified intensities could be renormalized as

$$G(\tau) = \frac{\langle I(t+\tau) I(t) \rangle}{\langle I(t) \rangle^2} - 1. \tag{4.8}$$

thus, all the pre-factors in the modified intensity cancel out in calculated FCS curves.

Finally as in chapter 2, calculating the intensity autocorrelation function, Eq.4.8, for the modified intensity profile Eq.4.6 leads, under the assumption the Gaussian form of PDF, tothe standard formula for the FCS autocorrelation function for normal and for Gaussian anomalous diffusion:

$$G(t; \alpha, D_\alpha) = \left(\frac{4 D_\alpha}{r_0^2} t^\alpha + 1 \right)^{-1} \left(\frac{4 D_\alpha}{s^2 r_0^2} t^\alpha + 1 \right)^{-\frac{1}{2}} \tag{4.9}$$

where α is the exponent of anomalous diffusion; the case of normal diffusion corresponds to $\alpha = 1$ (**?**).

4.1.1 Shot Noise, Binning and Smoothing Kernel

As discussed in the last section, having the intensity profile of detected photons from a single run ordinary FCS measurement is sufficient to calculate the FCS curves for the mimicked sizes of confocal volumes which are effectively smaller than the initial one. This size reduction according to the Eq.4.6, can be done for any size of the confocal volume, ranging from r_0 down to zero (corresponding to the tracer's size) with any desired step size. In other words, the whole information is essentially contained in the single photon count time series, such that the spot variation is essentially superfluous. However, the realistic situation is somewhat more involved. Having look at the non-linear transformation, one notices that the transformation works by tuning the intensity at arbitrary time by a factor of the intensity at the same time. This means that the higher intensities in the initial intensity profiles are magnified exponentially with the factor of the intensity itself in the modified one. Thus, applying this non-linear transformation demands an intensity profile which varies considerably for different times according to the position of the particle in the confocal volume (distance from the center). This is, however, not the case for the typical measurements in ordinary FCS experiment where the outcomes are single

photon counts.

In typical FCS measurements the FCS curves are calculated from the photon arrival times (**?**). Thus, the intensity profile is a binary file containing zero or one photon count per detection bin. For our approach, however, this shot noise is very disturbing. In this case, the proposed method would not work and applying the non-linear transformation would lead to the same FCS curve as the initial one. Here, we discuss two ways to circumvent the problem.

I) Binning the photon counts: The immediate idea to have a varying intensity profile is to use the binning method. In this approach, the photon counts in each instant of detection time, normally nanosecond, are collected in time intervals which are larger than the detection accuracy. Choosing the binning time interval, two important points should be taken in account. First, the time interval must be chosen such that the summation of photon counts inside bins differ considerably from each other. This, naturally, demands the binning time to be large enough. The second parameter in defining the time interval is the accuracy, which one loses by increasing the bin size. In another word, the bin size determines the minimum time resolution of the analysis. Thus, it should not be larger than the dynamical time range of the interest in investigation of the process. Therefore, one has to optimize the binning time such that it finally satisfies these to conditions in order to work with this piecewise-continuous intensity profile. Our investigations on the experimental data, as will be discussed in the following chapter, indicate that having the intensity profile varying from zero to roughly 20 photon counts per bin is sufficient to perform our analysis. Note, that this method works perfectly in the situations when the diffusion process is slow, and the diffusion time through the spot is much longer than the binning time necessary to achieve the required accuracy. However, there are diffusion processes which are not slow enough to optimize the conditions in order to find a proper binning time. In this case, the second developed method is recommended to be performed.

II) Smoothing kernel: The alternative way to circumvent the problem of shot noise in fast diffusion processes is to transform the initial binary intensity profile into a continuous fluorescence intensity trace (photon counting rate) which considerably varies in time according to the position of the tracer. In the smoothing method, instead of summation of photon counts with the same importance factor in a bin, the photons are attributed to a magnifying factor based on their time distance from the next and previous detected photons. The reason for this discrimination between photon counts with respect to their neighbours is as follows: when the fluorescent particle is closer to the center of the confocal volume, it is exposed to higher number of exciting photons and consequently it emits the fluorescence photons with a higher rate. Thus, the time distances between the detected photons are smaller as they are

closer to the center.

Finding a proper function for this approach was, indeed, a hard task. Several approaches based on kernel smoothing and on the statistics of the inter-event times weretested. Finally, a smoothing function with the double-sided exponential kernel was found to provide the best results among all tested variants. Thus, our estimate for the intensity is

$$I(t) = 1/2\sigma \sum_{i=0}^{N} \exp\left(-|t - t_i|/\sigma\right) \tag{4.10}$$

where t_i are the photon arrival times, N is the total number of records during the measurement time T, and σ is the effective smoothing time which also defines the temporal resolution. The optimal value of σ depends on the total number of photons collected from the particle diffusing inside the confocal volume. This has to be taken such that the autocorrelation function $G'(t)$ calculated from the reconstructed intensity trace $I'(t)$ for $r_c \gg 1$ (i.e. when $I'(t) \to I(t)$) show the minimal deviation from original FCS curve $G(t)$.

4.1.2 Proof of Principles, Simulation and Test Experiments

Before applying the method to the experimental data, we discuss the proposed method at the simulation level in this section. Since the binning method is somewhat trivial, the kernel smoothing approach is investigated in an extensive simulation study of normal and anomalous diffusion. Introducing the simulation details from the well-established methods and the results, the suitability of the proposed method is then investigated experimentally for two cases of normal and anomalous diffusion of AlexaFluor647-labeled streptavidin in pure phosphate-buffered saline (PBS) and in PBS crowded with 30% PEG1500 which are known to be homogeneous. In this test experiments, we used both approaches, namely binning and kernel smoothing.

Simulation

To support our theoretical finding by means of simulation with emphasis on the kernel smoothing method, simulations for the cases of normal and anomalous diffusion were performed. Simulation details for the medium and the particles were as follows: A box in three dimensions with the size of $L = 4$ μm in each direction, with periodic boundary conditions was considered as a homogeneous medium in which the tracer particles performing the diffusion process. Then a confocal volume, for the purpose of recording the fluorescent intensity, was placed in the center of box with parameters in Eq.4.4 being $r_0 = 0.3$ μm, as the radius in x-y plane and $s = 4$ as the elongation in z direction. we set the characteristic intensity I_0 and the total quantum efficiency ,ϵ, to be unity. Then, the tracer particles were distributed randomly in the box with a total number to be such that their mean number within

the confocal volume did not exceed 0.5. We note that the particles here assumed not to have any interaction with each other, with the particle size of zero (i.e. point particles). When the diffusing particle reaches the centred confocal volume, depending on the distance from the center of the spot in x-y plane and the position in z direction, the fluorescence intensity is calculated according to the Eq.4.4.

In our numerical simulations for normal and anomalous diffusion, the trajectories of each tracer were obtained from their coordinates simulated as three independent one-dimensional Brownian and fractional Brownian motions along each axis. The trajectories for normal diffusion were generated using the Box-Muller method (**?**). For the case of anomalous diffusion, we first generated the fractional Gaussian noise using Lowen's method (**?**). Then the trajectories were calculated as integrating the fractional Gaussian noise in discreet time steps.The trajectories of each tracer were recorded up to 10^8 time steps.The time step of simulation corresponds to 1 μs in a real experiment. The value of the Hurst parameter for anomalous diffusion was $H = 0.37$, corresponding to sub-diffusion with the exponent of anomalous diffusion $\alpha = 0.75$. Diffusion coefficients were set to be 11.8 $\mu\mathrm{m}^2/\mathrm{s}$ for normal and 80.1 $\mu\mathrm{m}^2/\mathrm{s}^{0.75}$ for anomalous diffusion.

Having the simulated particles' trajectories and the known form of the confocal volume, the intensity traces $I_0(t)$ for the initial continuous form, according to the Eq.4.4, were generated. The upper purple color coded plots in Fig.4.3 and Fig.4.4 indicate the calculated intensities for the normal and for anomalous diffusion processes, respectively. Note that the intensities are shifted by two units for sake of clarity. These intensity profiles are the starting point in the simulation which are not available in the real experiments. In principle, the main aim here is to reproduce such continuous intensity profiles in the last stage using the kernel smoothing method on the photon counts. Then the non-linear transformation can be conveniently applied to such intensity profiles.

To mimic the detected photon counts, I_p as in real experiment, we attributed the intensity at each time to the probability of the detection or absence of a photon. Thus, one has for the probability of detection a photon at each time step Δt, $1 - \epsilon I_0(t)\Delta t$ and the probability of having no detection, $\epsilon I_0(t)\Delta t$ respectively, with $\epsilon = 1$. Therefore, the binary intensity of photon counts profile, I_p is generated being zero or one. The middle purple color coded plots in Fig.4.3 and Fig.4.4 show the binary intensity profile for normal and anomalous diffusion. This situation can be generalized for the experimental cases with larger binning times. In such case, one can attribute the maximum probability (maximum intensity is unity) to the maximum number of photons, which the tracer particle can emit in the corresponding time interval. Consequently, one obtains a piecewise-continuous intensity profile, similar to the result of binning method. One of the main assumptions made here, was that the fluorophor tracer responses linearly to the intensity. In other words, the number of emitted photons changes is a linear function of the intensity. This is

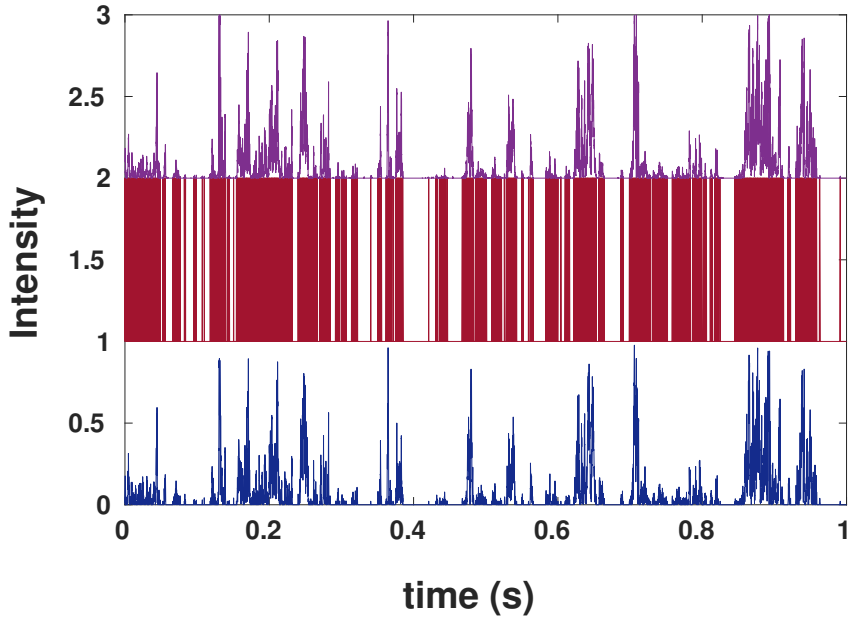

Figure 4.3. Simulation results for fluorescence intensities for the case of normal diffusion: (upper, purple) the original intensity trace I_0 shifted up by 2 units; (middle, red) photon counts (I_p) shifted up by 1 unit, and (lower, blue) restored intensity trace $I(t)$ with $\sigma = 23$ μs.

however, the assumption which is considered when deriving the basic equations in the ordinary FCS theory and can be surely used for moderate intensities.

In the next step, the binary intensity profile, I_p, may be transformed to the continuous intensity trace, $I(t)$, using the kernel smoothing method. This can be done by tuning the parameter σ such that the deviation between the original and the restored intensity profiles are minimized. The bottom blue plots in Fig.4.3 and Fig.4.4 show the restored intensity profiles by using the Eq.4.10 with $\sigma = 23$ μs for the normal and $\sigma = 12$ μs for anomalous diffusion. Finding these σ values, one may start from two lower and higher limits for the σ value, depending one the number of photon counts and try to perceivethe an optimum value. this value should result in minimum difference between the initial and final intensity profiles. It is a tautology that in real experiments, we do not have access to the original intensity trace $I_0(t)$, but only to the photon counts. In such situation, finding the optimal value of σ can be done by comparing the FCS curves $G(t)$ and $G'(t)$ as calculated from the photon counts and from the smoothed intensity trace in the relevant time domains. Here, we compare both the intensity traces and corresponding autocorrelation functions. The

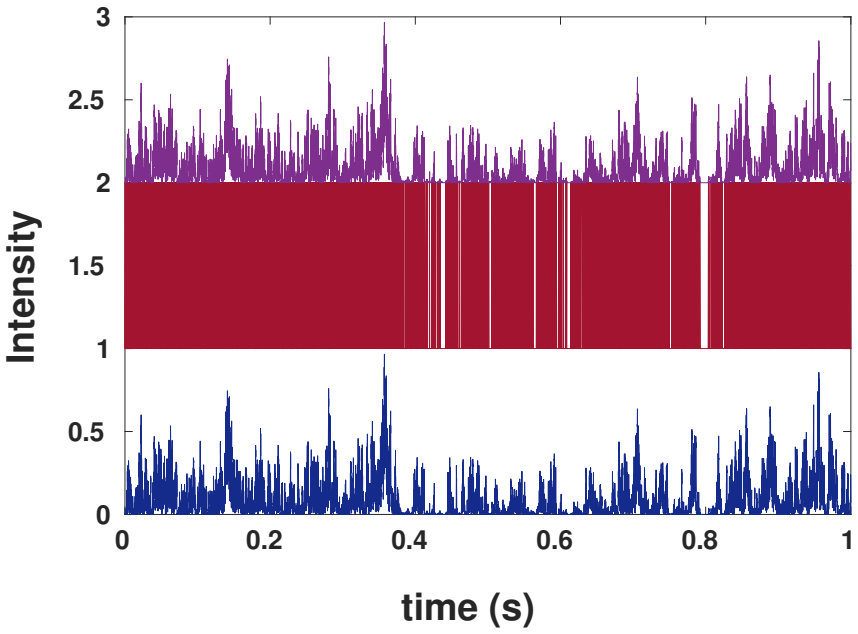

Figure 4.4. Simulation results for fluorescence intensities for the case of anomalous diffusion: (upper, purple) the original intensity I_0 shifted up by 2 units; (middle, red) photon counts (I_p) shifted up by 1 unit, and (lower, blue) restored intensity trace $I(t)$ with $\sigma = 12$ μs.

aim is to show that if the autocorrelation functions from binary data and from the reconstructed intensity coincide, the initial and the reconstructed intensity traces are indeed the same to a good extent.

Fig. 4.5 shows the autocorrelation functions calculated from the photon counts and from the restored intensities for normal and for anomalous diffusion. Fig.3 indicates that both in the normal and in the anomalous diffusion cases the autocorrelation functions of reconstructed intensities reproduce the autocorrelation functions of original data at longer time lags. We note that for the lag times of the order and below σ values the deviations may increase considerably. Given typical times between photon counts in real experiments this limitation is not an important issue, however, care must be taken when fitting the corresponding curves: time lags below σ must be excluded from the fit.

In order to apply the proposed method to mimic the size change of the confocal volume, we used Eq.4.5 with changing parameter r_c such that the size of the resulting confocal volume decreases from initial size r_0 to $0.2r_0$ with steps of $0.1r_0$, both for normal diffusion, Fig.4.6, and for anomalous diffusion, Fig.4.7.

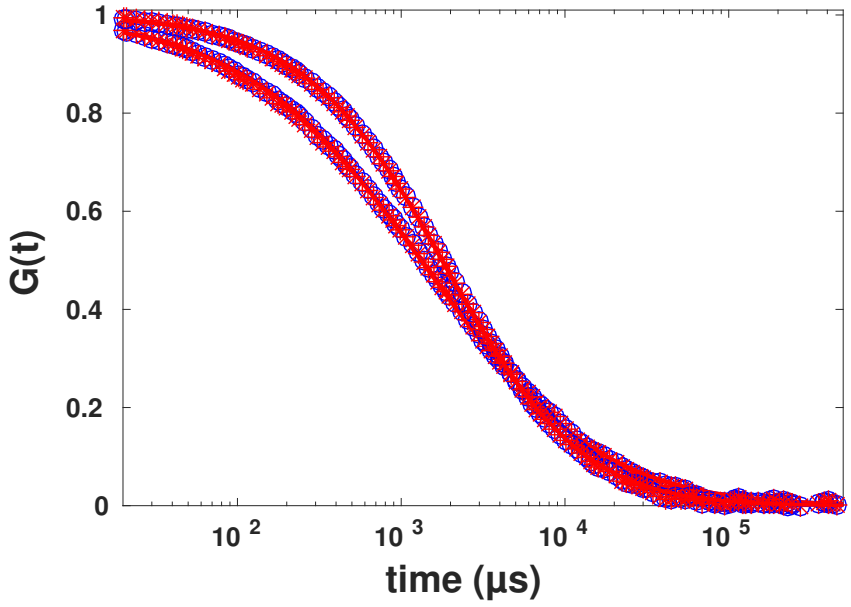

Figure 4.5. Simulation results for FCS curves calculated from photon counts (bluecircles) and from restored intensity traces (erd asterisks) fitted to Eq.4.9 (lines) for normal (upper line) and anomalous (lower line) diffusion.Note the almost complete coincidence of data.

Plotted in Fig.4.7 are the initial FCS data for the beam waist r_0, the results for the beam waists $r < r_0$ as obtained by the procedure discussed, and the theoretical curves, according to Eq.4.9, as calculated for the corresponding beam waists and for the known values of the coefficient of the normal or anomalous diffusion. Note that the curves in Figs. 4.6 and 4.7 *are not fits*, but the theoretical curves showing the behaviour given by Eq.4.9 for the values of parameters used in simulations. Additionally, the simulated data were fitted to Eq.4.9 to obtain the exponents of anomalous diffusion and diffusion coefficients. Results of fittings in all data for diffusion coefficients and exponents of anomalous diffusion being $D = 12.2 \pm 1.2\ \mu\text{m}^2/\text{s}$ and $\alpha = 0.99 \pm 0.01$ for normal diffusion and $D = 78.5 \pm 4.8\ \mu\text{m}^2/\text{s}^{0.75}$ and $\alpha = 0.75 \pm 0.03$ for anomalous diffusion, i.e. practically do not deviate from the values which were used for the trajectories' simulation. As it is seen in the FCS curves from the spot variation, the results of mimicked FCS for smaller sizes of confocal volume tends to deviate slightly from the theoretical line. These errors in smaller sizes are , in principle, expected as in this measurement time (i.e. simulation running time) the particles cross the central part of the spot less often compared to the outer layers

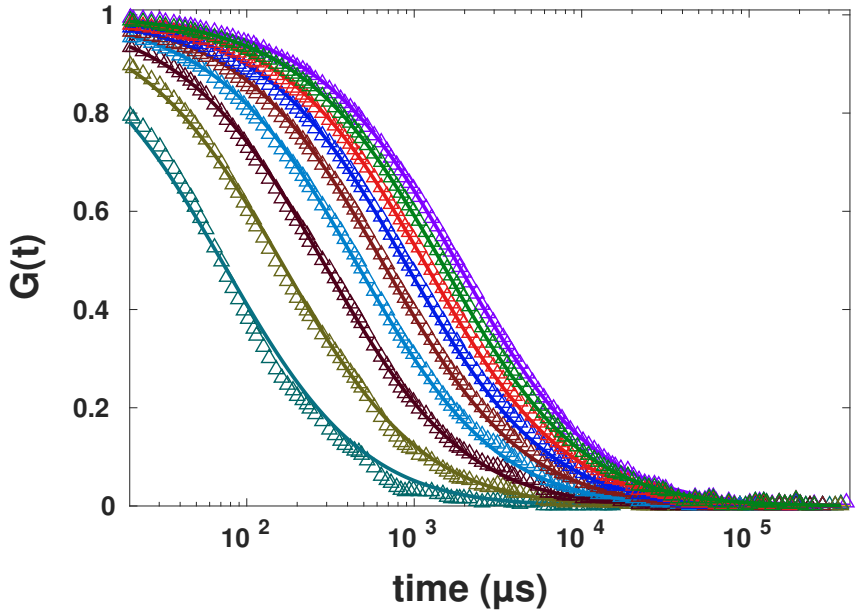

Figure 4.6. Simulation results for mimicked spot variation FCS for the values of the effective beam waist ranging from r_0 to $0.2r_0$ (from right to left) for normal diffusion (symbols), together with theoretical FCS curves for the same beam waists according to Eq.5.

of the spot. Therefore, the lack of statistics is simply acceptable. This deficiency in the data for small sizes can be fixed by increasing the measurement time which provides more reliable statistic for arbitrary small sizes.

Test Experiments: Normal and Anomalous Diffusion in Homogeneous Media

The findings in the simulation level give a direct support of the method. In the next step of corroborating the method, we will apply the proposed approach to the experimental data. This will give additional support for the applicability of the method and show its potential usefulness for investigations of biological systems. From the experimental results in the chapter 2, it was known that the normal diffusion of a particular tracer in a homogeneous medium such as water, may change to the anomalous diffusion with adding some crowding materials in the system. The size of the crowding material as well as its concentration determines the deviation of diffusion process from normal diffusion in favour of sub-diffusion. To create such systems of normal and sub-diffusion processes, for investigation of our new method, we chose the AlexaFluor647-labeled streptavidin as the tracer particle. Since this

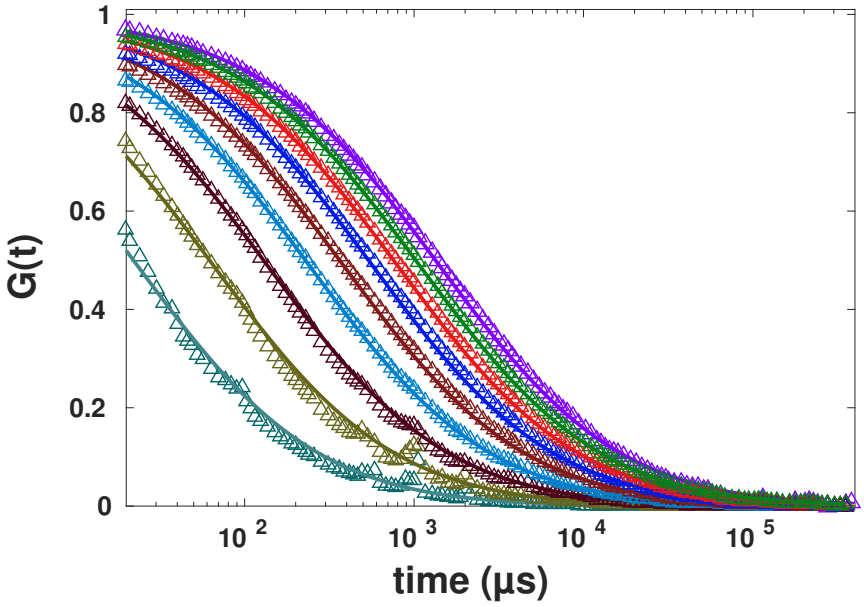

Figure 4.7. Simulation results for mimicked spot variation FCS for the values of the effective beam waist ranging from r_0 to $0.2r_0$ (from right to left) for anomalous diffusion (symbols), together with theoretical FCS curves for the same beam waists according to Eq.5.

tracer must be kept in the buffer environment, we replaced the water solution in chapter 2 with PBS buffer solution for normal diffusion. To obtain the sub-diffusion in a homogeneous system, we then added PEG1500 molecules as crowding material, noting that the concentration should not reach the solubility level. In low concentration of this type of crowding molecules, the PBS system becomes strongly viscose and Gaussian anomalous processes are observed. This has been checked by the asymptotic analysis as introduced in chapter 2. This assures that, there exist no trapping site in the medium. In other words, the motion of the particle does not differ in different points in the system. Thus, we performed FCS measurements for the cases of diffusion of 0.5nM AlexaFluor647-labeled streptavidin in PBS buffer solution and in PBS buffer solution crowded by 30% PEG1500.

Choosing a low concentration of fluorescence tracer, provides the possibility that, at any time there would be, in average, not more than one tracer particle in the confocal volume. Generally, a good test for performing a single molecule FCS measurement is to observe the fluorescence intensity profile for a single molecule experiment. One should in this case observe strong fluctuations of the count rates arising from

entering and exiting of the tracers in and out of the confocal volume. In our experiments, the photon count rate in background was roughly $1,000$ *cps* with maximum change to roughly $10,000$ *cps*, depending on the trajectories intersecting different parts of the confocal volume. To filter out the unwanted background photons coming from reflection, one may use the time gating technique. The disturbing photon counts as a result of the reflection of incident laser light from the glass surface and other parts of the set-up such as filters, generally have different arriving times in the detectors compared to the fluorescent photons. Therefore, choosing a proper window of arriving time for the detection of fluorescent photons compared to the incident photons, leads to the elimination of unwanted background. Nevertheless, there will be always some photon count background from other light sources in the room which their impact to the final FCS curves could be neglected.

Autocorrelation functions for the corresponding cases, calculated from recorded photon counts, are shown as blue symbols in Fig.4.8. The upper curve belongs to the diffusion in PBS and the lower one corresponds to the diffusion in PBS crowded with PEG1500 molecules. The data were then fitted to the standard formula of FCS. The results of the fits accord to our expectation in generating normal and anomalous diffusion process. The fit for the case of crowded buffer with 30% PEG1500 led to the exponent of anomalous diffusion and diffusion time being 0.89 ± 0.03 and $1,084.3 \pm 38.6$ μs. The case of diffusion in pure buffer solution were fitted to the normal diffusion and resulted in diffusion time being 243 ± 20 μs. The standard deviations were calculated from $N = 6$ repeated experiments for both.

Then, we formed the restored intensity profiles for both processes according to Eq.4.10 with $\sigma = 3$ μs and calculated the FCS curves, respectively. The equal σ values for both processes stems from the similar experimental situations, namely the same sizes of the confocal volumes, same incident laser intensities and the same fluorescent molecules. Although one can go beyond this accuracy and find the corresponding results with next digits for σ value, this satisfies our considerations in establishing the method. The differences between fits to the original FCS data and reconstructed ones using kernel smoothing method for both normal and anomalous diffusion were very small and here we reported the fit for smoothed curves. Similar to our simulations in the previous section, the FCS curves as calculated from the photon counts and from the restored intensity traces coincide (compare *blue* and *red* solid lines in Fig.4.8). We also mention that, only lag times longer than 20 μs entered our calculations in the analysis of the FCS curves for sake of avoiding the photophysics of AlexaFluor647 dyes. However, since the diffusion processes are slow, this does not impact our analysis significantly. Note that this lag time is of the order of the time limitation of our method as defined by the used value for σ .

Parallel to the kernel smoothing method, we investigated the binning method for generating the piecewise-continuous intensity profile from the original experimental data. In this manner, the original binary photon counts were binned with a bin

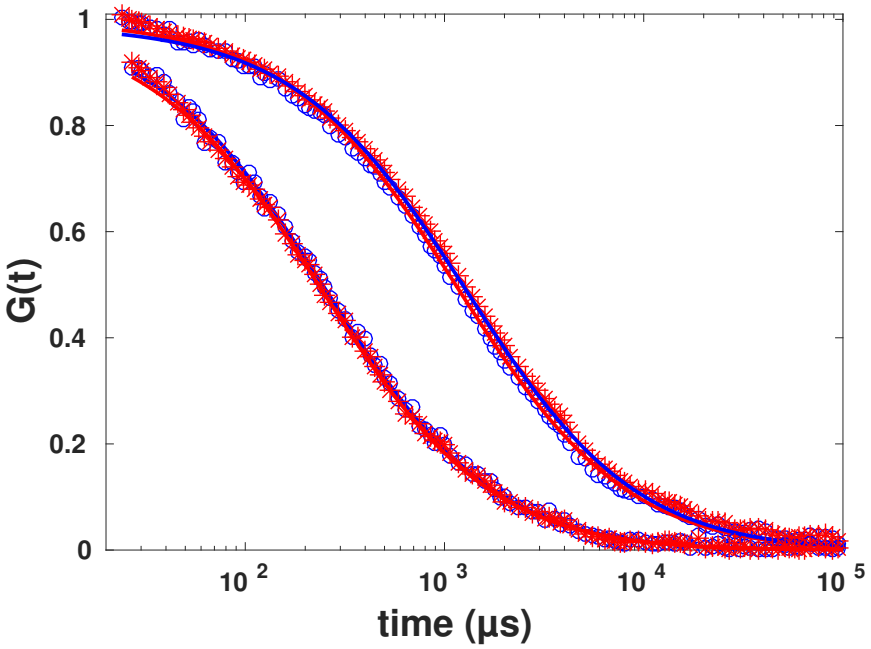

Figure 4.8. Experimental results for FCS calculated from photon counts (blue circles) and from the restored intensity trace according to Eq.4.10 (red asterisks) for streptavidin diffusion in pure PBS (lower line/symbols) and in PBS crowded with 30% PEG1500 (upper line/symbols) fitted to the standard formula (solid lines). Each curve is representative for $N = 6$ independent experiments.

width of 10 μs, which resulted in intensity profiles varying from zero to maximum of 20 and 31 counts for normal and anomalous diffusion, respectively. This number of detected photons per bin may be, trivially, increased with intensifying the incident laser light. However, to check the method's applicability for standard situation of FCS experiment, we let the intensity to be low. Having both intensity profiles at hand, we could apply the non-linear transformation according to Eq.4.5 to these restored intensity traces and mimic the spot variation FCS. Results of applying Eq.4.5 to these intensity traces for the cases of pure buffer and crowded one are shown in Fig. 4.9 and 4.10. In each figure, the left plot corresponds to the spot variation FCS without spot variation using the kernel smoothing method and the right one, belong to the same results with the binning method.

As it can be seen in Fig. 4.9 and 4.10, two different approaches of kernel smoothing and binning in both experiments revealed qualitatively similar results. In both methods, the FCS curves decayed faster as the spot size became smaller, However,

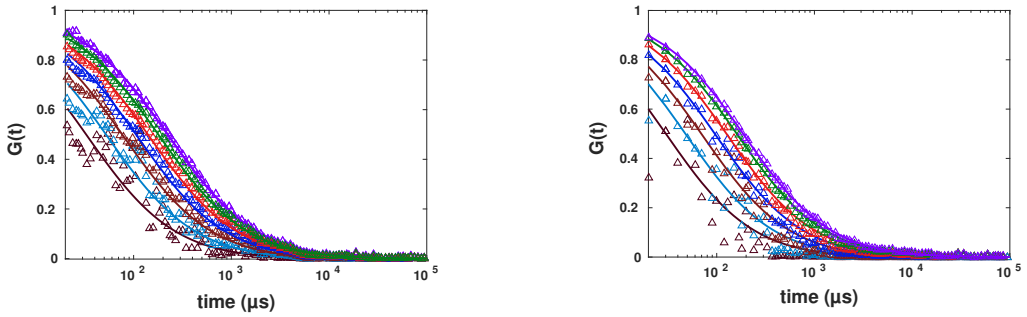

Figure 4.9. Experimental results for spot variation FCS (with the effective beam waist varying from r_0 to $0.4r_0$ from right to left) for diffusion of AlexaFluor647-labeled streptavidin in buffer fitted to the standard formula. The intensity time traces were generated using kernel smoothing method for the left panel and binning for the right panel.

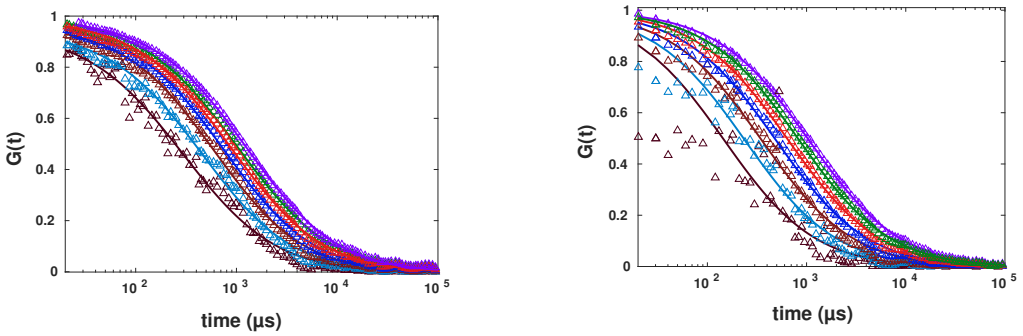

Figure 4.10. Experimental results for spot variation FCS (with the effective beam waist varying from r_0 to $0.4r_0$ from right to left) for diffusion of AlexaFluor647-labeled streptavidin in buffer crowded by 30% PEG1500 fitted to the standard formula. The intensity time traces were generated using kernel smoothing method for the left panel and binning for the right panel.

there exist some apparent differences between them. The first main difference is the fact that, the FCS curves generated by binning approach have less data points in the first decade (10 μs - 100 μs) compared to that of generated by kernel smoothing method. This could, essentially, lead to more uncertainties in fitting process and data analysis. On the other hand, binning approach has the advantage of fast analysis and less complexity and does not demand a thorough choice of smoothing parameter required by the kernel smoothing method. The key advantage of kernel smoothing method is its applicability in case of low photon counts (arising from e.g. low laser power or low fluorescence quantum yield of dye). In such cases, to obtain a

sufficient varying intensity trace from binning method, one would have to make the bin larger, leading to a reduced time resolution. Therefore, choosing one of these approaches as the efficient method for the analysis, one should consider different parameters and the experimental situations.

Similar to the results in the simulation part, the data for smaller mimicked sizes of confocal volume contain more noise due to fairly short measurement duration, being 100 s. For in-vitro measurements, one could simply increase the measurement time and obtain quite smooth curves, see the FCS curves for the in-vitro measurements in chapter 2, also for smaller spots. We set the data acquisition time to be 100 s in all reported experiments to comply with limitations of in-vivo experiments, where longer illumination times harm the cell.

To obtain a quantitative result from the spot variation method without spot variation, to see how correct it could reproduce the FCS curves for the smaller sizes of the confocal volume, we performed the diffusion law analysis. FCS curves, shown in Figs. 4.9 and 4.10, for different sizes of confocal volume were fitted to Eq.4.9 with the exponent of anomalous diffusion acquired from the initial fit to the autocorrelation function of the data (i.e. for the original size of confocal volume equal to 1.0 r_0). Then the relation between the diffusion time and size of the confocal volume was investigated, see Fig. 4.11. To obtain the intercept, the diffusion time for zero size of the confocal volume, we interpolated the data with a linear fit. These fits resulted in the intercepts t_0 being -11 ± 13 μs and -23 ± 54 μs for pure PBS buffer solution and the PBS solution crowded by PEG1500. Larger error bars in results for diffusion in buffer solution crowded by 30% PEG solution were due to including the exponent of anomalous diffusion as a free fit parameter. The parameter α has a standard deviation of 0.03. Such a small variation in exponent of anomalous diffusion has a larg impact in the diffusion time calculation. In summary, these results show that in fact no barrier or domain is present in these homogeneous solutions. This is a strong witness in favour of the applicability of our approach to experimental data to prove the homogeneity of a structure concerning nano-domains.

4.1.3 Heterogeneity in in-Vitro Experiments

In previous sections, we have introduced an alternative approach to the experimental spot variation in FCS measurements based on post-processing of the obtained data from a single ordinary FCS measurement. The application of the method for situation of normal and anomalous diffusion in homogeneous media, in simulation level and in-vitro experiments, has been so far demonstrated. This could be a direct test for investigation of the homogeneity in nano-scale, such that any deviation from the expected trend in the diffusion law analysis means at inhomogeneity of the system. Beside this possibility, we attempted to provide a robust experimental corroboration for the proposed method, in order to directly observe the presence of

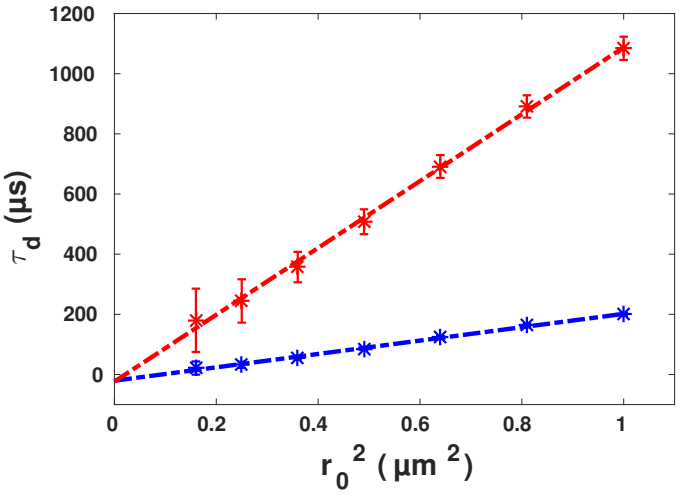

Figure 4.11. Diffusion time of AlexaFluor647-labeled streptavidin in buffer (blue) and in buffer crowded with 30%PEG1500 (red) versus spot size, together with corresponding linear fits being $\tau_d = 222{r_0}^2 - 11$ with $Pearson\ r^2 = 0.995$ and $\tau_d = 1111{r_0}^2 - 23$ with $Pearson\ r^2 = 0.997$. Data are presented as means $\pm$ standard deviation from $N = 6$ independent experiments.

nano-scale domains or barriers. Seeking for such a test system, we found the binary mixture of Dimethyl sulfoxide (DMSO) and glycerol as a generally accepted in-vitro systems which exhibits the desired properties.

As a protocol to the method, the ideal way to proceed the proposed analysis is to start with a system which shows a normal diffusion behaviour in a homogeneous system. Aside from calibration purposes, which is needed in $3-D$ measurements for determination of the elongation parameter s, demonstration of applicability of the method in simple systems before the main experiment makes the final results more reliable and comparable. Due to this reasoning, we started first with investigation of diffusion process in Pure DMSO solution. DMSO is, in fact, a homogeneous system with uni-modal diffusion time distribution of tracer particles. However, binary mixture of DMSO and glycerol has been reported to be extremely heterogeneous. Broad range of nano- and micro-domains are created by glycerol with considerably higher viscosity. Therefore, diffusion in such system takes place with a broad range of diffusion time distribution in FCS measurements (**?**). Such a system provides an ideal test for the capability of our method to unravel local inhomogeneities.

Compatible with other experiments in this work, we chose AlexaFluor647-labeled streptavidin tracers and performed the FCS measurements with tracer concentration being 0.5 nM. We started with the homogeneous system (pure DMSO) and performed FCS measurements for four independent experiments. Results of the

consequent FCS measurement are given in the left panel in Fig.4.12. In accordance with the assumption about the homogeneity of the system similar FCS curves were obtained in all experiments. All FCS curves fell on each other resulting in a normal diffusion with uni-modal diffusion time distribution with a mean value being $2,969 \pm 25\ \mu s$. In analysis of the corresponding FCS curves, we have included the triplet dynamics (**?**) into Eq.4.9 as:

$$G(t;\alpha,D_\alpha) = \frac{(1-F+Fe^{-\tau/\tau_F})}{(1-F)} \left(\frac{4D_\alpha}{r_0^2}t^\alpha + 1\right)^{-1} \left(\frac{4D_\alpha}{s^2 r_0^2}t^\alpha + 1\right)^{-\frac{1}{2}} \tag{4.11}$$

with F and τ_F being the fraction of the tracer particles at triplet state and the relaxation time of corresponding triplet state, respectively. We note that, one may introduce a summation to thee pre-factors of standard FCS formula including other possible triplet states. This, however, corresponds to the second order of correction in fitting procedure and for simplicity could be neglected.

In preparation of suitable intensity profile from the originally single photon counts, for performing the spot variation without spot variation, we used the binning method. Since the medium is quite viscose, the tracer particles diffuse quite slowly. Therefore, the fluorescent particles are exposed longer to laser light and consequently re-emit more fluorescent photons, resulting in a fairly good piecewise-continuous intensity profile with binning method. With same reasoning, losing the information in the short times due to less data points in binning method is not disturbing, while the dynamic of interest containing the main information is much larger than binning time, 10 μs.

The results of performing the spot variation for size range of r_0 - $0.4r_0$, with corresponding fitted curves are shown in the right panel of the Fig.4.12. The diffusion law analysis of the FCS curves is given in Fig.4.13. The intercept of linear fit to the diffusion time was obtained $35 \pm 133\ \mu s$, which means that one can assume the intercept to be zero within the errors. This in principle confirms our previous knowledge on the homogeneity of the system not only in the macro but also in nano-scale. The

The same procedure was then repeated for the binary mixture of DMSO:glycerol (77% : 23% , v/v). As it is known from literature, presence of the glycerol droplets with different micro and nano-sizes in the DMSO solution, creates some highly viscose spots in which the diffusing particles are trapped. This leads to a heterogeneous system which exhibits different behaviours in different repetition of the FCS measurements. To illustrate the point, four independent samples with the same ratio of DMSO and glycerol and 0.5 nM AlexaFluor647-labeled streptavidin were prepared. For each sample, we performed two FCS measurements at two different positions. Fig.4.14 shows the FCS curves of four measurements (one of the two measurements

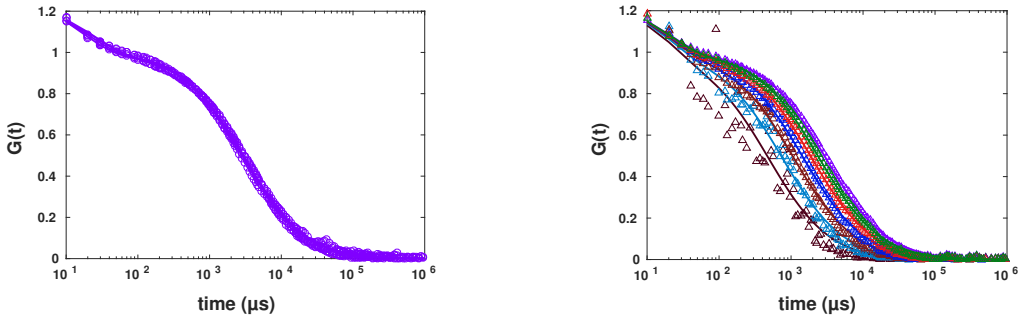

Figure 4.12. Experimental results of FCS measurements (left) for diffusion of AlexaFluor647-labeled streptavidin in pure DMSO fitted to the standard formula including triplet dynamics. Spot variation FCS with post-processing (r_0 - $0.4r_0$ from right to left) . The intensity time traces were generated using binning method (right).

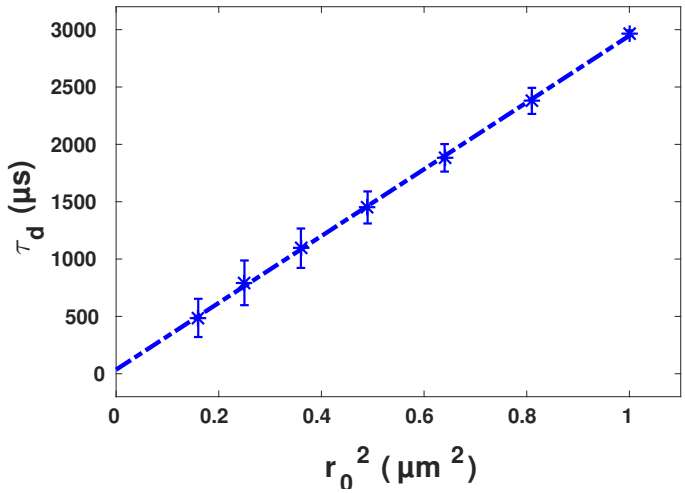

Figure 4.13. Diffusion time of AlexaFluor647-labeled streptavidin in pure DMSO versus size, together with the linear fit of $\tau_d = 2912{r_0}^2 + 35$ with $Pearson\ r^2 = 0.999$. Data are presented as means +/- standard deviation from $N = 4$ independent experiments.

for each sample). A strong variation of diffusion time and exponent of anomalous diffusion was observed, indicating the heterogeneity of the system at larger scales. For curves shown in this figure, the exponents of anomalous diffusion were 0.79, 0.91, 0.87 and 0.52 and the corresponding diffusion times being $26,704\ \mu s$, $1,072\ \mu s$, $1,505\ \mu s$ and $6,241\ \mu s$.

After analysing this heterogeneity at the diffraction-limited scale using FCS, we also performed the spot variation with post-processing to investigate the existence of nano-scale domains in the diffraction-unlimited detection volume.

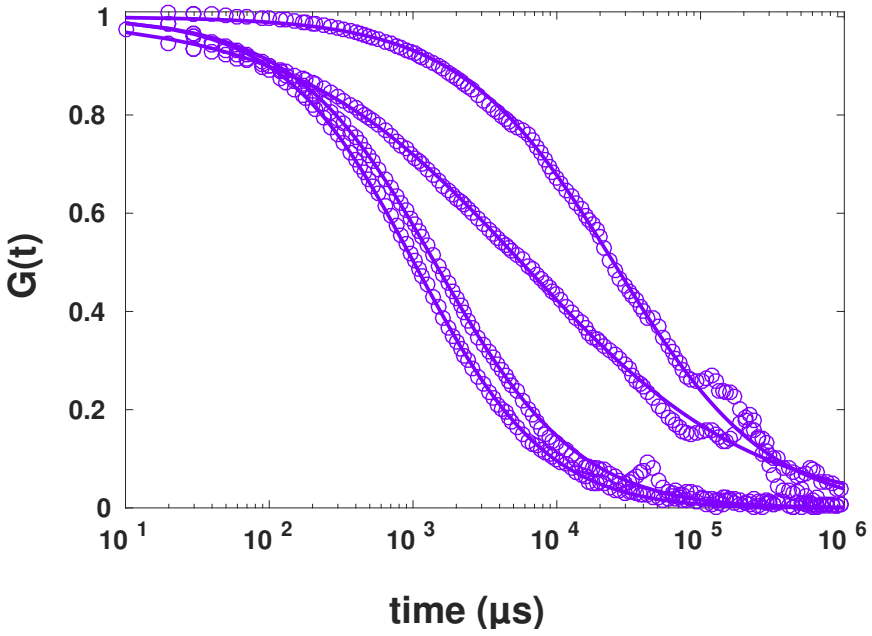

Figure 4.14. Experimental results of FCS measurements for diffusion of AlexaFluor647 labeled streptavidin in DMSO:glycerol solution fitted to the standard formula.

The post-processed data for smaller spot sizes were shown in Fig.4.15. Only one of the measurements (shown in the right panel) shows the linear decrease of the diffusion time with decreasing the spot size. Three other set of data show extreme deviations from the expected behaviour for homogeneous systems: Even the obtained exponents of anomalous diffusion for smaller r_0 deviate considerably from the those obtained from the experimental confocal FCS data. Most of them tend to unity (normal diffusion) for smaller spot sizes. In some cases the fit indicates $\alpha > 1$, which is probably an artefact due to an inappropriate fit function (**?**).

In order to apply the diffusion law analysis, one can not simply average the diffusion times resulting from the different exponents of anomalous diffusion; different exponents for different measurements and spot variation data. An alternative way to analyse data, in a form which is applicable to the diffusion law analysis, is to fit the data to the normal diffusion with different diffusion times. Taking into account the binary nature of the system, we performed two-component fits for all original

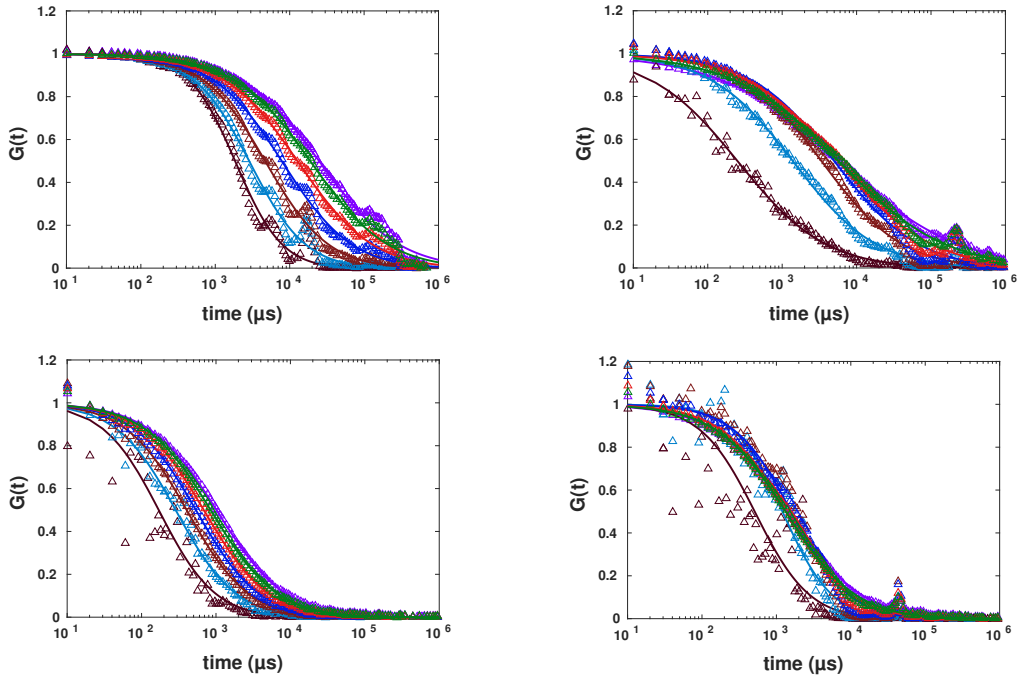

Figure 4.15. Spot variation FCS with post-processing for four independent measurements in four different samples (r_0 - $0.4r_0$ from right to left). The curves were fitted to the standard formula with free fit parameter of exponent of diffusion. The intensity time traces were generated using binning method.

and spot variation FCS curves as:

$$G(t;\alpha,D_\alpha) = A_1\left(\frac{4D_1}{r_0^2}t+1\right)^{-1}\left(\frac{4D_1}{s^2r_0^2}t+1\right)^{-\frac{1}{2}} + A_2\left(\frac{4D_2}{r_0^2}t+1\right)^{-1}\left(\frac{4D_2}{s^2r_0^2}t+1\right)^{-\frac{1}{2}} \tag{4.12}$$

where A_1 and A_2 are attributed to the contribution of two components of diffusion processes, respectively with their diffusion coefficients, D_1 and D_2.

Although the two component fit was suboptimal, requiring higher number of components, our analysis indicates the existence of the slow component with the diffusion time of $31,907 \pm 2,726$ μs. This is roughly ten fold larger than the diffusion time in pure DMSO, which is in agreement with previous results (**?**). The spot size dependence of slow (blue) and fast (red) diffusion times are shown in Fig.4.16. The diffusion time for the slow diffusion did not follow the expectation for a homogeneous system, and the intercept of a linear fit was $28,133 \pm 2,726$ μs indicating the existence of nano-domains within the confocal volume, in which tracer molecules

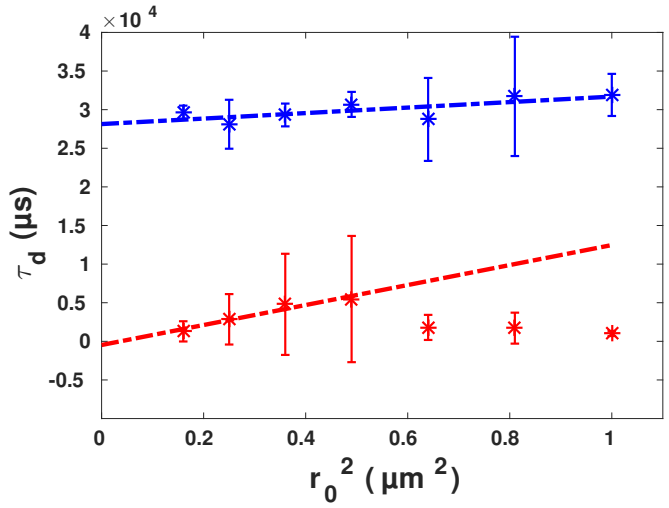

Figure 4.16. Diffusion time of AlexaFluor647-labeled streptavidin in DMSO:glycerol solution for slow component (blue) and fast component (red) versus spot size, together with corresponding linear fits $\tau_d = 3555{r_0}^2 + 28133$ with $Pearson\ r^2 = 0.45$ and $\tau_d = 12941{r_0}^2 - 474$ with $Pearson\ r^2 = 0.91$. Standard deviations were calculated from eight measurements in four sample preparations.

spends much longer time compared to the free diffusion in the DMSO phase, indicated by the fast time component of $1,019 \pm 3,360\ \mu s$. This result could in principle be considered as an experimental proof of the capability of the method to detect nano-domains.

The analysis of the fast component for larger spot sizes is very inaccurate due to the overall very slow decay of the curves. Nevertheles, when the size of the spot is reduced using spot variation, the influence of slow diffusion due to nano-domains is diminished in most of the FCS curves. For $< 0.5r_0$ the behaviour of the diffusion time is similar to those for pure DMSO. Excluding the data for larger effective spot sizes from the linear fit results in intercept being: $-474 \pm 3,323\ \mu s$.

4.1.4 In-vivo Exemplary Experiments

As an application of our method to living cell studies, we performed intracellular FCS measurements. The microscopic picture corresponding to successful injection of AlexaFluor647-labeled streptavidin is given in Fig. 4.17.

To check the successful injection process, fluorescence lifetime histograms before and after the injection process were recorded. Results shown in Fig.4.18 indicate the broad lifetime distribution of autofluorescence (blue) before injection. After

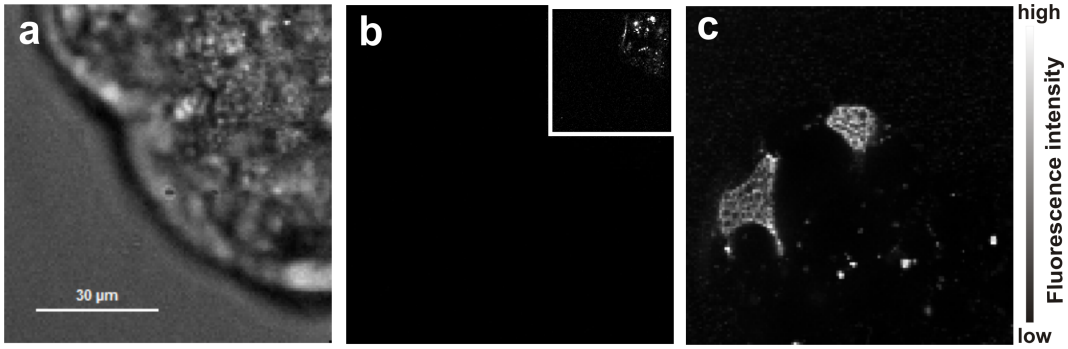

Figure 4.17. a) Bright field image of chosen cell region to be injected, b) fluorescence image of cell region before injection, (inset) fluorescence image before injection boosted 40 times for visibility of autofluorescence, c) fluorescence image of cell region after injection showing AlexaFluor647 fluorescence in two different injection points.

injection of AlexaFluor647-labeled streptavidin, the lifetime histogram is enhanced and centred around 1.5 ns. The biexponential fluorescence decay analysis (not shown) resulted in average decay time 1.6 ns. This is in agreement with reported lifetime for AlexaFluor647-labelled streptavidin in buffer solution indicating a bi-exponential fluorescence decay with an average lifetime of 1.5 ns (**?**).

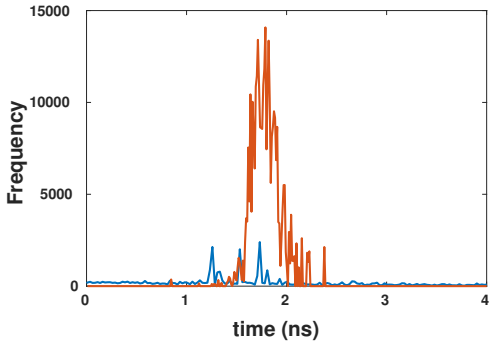

Figure 4.18. Fluorescence lifetime histograms extracted from both images, before (blue) and after (red) injection. Additional photon counts after injection and their lifetime distribution indicate successful injection process of AlexaFluor647-labeled streptavidin.

After injection, we performed intracellular FCS measurements. The calculated autocorrelation functions are shown in Fig.4.19. Similar to the case of binary mixture of DMSO:glycerol, we have observed different results for four different cell preparations. Plotted in Fig.4.19 are the FCS curves corresponding to four different

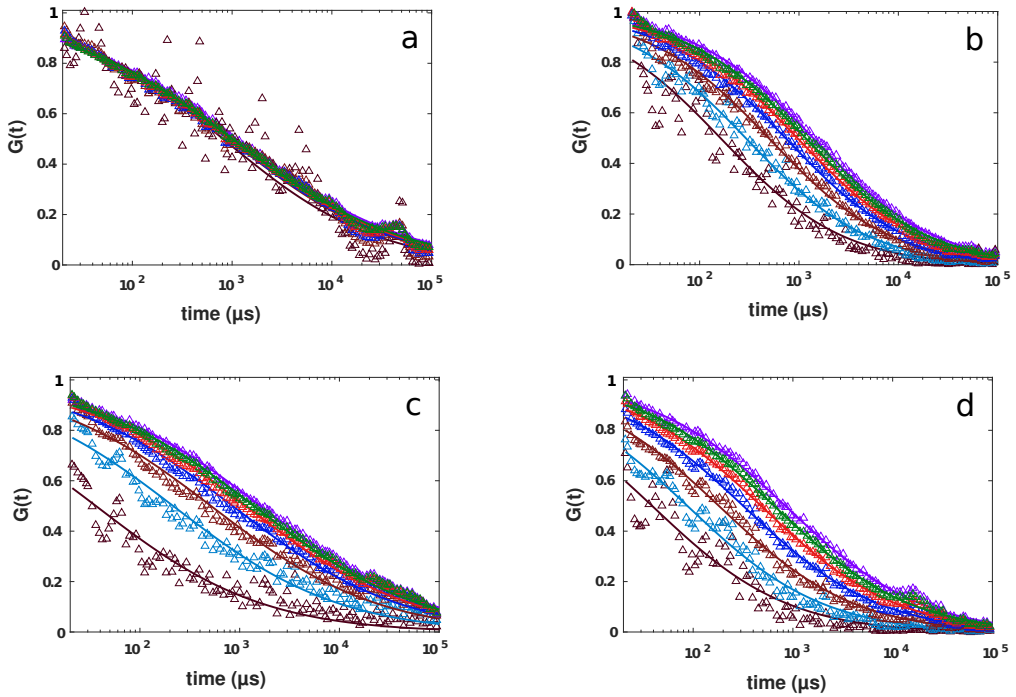

Figure 4.19. Experimental results for FCS calculated from smoothed FCS curves with $\sigma = 3$ μs (circles) together with results for mimicked spot variation FCS (with spot size varying from r_0 to $0.4r_0$ from right to left) for the diffusion of AlexaFluor647-labelled streptavidin in a living cell in different preparations fitted to the standard formula.

measurements together with post-processed spot variation data, respectively. The exponents of anomalous diffusion changed considerably from one to another measurement and were 0.49, 0.68, 0.50 and 0.62 with corresponding diffusion time being $1,199$ μs, $1,496$ μs, $1,770$ μs and 903 μs. The spot variation FCS results apparently differ from one to another sample and except for one measurement, the results unravel presence of either transient interaction with other macromolecules or trapping due to geometrical confinement bellow the diffraction limit.

The dependence of the effective diffusion time on the spot size is shown in Fig.4.20. These data and the corresponding linear fits indicate different behaviour of diffusion time with change of the spot size. Observed positive and negative intercepts in diffusion law analysis for different independent experiments underlie the existence of a complex intracellular-environment. Here, streptavidin seems to transiently interact with other macromolecules or its diffusion is hindered due to existing of nanobarriers. Similar experimental results were observed recently using STED-FCS (**?**).

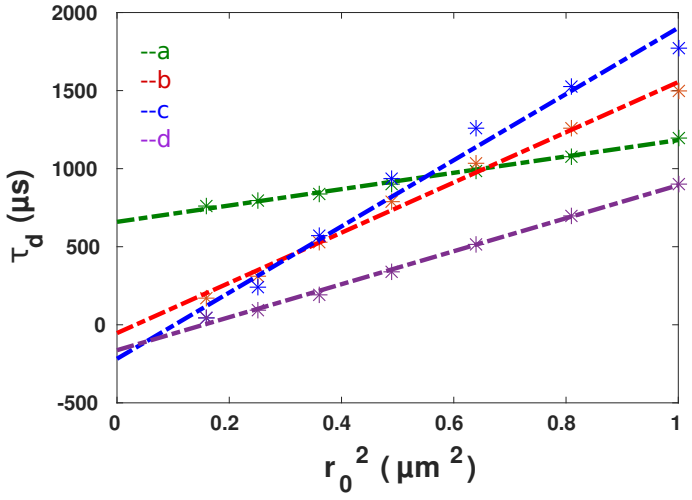

Figure 4.20. The diffusion law analysis for four living cell FCS measurements (shown in Fig.4.19) together with the linear fits.

Generally, intracellular organellesin living cells and membrane systems as well as cytoskeleton elements form a dynamic three-dimensional maze through which tracer molecules have to find their way, leading to hopped diffusion. This kind of trapped diffusion can be the result of transient protein-specific interactions with intracellular components. Such transient complexes would then diffuse slower or could be locally immobilized or geometrically repulsed (**????**).

4.2 Summary

In this chapter, we introduced a method for mimicking the spot variation fluorescence correlation spectroscopy (SV-FCS) using post-processing of recorded photon counts from an ordinary diffraction-limited confocal FCS measurement. Recorded photons counts from FCS measurements are transformed to a smoothed intensity trace using kernel smoothing method with a double-sided exponential kernel or to a piecewise-continuous intensity trace using binning. The resulting intensity trace is then non-linearly transformed. The transformed trace corresponds to the one which would be obtained for the same particle's trajectories in a smaller confocal volume, whose waist is controlled by a free parameter r_c of the transformation. The method is checked in extensive numerical simulations, and is applied to experimental situations.

Applying the method to diffusion of AlexaFluor647-labelled streptavidin in PBS buffer solution and in buffer crowded by 30% PEG1500, we have shown that for

these homogeneous systems the effective diffusion coefficient does not depend on the mimicked spot size and equals to the one obtained in normal FCS. This gives an additional (although indirect) support for the validity of our approach. Applying the method to the diffusion of the same tracer in DMSO and the binary mixture of DMSO:glycerol we tested the method's ability to detect nano-domains at sub-diffraction level. Finally, the same procedure was applied for the case of diffusion of streptavidin in living cells. As expected, the results of such application indicate strong inhomogeneity of the intracellular medium.

5 Conclusion and Outlook

Fluorescence correlation spectroscopy is a strong single molecule technique which provides important information about the diffusion process and the medium in which the diffusion takes place. Methods for performing FCS experiments in artificial and biological systems are well-established and obtaining the FCS curves in laboratory is nowadays a routine task . The analysis of data obtained from this technique is, however, a hard task. The protocol for the analysis of normal diffusion in the FCS results is so far trivial and generally accepted. However, data processing for the case of anomalous diffusion, typical for strongly inhomogeneous and crowded biological systems was missing. Such a toolbox was strongly needed not only to obtain some specific parameters of the undergoing processes, but also for understanding the physics behind them. In this thesis, we looked deeper at different temporal and special aspects of the FCS data and developed methods not only to robustly analyse the FCS data for anomalous diffusion, but also obtain much more information which was not known using standard methods.

In chapter 2, we performed a deep mathematical investigation of the theory behind FCS data. With minimal assumptions made on the PDF of the particle's displacement, we derived a general formula which represents the FCS curve for more complicated three dimensional case. Using this formula, we investigated the robustness of data one obtains from the standard method of data analysis which is often used in most of literatures. We used some toy models as functions for PDF and calculated the corresponding FCS curves. The results of the standard fits happened to be considerably different from the initial input values for all the cases, but the Gaussian form of PDF. We then proceeded to show that a FCS curve is, essentially, constructed of the moments of its displacement PDF which allows one to confirm or reject the Gaussian nature of PDF. In case of scaling form of PDF, we demonstrated that the robust information can be obtained from the short time asymptotic. Using this facts, we established a protocol which enables one to choose a proper model for explanation of observed anomalous diffusion. The obtained theoretical results were then supported by extensive FCS experiments in in-vitro and in-vitro systems.

Besides these progresses we made in the theory of ordinary FCS, still there are some questions left regarding to the possibility of extraction of the full form of the PDF. As we discussed, in the Eq.2.1, the unknown $P(r,t)$ is function of two parameters and obtaining its full form requires that the known part $G(t)$, to be also a function of position. This possibility was discussed in chapter 4 and here we

propose other possible approaches. One method to reach this aim, which deserves further investigations, could be to transform Eq.2.1 to a Fredholm's type equation with some changes of variables. For this, one needs to assume that the PDF scales. In such case, the relation between position and time (as in MSD) could be exploited to reduce the unknown two parameters to only one parameter and then try to solve the inverse problem. For instance, in the two dimensional case which is realistic for diffusion in the plasma membrane, the apparatus function contains no dependency on the elongation parameter and has a Gaussian form. With the change of variables one could show that Eq.2.1 may be re-written as a Laplace transform of $P(r,t)$. Although this step is possible, the inversion part still demands further investigation. The main problem is that the Inverse problem is formally solvable, but highly ill-posed. In other words, the noise in the data creates extreme fluctuations in the inverse problem. Therefore, one needs to somewhat smooth the noisy FCS data such that the nature of data remains still untouched.

The other possibility to gain the full form of the PDF from Eq.2.1 is fitting. For this, one may consider a general form of the PDF, similar to the Eq.2.24. This general form contains four unknown parameters which have to determined from fitting to the FCS data. Although taking this type of functions for the form of the PDF imposes some assumptions on it, still is more general than assuming a Gaussian nature of the process. In the situation where the system is simple (e.g in water) one would expect the results to generate a Gaussian form from fitting. This can be considered as a test for fitting approach. The initial values for the fitting may be determined by performing the standard fit model for the first run. The first and main issue in this approach is that the integral in Eq.2.13 does not have an analytical solution with these types of functions, or at least the answers are very complicated. Thus, one has to perform the fitting with the numerical results of the integral. Therefore, one has to develop a fitting toolbox which provides reliable results from fitting to the noisy data in a numerical way. Our investigation indicated that the numerically calculated noiseless FCS data as in toy models, could be accurately fitted and this approach provides the exact form of the PDFs.

In chapter 3, we formulated the theory of FCS technique for the situation where the PDF of displacement lacks the scaling property. A good example of such phenomena is "anomalous yet Brownian" process. In such a process, the MSD grows linearly in time but the PDF deviates from Gaussian form at short times. An analytically solvable model which shows such behaviour is the CTRW model with a waiting time PDF being the Lévy-stable distribution with an exponential cut-off. We considered the system to be in equilibrium, to comply the real situation in experiments where the samples are prepared long time before the measurements start. Using the general formula derived in chapter 2, we showed that the body of the FCS curves for such a model may be nicely fitted to the normal diffusion and without short time analysis, such phenomena may not yet be seen in the FCS data.

Here we investigated the equilibrated CTRW in the FCS thechnique and the ordinary CTRW was generically studied by **?**. Nevertheles, there are still some questions which could be addressed in this area. Observation of aging which is a characteristic property of the ordinary CTRW process in a single FCS measurement is an example. For this, one could obtain the fluorescence intensity of single measurement and calculate the autocorrelation functions with truncating the initial parts of the intensity traces. This in fact leads to the change of the starting point of the measurements. Therefore, one may observe a shift of diffusing time to longer times. This would indicate the decreasing of the jump rates due to the aging of the processes. For instance, we have observed such phenomena in analysing the FCS data obtained in living cell measurements. The main issue in this type of analysis would be as follows: for the experiments where the preparation has been done long ago, the system is already aged and equilibrated. Therefore, changing the starting point of the analysis would not result in a considerable difference between the corresponding FCS curves. Thus, one has to perform the experiment right after injection process of tracer particles into the sample. Here also care must be taken, not to misinterpret the changes in the FCS curves due to the injection process as aging. The ideal case, would be to prepare the system and freeze the process with some external conditions (e.g temperature) and then to perform the experiment as the process starts (**?**).

Another interesting question to be answered, could be to develop a theoretical strategy to capture more information concerning the energetic landscape of the medium (e.g waiting time distribution function PDF) form FCS data analysis. Assuming that the waiting time and jump length PDFS are decoupled in PDF of displacement and additionally, considering a Gaussian form for the jump length distribution, one may seek for a way to extract information about the waiting time distribution with fitting the FCS data in Laplace domain. Using the connection between the mean waiting time and the energy of the traps, one can in principle, study the chemical reactions between the trapping and diffusing elements. Another issue in this section is to demonstrate the artefacts from many component fit method. Normally in analysing FCS curves, one observes the quality of fits from the error bar windows. when the standard formula does not well fit the curves, the curves are fitted to the many component normal diffusion model. The connection between the diffusion times obtained from this type of fit and our analysis may also be studied to compare the accuracy of different methods for exact analysis of FCS data.

In chapter 4, we developed a new strategy to perform SV-FCS by data analysis. The main idea behind our work here, was to exploit the form of the confocal volume which nicely connects the position of the tracer (distance from the center) and the recorded fluorescence intensity profile. The initial binary intensity profiles were first transformed to continuous or piecewise-continuous profiles using smoothing kernel or binning methods. We then introduced a non-linear transformation in order to continuously manipulate the intensity profile to eliminate the photon counts

resulting from outer parts of the confocal volume. The autocorrelation functions of newly generated intensity profiles represented the FCS curves for the sizes of the confocal volume which were effectively smaller than the initial one. We tested our proposed method in an extensive simulation study and then successfully, applied it to investigate in-vitro and in-vivo systems.

Contrary to the existing experimental methods for SV-FCS, our proposed method requires no additional experimental complexity in set-up and no need for repetition of experiments. This prevents the errors due to recalibration, drifts and thermal instabilities. The limitation of the method is, however, its restricted applicability to experiments with a low concentration of tracer, below 1 nM for a typical size of the confocal volume. Therefore to obtain enough statistics, one may need longer data acquisition times. In our analysis, we showed that 100 s data acquisition time is sufficient to obtain reliable results for effective spot sizes down to 1/3 of the initial one. Further increasing of the measurement time would lead to a high quality data and allows to extract the effective FCS curves for the spot sizes up to an order of magnitude smaller than initial spot size. Then we concluded that SV-FCS using data post-processing is an experimentally simple and straightforward single-molecule technique which is feasible for studying the sub-cellular organisation of living cells.

The possibility of performing the spot variation in software level, in fact, opens a broad window for further developments in the FCS technique, especially in experimental part. Since our proposed method is a calibration free method in studying two dimensional cases, one can use it for a high precision study of lipid bi-layers and plasma membrane. Performing a long time measurement in two dimensional case and treating the FCS data as function of position and time, one can think of applying maximum like-hood method to find the best matching model for the corresponding experiment. Also, with independent analysis of all curves obtained from the SV-FCS in a single measurement, one can indirectly observe the trapping un-trapping phenomenon in a higher spacial resolution.

Another very interesting idea to pursue is to develop the spot variation fluorescence cross correlation spectroscopy (SV-FCCS) technique. In the FCCS technique, lasers sources with different colours create two overlapping spots in the sample. This set-up is normally used to study the interaction of two types of tracer molecules which are labelled according to the colours of lasers. Although performing SV-FCCS experimentally (i.e. using methods listed in this work) is possible, but practically is an extremely difficult task. Using our proposed method, one can first perform FCCS measurements and then, independently, apply the non-linear transformation on the intensity profiles obtained from each spot. With this, one can study not only the activity of two species, but also their interactions with their substrates. For instance, the spatio-temporal heterogeneity of lipid interaction in the plasma membrane of living cells has been revealed using STED (**?**). Applying the SV-FCCS to living cell systems, one may investigate this heterogeneity in language of FCS data.

The advantage would be the possibility of monitoring the interactions of different proteins with a single raft which is captured in the confocal volume. This also allows one to study the functionality of different proteins with respect to a specific part of the cell. On the other hand, having the same molecule as a diffusing particle and labelling it with different fluorescence molecules, one can investigate the influence of labelling in the activity of a specific protein.

A Appendix

A.1 Details of experimental procedures

A.1.1 In-Vitro Measurements

The measurements have been performed on a Micro-Time 200 time-resolved confocal microscope (PicoQuant, Berlin, Germany) at the Physical Chemistry group of University of Potsdam. Samples were excited by a laser diode (LDH-P, PicoQuant) with wavelength of 635 nm, repetition rate of 20 MHz and pulse width of 70 ps. The excitation beam was focused by a 100x/NA1.4 oil immersion objective (Olympus, Hamburg, Germany). Fluorescence light emitted from dye passes through the dichroic mirror (z467/635rpc, AHF Analysentechnik, Tübingen, Germany) and is guided through a 50 μm pinhole, is splited by a 50% mirror to be recorded by two single photon avalanche diodes detectors (SPAD)(SPCM-AQR-13 SPCM-CD-2801, Perkin-Elmer, USA). To calculate the autocorrelation functions, we used SymPhoTime 64 software (PicoQuant) and analysis of data was performed by software OriginPro 9.2. In order to obtain parameters r_0 and s entering the apparatus function, we performed a calibration experiment with Atto655 diffusion in water at 293.15 K where the diffusion is normal and the diffusion coefficient is known: $D = 392\mu\text{m}^2/\text{s}$ (**?**). Calibration leads to the values of parameters $r_0 = (0.260 \pm 0.006)\mu m$ and $s = 6.3 \pm 0.13$, which corresponds to the values of $a_2 = 0.675$ and $a_4 = 0.271$.

A.1.2 In-Vivo Measurements

In order to perform intracellular FCS measurements, salivary gland tissue of the American cockroach *Periplaneta americana* was dissected in physiological saline. Subsequently, the tissue was attached to a glass cover slip using the tissue adhesive Vectabond (Axxora, Lörrach, Germany) and the recording chamber was then mounted on the microscope stage. For dye-injection, micropipettes with tip sizes of approximately 2 μm were prepared from glass tubes with filaments (GB150F-10, Science Products, Hofheim, Germany) using a micropipette puller (P-97, Sutter Instruments, Novato, USA). Micropipettes were loaded with 100 nM of tracer molecules. The injection process into the salivary gland duct cells was performed with an injection system (FemtoJet, PatchMan NP2, Eppendorf, Hamburg, Germany) under microscopic view (IX71, Olympus, Hamburg, Germany).

A.2 Numerical Laplace Inversion

There are several numerical approaches for inversion of Laplace transform, no single method is optimal and each method is suitable for a particular function. One of the most popular inversion algorithms is the Gaver-Stehfest algorithm. This algorithm is very accurate for functions of type $e^{(-\alpha t)}$ but fails for functions with oscillatory behaviour. In the Gaver-Stehfest algorithm we should sample the Laplace sample function in real line, therefore the inverse integral is defined as:

$$f(t) = \frac{1}{2\pi i t} \int_c \tilde{f}(z/t) e^z dz.$$

Approximation of e^z with rational function one has

$$e^z \simeq \sum_{k=0}^{n} \frac{w_k}{\alpha_{(k-z)}}$$

w_k and α_k are weights and nodes respectively. Applying the Cauchy integral formula and considering weight and nodes are real numbers, we obtain:

$$f(t) \simeq \frac{(\ln(2))}{t} \sum_{k=1}^{N} w_k \tilde{f}(k ln(2)/t)$$

with

$$w_k = (-1)^{N/2+k} \sum_{j=(k+1)/2}^{min(k,N/2))} \frac{k^{(M+1)}}{(N/2)!} \binom{N/2}{j} \binom{2j}{j} \binom{j}{k-j}$$

The precision of $f(t)$ depends on the value of Stehfest number N. Theoretically, increasing N leads to preciser $f(t)$. On the other hand, when the Stehfest number becomes too large, the numerical errors extremely increases. Thus, there is an optimum value of N. For our calculation we set $N = 18$. The main limitation of this method is that, $f(t)$ should be smooth on the scale of the sampling function. Despite these limitations, this method has some desirable aspects. For instance, the coefficient w_k can be easily computed and the approximation does not need the value of function for complex number and it is simple to implement.

A.3 Details for Generation of Random Numbers

A.4 Box-Muller Method

The Box-Muller transform, is a pseudo-random number sampling method for generating pairs of Gaussian-distributed random numbers, given a source of uniformly distributed random numbers. Suppose x_1 and x_1 are independent random variables that are uniformly distributed in interval $(0, 1)$, then y_1 and y_2 are pseudo-random numbers with a standard normal distribution. The basic form of transformations are as follows

$$y_1 = \sqrt{-2\ln(x_1)}\cos(2\pi x_2)$$

$$y_2 = \sqrt{-2\ln(x_1)}\sin(2\pi x_2).$$

We used a prepared function in $C{+}{+}$ programming language which uses the above mentioned method for generating the Gaussian-distributed random numbers.

A.5 Metropolis-Hastings Algorithm

To generate a set of random variable with a desired distribution, one normally uses the inverse form of the function for the cumulative density function (cdf) of a random variable. But in most situation, one needs to obtain a sequence of random samples from a probability distribution for which direct sampling is difficult. The Metropolis-Hastings algorithm can draw samples from any probability distribution P(x), provided you can compute the value of function $f(x)$ that is proportional to the density of $P(x)$, rather than exactly equal to it. This makes the Metropolis-Hastings algorithm particularly useful. Metropolis-Hastings algorithm works in such a way that, as more and more sample values are produced, the distribution of values more closely approximates the desired distribution, P(x). To generate a collection of states according to a desired distribution, the algorithm uses a Markov process which asymptotically reaches a unique stationary $\pi(x)$, such that $\pi(x) = P(x)$.

To generate y_i according to $g(y, x_i)$, the approach is to separate the transition in two sub-steps; the proposal distribution $g(x, y)$ and the acceptance distribution $A(x, y)$ (the conditional probability to accept the proposed state):

$$x_{(i+1)} = \begin{cases} y_i, & \text{with probability } A(x_i, y_i) \\ x_i, & \text{with probability } 1 - A(x_i, y_i) \end{cases} \tag{A.1}$$

with

$$A(x, y) = min[1, (P(y))/(P(x))(g(x, y))/(g(y, x))]$$

Note that in general, it is not clear problem which distribution $g(x, y)$ should be

used. It is a free parameter of the method which has to be adjusted to the particular problem in hand.

In our case the desired distribution contains two parts. The first Lévy part is the distribution from which we can draw y_i and the exponential part is used to form the condition.

Acknowledgement

First of all, I would like to thank my first supervisor, Prof. Igor Sokolov, for his exceptional supervision. He was all the time open for discussion in order to develop different scientific ideas. It is a great honor for me to do my doctorate with him.

I would like to thank my second supervisor, Prof. Hans-Gerd Löhmannsröben, for his endless support during my work. He discussed with me and corrected me at each stage of my work and guided me to different national and international conferences. I learned a lot from him.

I also thank Dr. Carsten Hille for his kind supervision, especially, for performing the experiments. I appreciate the time he devoted for me and his effort in introducing the experimental techniques. He provided all the needed materials and set-ups for experiments.

I also would like to thank my family for their endless support from far distance. Talking to them always makes me more energetic to peruse my scientific carrier. Especially my parents for their love and caring.

I also would like to thank all my friends and colleagues from Golm, SALSA, Iran and especially our group in the Physics department of Humboldt University of Berlin.

Finally, I thank the school of analytical science Adlershof (SALSA) for providing this position for me. Participating the conferences, lectures and team works in SALSA was an amazing chance to meet great people, learn from experts and make good friends.

Selbständigkeitserklärung

Ich erkläre, dass ich die vorliegende Arbeit selbständig und nur unter Verwendung der angegebenen Literatur und Hilfsmittel angefertigt habe.

Berlin, den 5. Juni 2018 Seyed Mohsen Jebreiil Khadem

List of publications

1. **Seyed Mohsen Jebreiil Khadem**, C. Hille, H. G Löhmannsröben and I. M. Sokolov
   What information is contained in the fluorescence correlation spectroscopy curves, and where
   Physical Review E 94, 022407 (2016).

2. **Seyed Mohsen Jebreiil Khadem** and I. M. Sokolov
   Nonscaling displacement distributions as may be seen in fluorescence correlation spectroscopy
   Physical Review E 95, 052139 (2017).

3. **Seyed Mohsen Jebreiil Khadem**, C. Hille, H. G Löhmannsröben and I. M. Sokolov
   Spot variation fluorescence correlation spectroscopy by data post-processing
   Scientific Reports 7 , 5614 (2017).

4. Y Abdi, **Seyed Mohsen Jebreiil Khadem** and P. Afzali
   Resonantly excited ZnO nanowires for fabrication of high sensitivity gas sensor
   Current Applied Physics 14, 227-231 (2014).

5. **Seyed Mohsen Jebreiil Khadem**, Y Abdi and P. Afzali
   Investigating the effect of gas absorption on the electromechanical and electrochemical behavior of graphene/ZnO structure, suitable for highly selective and sensitive gas sensors
   Current Applied Physics 14, 1498-1503 (2014).